BioMed Research International

Trends and Future of Hearing Aid Implantation and Implant Technology

Guest Editors: Stefan Weber, Marco Caversaccio, Peter Brett, Nozomu Matsumoto, and Claus-Peter Richter

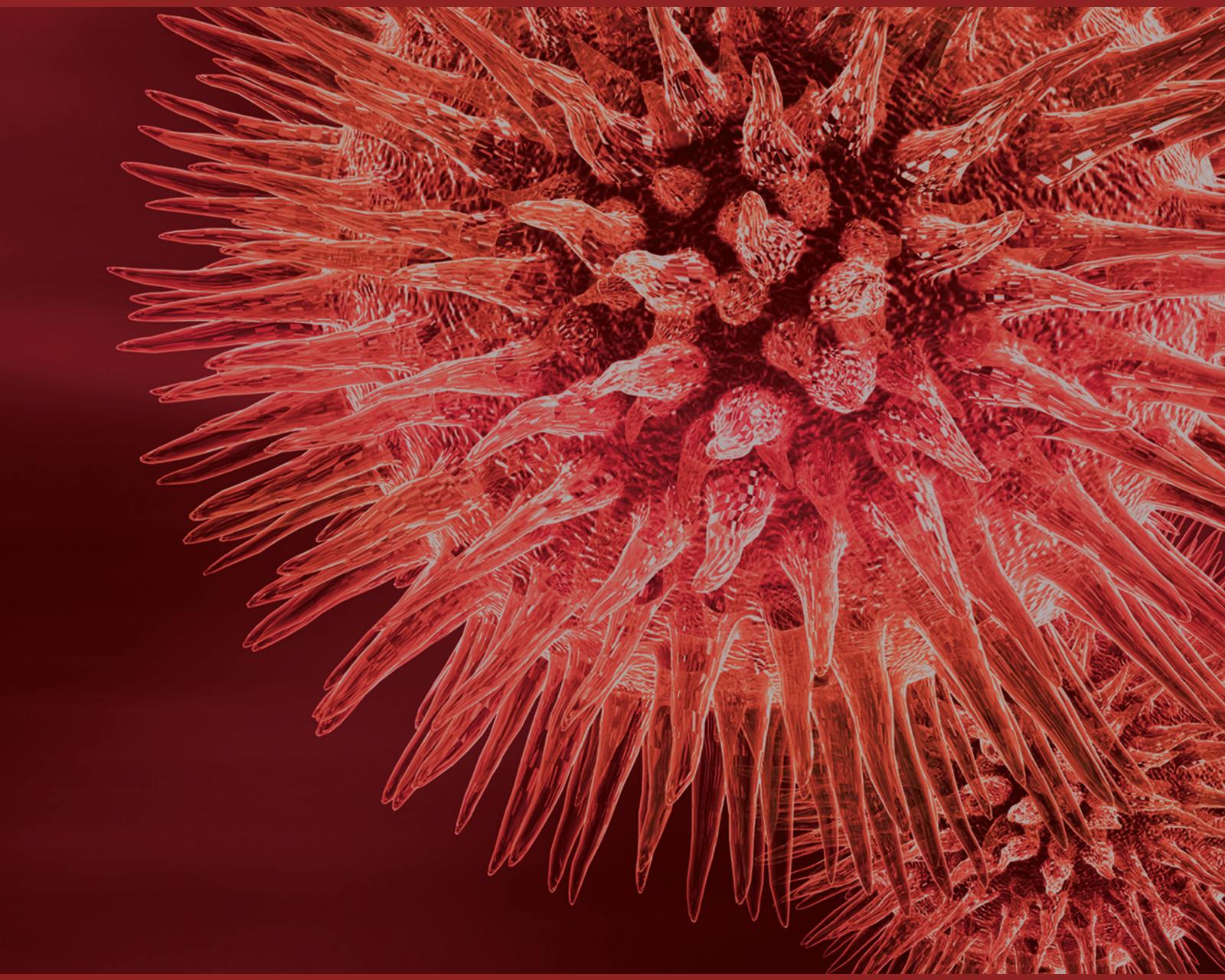

Trends and Future of Hearing Aid Implantation and Implant Technology

BioMed Research International

Trends and Future of Hearing Aid Implantation and Implant Technology

Guest Editors: Stefan Weber, Marco Caversaccio, Peter Brett, Nozomu Matsumoto, and Claus-Peter Richter

Contents

Hindawi Publishing Corporation
BioMed Research International
Volume 2014, Article ID 251814, 10 pages
http://dx.doi.org/10.1155/2014/251814

Research Article

Optical Coherence Tomography Guided Laser Cochleostomy: Towards the Accuracy on Tens of Micrometer Scale

Yaokun Zhang,[1] Tom Pfeiffer,[2] Marcel Weller,[3] Wolfgang Wieser,[2] Robert Huber,[4] Jörg Raczkowsky,[1] Jörg Schipper,[3] Heinz Wörn,[1] and Thomas Klenzner[3]

[1] *Institute for Anthropomatics and Robotics (IAR)-Intelligent Process Control and Robotics (IPR), KIT, Engler-Bunte-Ring 8, 76131 Karlsruhe, Germany*
[2] *Ludwig-Maximilians-University, Oettingenstraße 67, 80538 Munich, Germany*
[3] *Department of Otorhinolaryngology, Düsseldorf University Hospital, Moorenstraße 5, 40225 Düsseldorf, Germany*
[4] *Institute for Biomedical Optics, University of Lübeck, Gebäude 81, Raum R 67, Peter-Monnik-Weg 4, 23562 Lübeck, Germany*

Correspondence should be addressed to Jörg Raczkowsky; joerg.raczkowsky@kit.edu

Received 5 March 2014; Accepted 31 July 2014; Published 11 September 2014

Academic Editor: Peter Brett

Lasers have been proven to be precise tools for bone ablation. Applying no mechanical stress to the patient, they are potentially very suitable for microsurgery on fragile structures such as the inner ear. However, it remains challenging to control the laser-bone ablation without injuring embedded soft tissue. In this work, we demonstrate a closed-loop control of a short-pulsed CO_2 laser to perform laser cochleostomy under the monitoring of an optical coherence tomography (OCT) system. A foresighted detection of the bone-endosteum-perilymph boundary several hundred micrometers before its exposure has been realized. Position and duration of the laser pulses are planned based on the residual bone thickness distribution. OCT itself is also used as a highly accurate tracking system for motion compensation between the target area and the optics. During *ex vivo* experimental evaluation on fresh porcine cochleae, the ablation process terminated automatically when the thickness of the residual tissue layer uniformly reached a predefined value. The shape of the resulting channel bottom converged to the natural curvature of the endosteal layer without injuring the critical structure. Preliminary measurements in OCT scans indicated that the mean absolute accuracy of the shape approximation was only around 20 μm.

1. Introduction

The inner ear is embedded in the temporal bone as part of the human skull. Future inner ear surgery will require a highly precise and most atraumatic surgical approach to the human cochlea with the organ of hearing. This is mandatory to give the possibility for future treatment options for diseases of the inner ear, for example, to place devices like drug delivery systems, electrodes, or optical fibers with preservation of existing inner ear function such as hearing or balance [1–3]. As an important surgical step, cochleostomy provides the surgical approach to the human cochlea when a round window approach is inconvenient or impossible, enabling the implantation of intracochlea devices. Preservation of existing inner ear function such as hearing or balance during this process is required.

In clinical routine, a cochleostomy is manually drilled by the surgeon with diamond burrs (Figures 1(a) and 1(b)) to create an artificial channel for the implant on the bony shell of the cochlea. During this process, the cochlear endosteum should remain intact, preventing the bone-debris produced during the drilling process or blood from entering the scala tympani and meanwhile avoiding the leakage of the perilymph. Otherwise, the residual function of the cochlea will be damaged.

Due to the small diameter of the cochleostomy (approx. 1 mm) and the thickness of the fragile endosteal layer (<50 μm), the required reproducible accuracy of the drilling

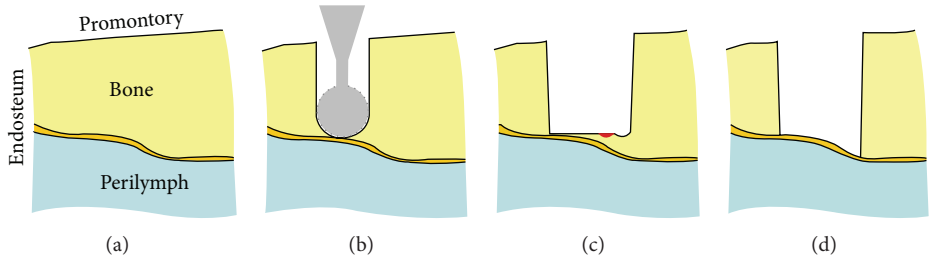

Figure 1: ((a)-(b)) Conventional cochleostomy: exposing the endosteum of the scala tympani with a small burr (diameter 0.6 mm); ((c)-(d)) conception of laser cochleostomy: the bony shell of the cochlea is ablated pulse by pulse using a short-pulsed CO_2 laser and the shape of the endosteum can be approximated more precisely. The red spot denotes the tiny tissue volume being ablated [18].

process reaches the limit of human capabilities. The achievable precision of the manually performed cochleostomy is mainly dependent on the skills and experiences of the surgeon. Although operated with great care, the burr frequently tears or perforates the cochlear endosteum despite the surgeons' best efforts [4]. According to the review study of Incerti et al. [5], an insertion of electrodes into the cochlea is possible with preservation of residual hearing. Nonetheless the patients treated for electric acoustic stimulation on the same ear suffered from a postoperative threshold shift up to 30 dB in the deep frequencies. A computer-assisted microsurgery system is therefore desired to support the surgeons to ensure a reproducible precision during this highly demanding surgery.

For this purpose, robotic systems are common choices, using either a highly precise hexapod [6, 7] or a standard robot arm [8, 9]. Based on preoperative planning in CT scans, the robot is navigated to perform the drilling without violating critical structures like the facial nerve and the chorda tympani until reaching the stop point located on the endosteum. Unfortunately, the accuracy of the stop point in the planning data is limited by the resolution of the CT scan, which is about 0.1–0.25 mm in clinical routine and is insufficient regarding the thickness of the endosteum that is only several tens of micros. Unavoidable intraoperative registration and navigation errors further worsen the situation. Du et al. [10] and Brett et al. [11] therefore developed autonomous surgical robotic systems with real time haptic feedback. The critical structure is discriminated by analyzing the force and torque measured from the tip of the drill bit. The drilling will be ceased when a significant change in force and torque occurs, indicating that the endosteum is reached.

An inherent shortcoming of mechanical drilling is that the resulting channel bottom has the same shape as the burr that is convex in the direction of the drilling (Figure 1(b)). But, the cochlea is convex towards outside (see also Figure 3), that is, in the opposite direction of the drilling. As a result, while the drill bit already touches the endosteum in the middle part of the channel, some residual bone tissue still remains near the wall of the cochleostomy. In such a case, it is a challenging task to expose a sufficiently large area of the endosteum that matches the diameter of the implant without damaging the already exposed thin membrane in the middle. Moreover, mechanical drilling is always accompanied by high frequency vibration of the surrounding tissue, which might bring additional acoustic trauma to the cochlea.

Researches throughout the last decade revealed the feasibility of using a short-pulsed CO_2 laser for hard tissue ablation [12–15] and more particularly for the inner ear surgery [16, 17]. Applying cooling water spray, the CO_2 laser is able to achieve clean cuts on bone with no significant thermal injury to the surrounding tissue [12–15]. Compared to conventional surgical burrs, lasers allow contactless removal of the bone tissue in the absence of any mechanical stress to the fragile structures, providing more safety to the patient. The tiny tissue volume ablated by each single pulse enables a precise control of the channel geometry, which makes it possible to approach the natural curvature of the critical structure (Figures 1(c) and 1(d)). Laser ablation also generates much less bone-debris, reducing the risk of inflammatory tissue reaction of the inner ear and consecutive loss of function. In other words, lasers provide an excellent solution to the shortcomings of the mechanical drilling-based systems stated above.

However, a key question of using a laser to create the cochleostomy remains unsolved: how can the position of the bone-endosteum-perilymph boundary be detected during the process, so that the laser-bone ablation can be guided without injuring the critical structure?

In the past years, efforts have been made to solve this issue. The most popular choice is to discriminate the tissue type at the bottom of the laser-ablated incision. As soon as a transition from hard tissue to soft tissue is detected, the ablation process will be terminated. The tissue type differentiation can be achieved either by monitoring the ablation induced process emissions such as the plasma [20, 21] and noises [22–24], as well as both of them [25, 26], or by analyzing the optical properties of the tissue [18, 27–31]. A significant drawback of these approaches is that they can detect the tissue transition only after the tissue boundary has been penetrated, so that an injury to the critical structure is almost unavoidable.

Recently, several research groups have been using optical coherence tomography (OCT) to control the laser ablation [19, 32, 33]. These approaches mainly focus on measuring the position of the target tissue surface in the OCT scans such that the current ablation depth can be determined online with high accuracy on the micrometer scale. The ablation

will be terminated as soon as the planned ablation depth is reached. However, these approaches will face the same problem as the robotic systems without haptic feedback [6–9] analyzed above, where the achievable accuracy is limited by the preoperative planning and intraoperative navigation.

Known as "ultrasonography with light," the most valuable feature of OCT is that it can provide cross-sectional images of the internal structures beneath the target tissue surface with a high resolution on the micrometer scale [34, 35]. Therefore, OCT is potentially able to detect the position of the subsurface critical structure before its exposure. Instead of only monitoring the ablation depth, the laser pulses can be guided according to the thickness of the residual bone layer above the critical structure. In this paper, we will propose a closed-loop control of laser cochleostomy under the monitoring of OCT and report on preliminary experiments of OCT guided laser cochleostomy.

2. Materials and Methods

2.1. System Setup. An in-house built swept source OCT system consisting of a 54 kHz FDML laser [36] with a 104 nm sweep range at a center wavelength of 1314 nm was used to acquire the OCT scans. Its Rayleigh range was 2.0 mm. The axial and lateral resolutions were measured to be 18 μm and 35 μm, respectively. The cochleostomy was performed with a short-pulsed CO_2 laser (wavelength 10.6 μm, spot diameter 200 μm, TEM_{00}, and Rayleigh range 2.4 mm) with pulse durations tunable from 20 μs to 100 μs, corresponding to energies ranging from 4.2 mJ to 28.5 mJ per pulse. The OCT system and CO_2 laser were equipped with separate scanning optics, which enabled simultaneous imaging and ablation of the target tissue surface. The angular resolution and repeatability of the scanning optics are <15 μrad (OCT, Thorlabs GVS002) and <20 μrad (CO_2 laser, ARGES Colibri 11), respectively, corresponding to a spatial accuracy of *circa* 2-3 μm within their working spaces.

A coaxial setup of both systems (Figure 2(a)) was constructed using a dichroic germanium mirror with high reflectivity coating for the wavelengths of the OCT, so that the working spaces of the OCT and CO_2 laser were overlapping. To create a three-dimensional mapping between both scanning optics, a calibration pattern was defined in the CO_2 laser coordinate system (Figure 2(b)) and ablated on the surface of a flat acrylic plate. The position of each point was detected in a subsequent 3D OCT scan (Figure 2(c)), resulting in corresponding point pairs in both systems. This procedure was repeated at predefined axial positions that are equidistant along the optical axis, using a new acrylic plate each time. A calibration point cloud covering the whole working space was then obtained (Figure 2(d)). The mapping from OCT to CO_2 laser $(x, y, z) = f(u, v, w)$ was determined by performing tricubic B-spline fitting to these points.

Given a point (x, y, z) in the CO_2 laser coordinate system and its corresponding point (u, v, w) in the OCT, the mapping error was defined as $|(x, y, z) - f(u, v, w)|$. We further defined an evaluation pattern consisting of the centers of all small squares (rotated for 45°) in the calibration pattern (Figure 2(b)). Using this pattern, the above ablation-detection procedure was repeated at the middle points of the equidistant axial positions that were used for the calibration. Thus, an evaluation point cloud containing points farthermost from the calibration points was obtained. The mean absolute mapping errors among the calibration points, among the evaluation points, and among all points together were 12.1 μm, 29.3 μm, and 19.6 μm, respectively.

Such a calibration procedure has to be done only once during system setup and a recalibration is not necessary as long as both scanning optics and the OCT reference arm length remain fixed.

2.2. Feasibility Study. As the first step, a feasibility study was conducted by acquiring OCT scans on diverse fresh porcine cochleae isolated from cadavers and comparing them to histological sections (Figure 3). It can be observed that the interface between the bony shell of the cochlea, endosteum, and the perilymph-filled scala is clearly visible in the OCT. These results evidence the possibility to detect the position of the critical structure in the OCT scans before the endosteal layer is reached.

By analyzing the OCT scans of a wedge-shaped bovine compact bone specimen, it could further be estimated that the imaging depth of OCT penetrating into compact bone tissue is about half a millimeter under laboratory condition. Compared to the ablation depth of a single CO_2 laser pulse ranging from 20 μm to 100 μm, the critical structure will be visible at least 4-5 ablation rounds before its exposure, so that the laser parameters such as pulse positions and pulse durations can be planned in advance to avoid injuring the fragile endosteum. Therefore, OCT is a very promising candidate for guiding the laser pulses during the laser cochleostomy.

2.3. OCT Guided Laser Cochleostomy. The control loop of the laser cochleostomy under the monitoring of OCT is designed as follows (Figure 4): the laser ablation and OCT scanning are performed alternately. After each round of ablation, a three-dimensional OCT volume scan of the cochleostomy is acquired. If the position of the bone-endosteum-perilymph boundary could be detected after proper image processing, the residual bone thickness above this critical structure can be calculated. Based on the obtained bone thickness distribution, the pulse positions and pulse durations for the next round of laser ablation are planned by a computer algorithm. After the compensation of potential relative displacement between the patient and the laser optics, the ablation parameters are transmitted to the corresponding control modules and the ablation pattern is executed. By repeating this procedure until the critical structure is reached, the desired endosteum preserving cochleostomy can be achieved.

2.4. Image Quality Enhancement. Obviously, the most crucial step in the control loop is the detection of the bone-endosteum-perilymph boundary. Unfortunately, lying beneath highly scattering bone tissue, the small signal coming from this critical structure is drowned out by multiple scattering. The speckle noise, which is inherent to OCT, further

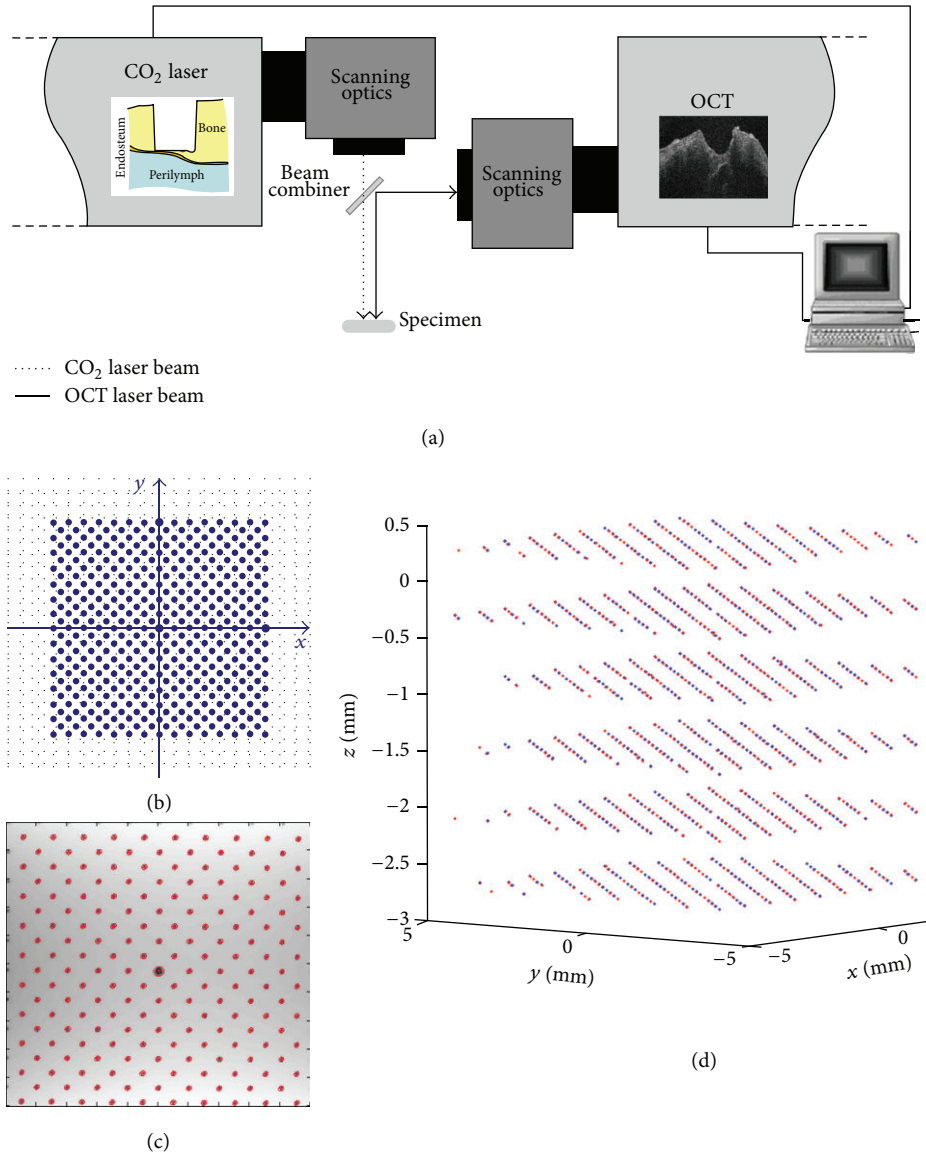

FIGURE 2: (a) Schematic diagram of the coaxial setup of the OCT system and the CO_2 laser with overlapping working spaces; (b) two-dimensional calibration pattern defined in the CO_2 laser coordinate system and (c) the corresponding points detected in the OCT coordinate system; (d) the corresponding point pairs filling the whole working space.

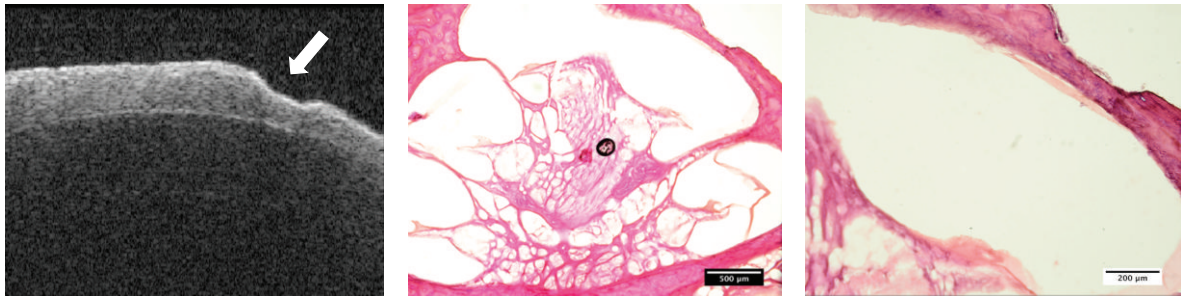

(a) (b) (c)

FIGURE 3: Feasibility study: (a) an OCT image of a fresh porcine cochlea with a laser-ablated crater on the surface (arrow). The interface between the bony shell of the cochlea, endosteum, and the perilymph-filled scala is clearly visible; ((b)-(c)) the corresponding histology under (b) 4x and (c) 10x magnification.

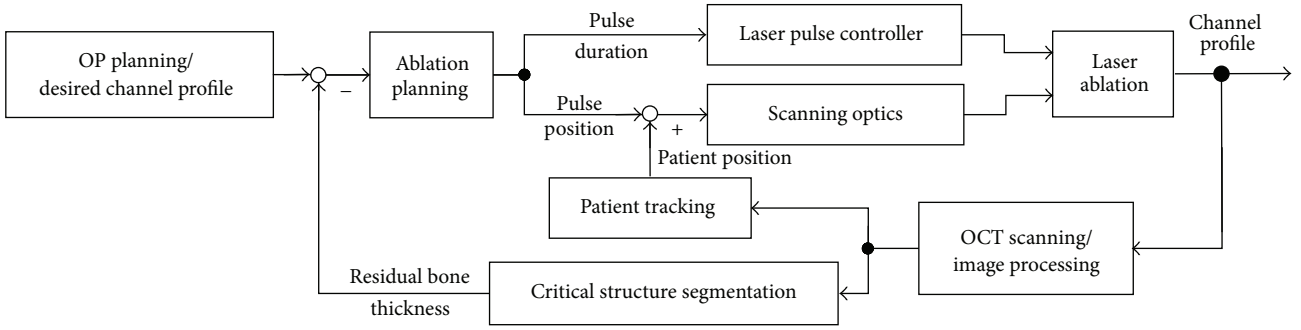

Figure 4: Control loop scheme of the OCT guided laser cochleostomy.

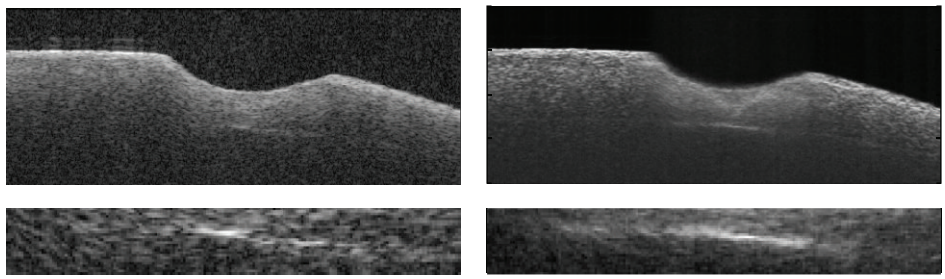

(a) (b)

Figure 5: Effect of image quality enhancement: (a) original OCT image of a cochleostomy on a fresh porcine cochlea (above) and the zoomed view of the bone-endosteum-perilymph boundary (bottom); (b) the enhanced image after applying history compounding and light attenuation compensation techniques.

degrades the image quality. Moreover, the full sensitivity of the OCT system cannot be used due to its limited dynamic range and the presence of specular reflexes. As a result, the critical structure appears to be rather weak in the OCT (Figure 5(a)) and its detection is difficult.

Therefore, image quality enhancement must be applied before proceeding. We developed a new speckle averaging technique called "History Compounding" [37] and further applied the light attenuation compensation method proposed by Girard et al. [38] to increase the contrast of the structures deep beneath the bone surface. The combination of these techniques significantly improved the image quality of the OCT scans and the bone-endosteum-perilymph boundary became much clearer in comparison to the original one (Figure 5(b)).

2.5. Segmentation and Ablation Planning. The segmentation of such a sharp structure shown in Figure 5(b) is straightforward using gradient-based edge detection and model-based edge linking in each single OCT frame (Figure 6(a)). A bicubic B-spline fitting is performed to all candidate edge points in the whole three-dimensional OCT volume, taking the full use of information from neighboring frames and resulting in a smooth 3D model of the critical structure (Figure 6(b)). The user is further allowed to define a "stop surface" (Figure 6(a)) parallel to the detected bone-endosteum-perilymph boundary and the distance between them can be chosen arbitrarily.

Owing to the significantly different refractive indices of bone tissue and air, the most superficial air-bone interface always has very high contrast in OCT images. It can therefore be detected using simple thresholding and reconstructed by three-dimensional morphological operation-based smoothing (Figure 6(a)). The residual bone thickness distribution above the "stop surface" can be derived easily. Pulse positions and pulse durations are planned accordingly. The basic strategy is to apply the next pulse to the position with the maximal residual bone thickness where no pulses have been planned yet. The pulse duration is chosen quasi proportional to the thickness of the local bone layer. The ablation pattern for the next round of laser ablation (Figure 6(c)) is determined by repeating this procedure until no more pulses can be appended.

2.6. Patient Tracking. Physical contacts to the patient, to the operation table, or to the laser optics due to incaution can cause relative displacements between the target area and the laser working space. As the diameter of the CO_2 laser pulses is approximately 200 μm, even tiny displacements less than 100 μm can make the best ablation planning pointless. In the worst case, pulses shot to wrong positions can damage the endosteum instantly if parts of it are already exposed (Figure 7(a)).

Such displacements must be detected and taken into account before passing the planned pulse positions to the scanning optics of the CO_2 laser. The gold standard for such a case is attaching special trackers to the patient as well as the laser optics and monitoring their positions using either optical or electromagnetic tracking systems, as illustrated in

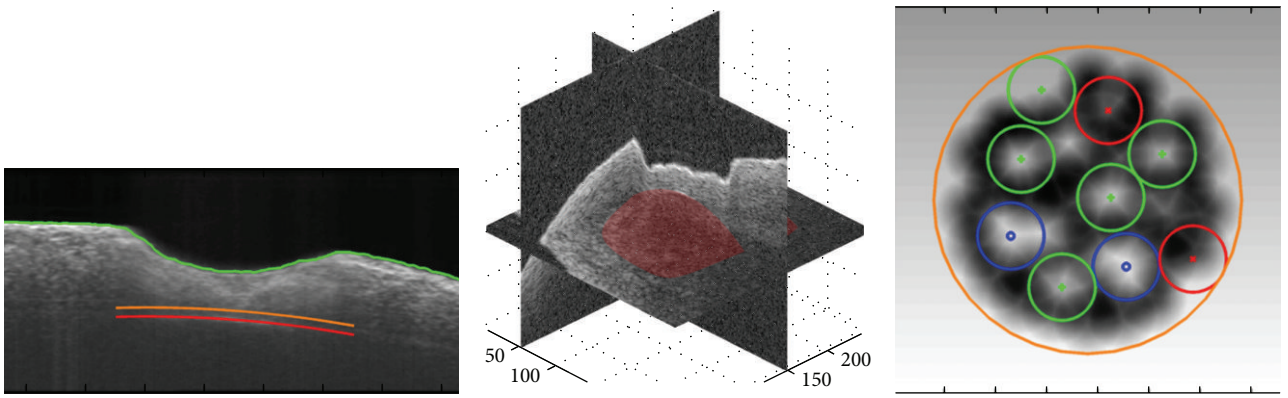

Figure 6: (a) The position of the bone surface (green), segmented bone-endosteum-perilymph boundary (red), and the user defined "stop surface" of the laser ablation (orange); (b) reconstructed 3D model of the critical structure; (c) ablation pattern planned according to the residual bone thickness map, where the blue, green, and red pulses are corresponding to long, middle, and short pulses; the gray scale in the background denotes the local residual bone thickness (lighter color for larger thickness).

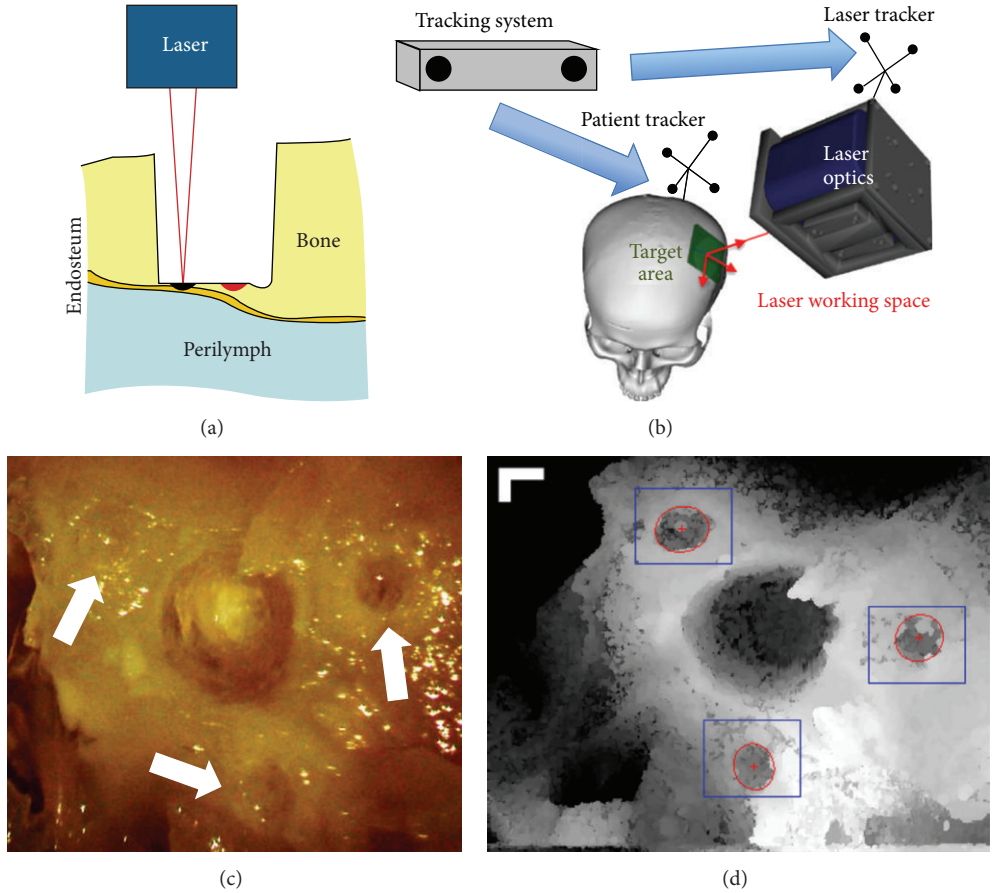

Figure 7: (a) Erroneously applied laser pulse (black) due to tiny relative displacement between target area and laser optics and the originally planned pulse position (red); (b) illustration of a typical setup using conventional tracking system; ((c)-(d)) OCT as highly accurate optical tracking system: (c) artificial landmarks surrounding the cochleostomy and (d) the corresponding top view in three-dimensional OCT scan, bar = 250 μm [19].

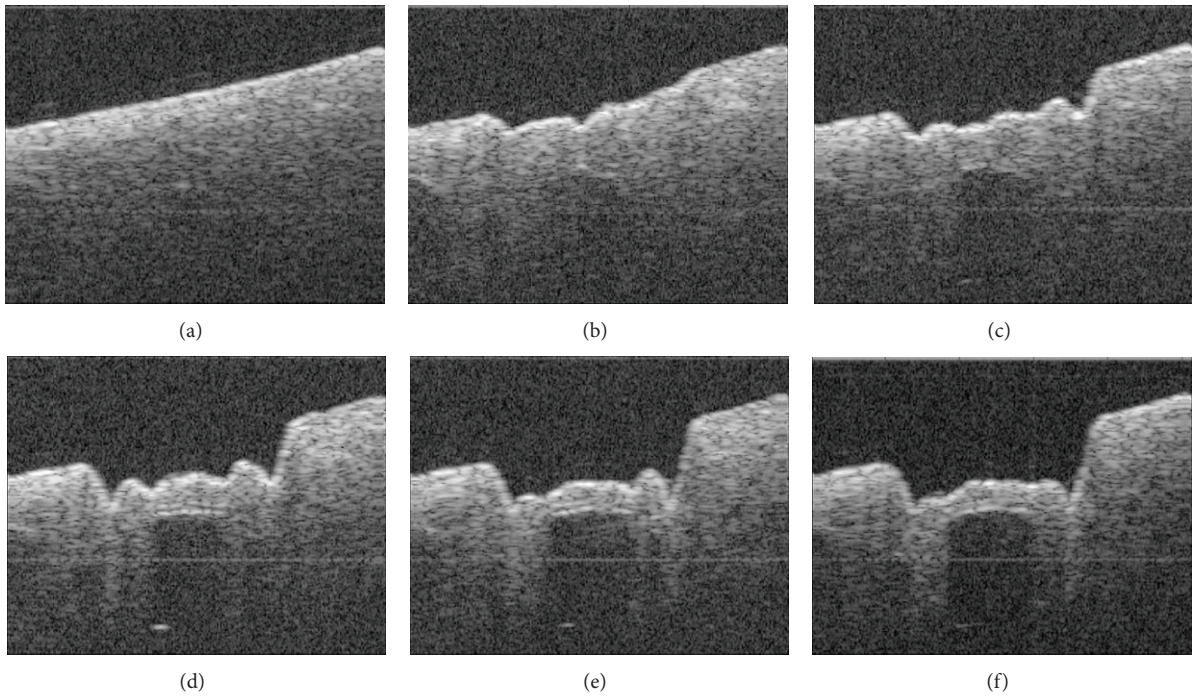

Figure 8: OCT frames passing through the center of the ablated cochleostomy showing the changing channel shape during the process of OCT guided laser cochleostomy on a fresh porcine cochlea.

Figure 7(b). Similar setups are widely used by many research groups to perform computer-assisted cochleostomy [6–10, 32]. However, most commercially available tracking systems can only provide an accuracy of several hundred micrometers for each single tracker, while what we need is an accurate measurement of the relative displacement between the laser working space and the target area. Due to the indirect tracking mechanism of the conventional setups, registration between the target area and the patient tracker as well as between the laser optics and the laser tracker is mandatory, resulting in a complicated transformation chain from the target area via the tracking system to the laser working space. The registration and tracking errors of each component along this chain are accumulated. The large distances between the involved components further magnify the rotational tracking errors of the trackers, resulting in additional inaccuracy. As a result, conventional tracking system-based setups are almost impossible to achieve a global tracking accuracy less than 100 μm regarding the relative displacement between the target area and the laser working space, which is insufficient in our case.

Therefore, we proposed a mechanism of using OCT itself as a more accurate optical tracking system [39] by locating small laser-ablated landmarks surrounding the cochleostomy (Figures 7(c) and 7(d)). The position of the target area can thus be determined directly in the OCT working space, bypassing the complicated transformation chain stated above. Because the cochleostomy is located near the centroid of the landmark layout, the rotational tracking error will not be magnified either. For the evaluation of the tracking accuracy, a specimen was moved along a predefined test grid within the laser working space using a hexapod (accuracy: $\pm 2\,\mu$m), whose position was tracked in the OCT. The global tracking accuracy of the target area with respect to the laser working space was measured by comparing the tracking results with the actual displacements performed by the hexapod, which was only about 25 μm (mean absolute error: $22.8 \pm 14.9\,\mu$m, root mean square: $27.2\,\mu$m).

3. Results and Discussion

3.1. Results. By now, the control loop conceived in Figure 4 has been successfully realized. The complete workflow was experimentally evaluated by conducting the worldwide first OCT guided laser cochleostomy on porcine cochleae isolated from cadavers.

Three cochleostomies were performed. No preoperative planning was made and the cochleae were manually positioned and oriented in the laser working space. The position of the bone-endosteum-perilymph boundary was unknown while starting the ablation process and the achieved accuracy was completely dependent on the proposed workflow. Before each round of ablation, water spray was manually applied to the target area, so that the ablation induced thermal injury could be effectively reduced and no significant carbonization was observed in the resulting cochleostomy. Meanwhile, the water spray also prevented tissue dehydration that can severely disturb the OCT imaging of the critical structure.

Figure 8 shows the changing channel shape during one of the cochleostomies. At the beginning (Figures 8(a) and 8(b)), the bone-endosteum-perilymph boundary was still barely visible due to the relatively thick overlying bone layer. During

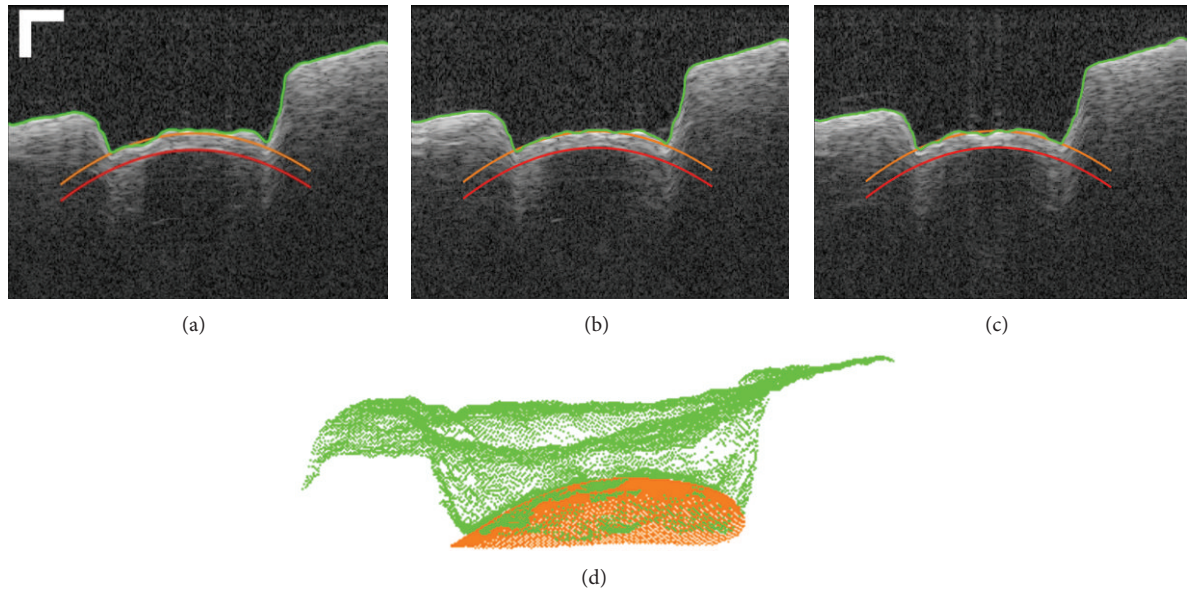

(a) (b) (c)

(d)

Figure 9: ((a)–(c)) Example OCT B-scans acquired near the center of a resulting cochleostomy, showing the final shape of the ablated cochleostomy, bar = 250 μm. (d) Comparison between the resulting channel bottom (green) and the three-dimensional "stop surface" (orange).

this phase, the ablation was planned according to a virtual critical structure located at infinity and parallel to the original bone surface, resulting in a channel bottom approximately parallel to it (Figure 8(b)). With the increasing channel depth, the critical structure became gradually visible (Figure 8(c)). After applying the image quality enhancement and critical structure segmentation, the ablation was planned according to the bone thickness distribution measured online. As a result, the channel bottom began to incline clockwise and its shape converged to that of the endosteal layer step by step as expected (Figures 8(d)–8(f)).

The target thickness of the residual layer was set to 100 μm. The control loop quitted automatically when the user defined "stop surface" was reached all over the channel bottom. Preliminary investigation in postoperative OCT scans indicates that the shape of the resulting cochleostomy macroscopically matches the curvature of the cochlear endosteum (Figures 9(a)–9(c)).

Instead of only evaluating the ablation accuracy at a single point, a more strict evaluation comparing the whole channel bottom with the "stop surface" was performed (Figure 9(d)). According to the measurement in the postoperative OCT scan, the mean absolute errors between the resulting channel bottom and the three-dimensional "stop surface" were 16.43 ± 14.90 μm, 19.62 ± 17.67 μm, and 21.01 ± 21.39 μm for the three cochleostomies, respectively. The corresponding maximal errors where the channel bottom penetrated the "stop surface" were 45.54 μm, 38.36 μm, and 46.73 μm. An evaluation of the accuracy based on histological studies is still to be made.

3.2. Discussion. The preliminary result of the experimental evaluation reveals that, under the monitoring of the OCT, the laser ablation can be directly guided according to the residual bone thickness above the bone-endosteum-perilymph boundary measured online. In contrast to the control conceptions using other sensor technologies [18, 20–31], a foresighted detection of the critical structure before its exposure has been realized. Compared to the workgroups who have also been using OCT to guide the laser ablation [19, 32, 33], our approach does not only rely on measuring the bone surface but also take the full advantage of the tomographic information provided by the high-resolution imaging system.

A unique feature of our system is that the laser control module does not only control the laser on and laser off, but also optimize pulse positions and pulse durations according to the residual bone thickness distribution. To our knowledge, a uniform convergence of the resulting channel bottom to the shape of the critical structure has been demonstrated for the first time.

Reviewing the control loop, it can also be noticed that the workflow is independent of the type of the integrated ablating laser. The CO_2 laser in the setup (Figure 2(a)) can be replaced by another kind of surgical lasers such as the commonly used Er:YAG laser.

On the other hand, our system is still an experimental setup and we have a long way to go before bringing it into real operation room. It can be observed that the resulting cochleostomy is not perfect and there exist in all three cochleostomies some positions where the channel bottom has penetrated the "stop surface" (Figure 9), indicating that a 100% protection of the endosteum has not been guaranteed yet. Meanwhile, the critical structure segmentation is currently semiautomatic. Due to the limited imaging depth of OCT, the critical structure is always invisible at the beginning (Figure 8(a)) or only a few pixels can be seen in the middle part (Figure 8(b)). The segmentation is impossible in the

first case and often returns a wrong result in the later one. A manual correctness check of segmentation result is still mandatory. Further improvement of the ablation strategy and a more intelligent segmentation algorithm are therefore necessary.

Time consumption is another critical issue in the current system implementation. The OCT imaging, processing, and the CO_2 laser control are done by three independent software packages and a manual data transfer between them is required. This has led to unnecessary overhead and allows human error to happen. Depending on the initial conditions including bone thickness and shape of the underlying endosteal layer, the OCT guided laser cochleostomy may cost up to more than one hour. Due to the manual data transfer, a real time tracking of the patient movements using the proposed tracking mechanism is also impossible in the current state. We are now working on speeding up the process by unifying the software packages and implementing GPU-based algorithms.

Further extensive systematic evaluations regarding the reliability, robustness, and repeatability of the system under different conditions are also essential.

4. Conclusions

In this work, we successfully solved a key problem hindering the clinical application of laser cochleostomy. Foresighted detection of the bone-endosteum-perilymph boundary in three-dimensional OCT volumes has been realized, enabling a residual bone thickness-based control mechanism of the laser ablation. An important step towards a standardized cochleostomy with reproducible ablation accuracy has been achieved. Future development of the OCT guided laser ablation system will provide the surgeon with a new intelligent microsurgical tool to perform the highly demanding surgical procedure in an easier but safer and more reliable way.

Conflict of Interests

The authors declare that there is no conflict of interests regarding the publication of this paper.

Acknowledgments

This research was supported by the German Research Foundation (DFG) project OCT-LABS. The authors acknowledge the publication support by Deutsche Forschungsgemeinschaft and Open Access Publishing Fund of Karlsruhe Institute of Technology.

References

[1] T. Klenzner, "Aspects of inner ear trauma in CI treatment," *HNO*, vol. 59, no. 6, pp. 568–569, 2011.

[2] E. E. L. Pararas, D. A. Borkholder, and J. T. Borenstein, "Microsystems technologies for drug delivery to the inner ear," *Advanced Drug Delivery Reviews*, vol. 64, no. 14, pp. 1650–1660, 2012.

[3] T. Lenarz, C. James, D. Cuda et al., "European multi-centre study of the Nucleus Hybrid L24 cochlear implant," *International Journal of Audiology*, vol. 52, no. 12, pp. 838–848, 2013.

[4] P. S. Roland and C. G. Wright, "Surgical aspects of cochlear implantation: mechanisms of insertional trauma," *Advances in Oto-Rhino-Laryngology*, vol. 64, pp. 11–30, 2006.

[5] P. V. Incerti, T. Y. C. Ching, and R. Cowan, "A systematic review of electric-acoustic stimulation: device fitting ranges, outcomes, and clinical fitting practices," *Trends in Amplification*, vol. 17, no. 1, pp. 3–26, 2013.

[6] T. Klenzner, C. Ngan, F. Knapp et al., "New strategies for high precision cochleostomy using a hexapod robot system," *Wiener Medizinische Wochenschrift*, vol. 156, supplement 119, p. 27, 2006.

[7] C. C. Ngan, *Atraumatic and Function-Preserving High Precision Surgery of the Human Temporal Bone*, Der Andere, 2006.

[8] O. Majdani, T. S. Rau, S. Baron et al., "A robot-guided minimally invasive approach for cochlear implant surgery: preliminary results of a temporal bone study," *International Journal of Computer Assisted Radiology and Surgery*, vol. 4, no. 5, pp. 475–486, 2009.

[9] H. Eilers, S. Baron, T. Ortmaier et al., "Navigated, robot assisted drilling of a minimally invasive cochlear access," in *Proceedings of the IEEE International Conference on Mechatronics (ICM '09)*, pp. 1–6, IEEE, April 2009.

[10] X. Du, M. Z. Assadi, F. Jowitt et al., "Robustness analysis of a smart surgical drill for cochleostomy," *International Journal of Medical Robotics and Computer Assisted Surgery*, vol. 9, no. 1, pp. 119–126, 2013.

[11] P. Brett, X. Du, M. Zoka-Assadi, C. Coulson, A. Reid, and D. Proops, "Feasibility study of a hand guided robotic drill for cochleostomy," *BioMed Research International*, vol. 2014, Article ID 656325, 7 pages, 2014.

[12] M. Frentzen, W. Götz, M. Ivanenko, S. Afilal, M. Werner, and P. Hering, "Osteotomy with 80-μs CO_2 laser pulses—histological results," *Lasers in Medical Science*, vol. 18, no. 2, pp. 119–124, 2003.

[13] M. Ivanenko, R. Sader, S. Afilal et al., "In vivo animal trials with a scanning CO_2 laser osteotome," *Lasers in Surgery and Medicine*, vol. 37, no. 2, pp. 144–148, 2005.

[14] M. Werner, M. Ivanenko, D. Harbecke, M. Klasing, H. Steigerwald, and P. Hering, "Laser osteotomy with pulsed CO2 lasers," *Advances in Medical Engineering*, pp. 453–457, 2007.

[15] J. Burgner, M. Müller, J. Raczkowsky, and H. Wörn, "Ex vivo accuracy evaluation for robot assisted laser bone ablation," *International Journal of Medical Robotics and Computer Assisted Surgery*, vol. 6, no. 4, pp. 489–500, 2010.

[16] A. J. Fishman, L. E. Moreno, A. Rivera, and C.-P. Richter, "CO_2 laser fiber soft cochleostomy: development of a technique using human temporal bones and a guinea pig model," *Lasers in Surgery and Medicine*, vol. 42, no. 3, pp. 245–256, 2010.

[17] M. R. Marchese, A. Scorpecci, F. Cianfrone, and G. Paludetti, "'One-shot' CO_2 versus Er:YAG laser stapedotomy: is the outcome the same?" *European Archives of Oto-Rhino-Laryngology*, vol. 268, no. 3, pp. 351–356, 2011.

[18] L. A. Kahrs, *Bildverarbeitungsunterstützte Laserknochenablation am humanen Felsenbein [Ph.D. thesis]*, KIT Scientific Publishing, Karlsruhe, Germany, 2010.

[19] A. Fuchs, M. Schultz, A. Krüger, D. Kundrat, J. Diaz Diaz, and T. Ortmaier, "Online measurement and evaluation of the Er:YAG laser ablation process using an integrated oct system," *Biomedizinische Technik*, vol. 57, no. 1, pp. 434–437, 2012.

[20] R. Kanawade, F. Mehari, C. Knipfer et al., "Pilot study of laser induced breakdown spectroscopy for tissue differentiation by monitoring the plume created during laser surgery—an approach on a feedback Laser control mechanism," *Spectrochimica Acta B: Atomic Spectroscopy*, vol. 87, pp. 175–181, 2013.

[21] R. Kanawade, F. Mahari, F. Klämpfl et al., "Qualitative tissue differentiation by analysing the intensity ratios of atomic emission lines using laser induced breakdown spectroscopy (LIBS): prospects for a feedback mechanism for surgical laser systems," *Journal of Biophotonics*, 2013.

[22] A. Rätzer-Scheibe, M. Klasing, M. Werner, M. Ivanenko, and P. Hering, "Acoustic monitoring of bone ablation using pulsed co2-lasers," *Aktuelle Methoden der Laser-und Medizinphysik*, pp. 281–286, 2004.

[23] H. Steigerwald, M. Werner, M. Klasing et al., "Spectral analysis of the acoustic signal during ablation of biological tissue with pulsed CO_2-lasers," in *Advances in Medical Engineering*, vol. 114 of *Springer Proceedings in Physics*, pp. 425–430, Springer, Berlin, Germany, 2007.

[24] M. Leinung, D. Hagner, T. Lenarz, and B. Schwab, "Akustische Analyse zur Grenzflächendetektion bei der Er:YAG -Cochleostomie," Tagungsband der 6. Jahrestagung der Deutschen Gesellschaft für Computer- und Roboterassistierte Chirurgie e.V, 2007.

[25] S. Rupprecht, K. Tangermann, P. Kessler, F. W. Neukam, and J. Wiltfang, "Er:YAG laser osteotomy directed by sensor controlled systems," *Journal of Cranio-Maxillofacial Surgery*, vol. 31, no. 6, pp. 337–342, 2003.

[26] S. Rupprecht, K. Tangermann-Gerk, J. Wiltfang, F. W. Neukam, and A. Schlegel, "Sensor-based laser ablation for tissue specific cutting: an experimental study," *Lasers in Medical Science*, vol. 19, no. 2, pp. 81–88, 2004.

[27] L. A. Kahrs, J. Raczkowsky, M. Werner et al., "Visual servoing of a laser ablation based cochleostomy," in *Medical Imaging*, Proceedings of SPIE, pp. 69182C–69182C, International Society for Optics and Photonics, 2008.

[28] L. A. Kahrs, M. Werner, F. B. Knapp et al., "Video camera based navigation of a laser beam for micro surgery bone ablation at the skull base-setup and initial experiments," in *Advances in Medical Engineering*, pp. 219–223, Springer, New York, NY, USA, 2007.

[29] A. Zam, F. Stelzle, E. Nkenke et al., "Tissue-specific laser surgery: hard tissue differentiation by diffuse reflectance spectroscopy ex vivo," in *Frontiers in Optics*, Optical Society of America, 2009.

[30] F. Stelzle, W. Adler, A. Zam et al., "In vivo optical tissue differentiation by diffuse reflectance spectroscopy: preliminary results for tissue-specific laser surgery," *Surgical Innovation*, vol. 19, no. 4, pp. 385–393, 2012.

[31] T. Klenzner, F. B. Knapp, J. Schipper et al., "High precision cochleostomy by use of a pulsed CO_2 laser—an experimental approach," *Cochlear Implants International*, vol. 10, supplement 1, pp. 58–62, 2009.

[32] J. Diaz Diaz, D. Kundrat, K.-F. Goh, O. Majdani, and T. Ortmaier, "Towards intra-operative oct guidance for automatic head surgery: first experimental results," in *Medical Image Computing and Computer-Assisted Intervention-MICCAI*, vol. 8151 of *Lecture Notes in Computer Science*, pp. 347–354, Springer, New York, NY, USA, 2013.

[33] B. Y. Leung, P. J. Webster, J. M. Fraser, and V. X. Yang, "Real-time guidance of thermal and ultrashort pulsed laser ablation in hard tissue using inline coherent imaging," *Lasers in Surgery and Medicine*, vol. 44, no. 3, pp. 249–256, 2012.

[34] J. Fujimoto, "Optical coherence tomography," in *Proceedings of the Conference on Lasers and Electro-Optics*, Optical Society of America, 2006.

[35] W. Drexler and J. G. Fujimoto, *Optical Coherence Tomography: Technology and Applications*, Springer, New York, NY, USA, 2008.

[36] R. Huber, M. Wojtkowski, and J. G. Fujimoto, "Fourier Domain Mode Locking (FDML): a new laser operating regime and applications for optical coherence tomography," *Optics Express*, vol. 14, no. 8, pp. 3225–3237, 2006.

[37] Y. Zhang, T. Pfeiffer, W. Wieser et al., "History compounding: a novel speckle reduction technique for OCT guided cochleostomy," in *Optical Coherence Tomography and Coherence Domain Optical Methods in Biomedicine XVII*, vol. 8571 of *Proceedings of SPIE*, 2013.

[38] M. J. A. Girard, N. G. Strouthidis, C. R. Ethier, and J. M. Mari, "Shadow removal and contrast enhancement in optical coherence tomography images of the human optic nerve head," *Investigative Ophthalmology & Visual Science*, vol. 52, no. 10, pp. 7738–7748, 2011.

[39] Y. Zhang, T. Pfeiffer, J. Ding et al., Optical coherence tomography as a tracking device for OCT guided laser cochleostomy : algorithm and first results, Tagungsband der 11. Jahrestagung der Deutschen Gesellschaft für Computer- und Roboterassistierte Chirurgie e.V., 2012.

Hindawi Publishing Corporation
BioMed Research International
Volume 2014, Article ID 891742, 10 pages
http://dx.doi.org/10.1155/2014/891742

Research Article

Middle-Ear Microsurgery Simulation to Improve New Robotic Procedures

Guillaume Kazmitcheff,[1,2,3] Yann Nguyen,[1,2,4] Mathieu Miroir,[1,2] Fabien Péan,[3] Evelyne Ferrary,[1,2,4] Stéphane Cotin,[3] Olivier Sterkers,[1,2,4] and Christian Duriez[3]

[1] *INSERM, "Minimally Invasive Robot-Based Hearing Rehabilitation", UMR_S 1159, 75005 Paris, France*
[2] *Sorbonne University, UPMC Univ Paris 06, UMR_S 1159, 75005 Paris, France*
[3] *Shacra, INRIA, University Lille 1, 59650 Villeneuve d'Ascq, France*
[4] *AP-HP, Otolaryngology Department, Unit of Otology, Auditory Implants and Skull Base Surgery, Hospital Pitié Salpêtrière, 75013 Paris, France*

Correspondence should be addressed to Guillaume Kazmitcheff; guillaume.kazmitcheff@inserm.fr

Received 14 February 2014; Accepted 2 June 2014; Published 23 July 2014

Academic Editor: Marco Caversaccio

Otological microsurgery is delicate and requires high dexterity in bad ergonomic conditions. To assist surgeons in these indications, a teleoperated system, called RobOtol, is developed. This robot enhances gesture accuracy and handiness and allows exploration of new procedures for middle ear surgery. To plan new procedures that exploit the capacities given by the robot, a surgical simulator is developed. The simulation reproduces with high fidelity the behavior of the anatomical structures and can also be used as a training tool for an easier control of the robot for surgeons. In the paper, we introduce the middle ear surgical simulation and then we perform virtually two challenging procedures with the robot. We show how interactive simulation can assist in analyzing the benefits of robotics in the case of complex manipulations or ergonomics studies and allow the development of innovative surgical procedures. New robot-based microsurgical procedures are investigated. The improvement offered by RobOtol is also evaluated and discussed.

1. Introduction

Surgical robot-based systems raise a great expectation for medical care. These systems are designed to improve quality and safety of surgical interventions and to lead to clinical benefits for the patient such as a reduction of the hospitalization duration [1]. Moreover robot-based and computer assisted surgeries enhance conventional gestures, with improved ergonomics and accuracy. In some case, as discussed in this paper, they even allow innovative procedures. However, when the use of robot changes the clinical practice, new procedures need to be designed, evaluated, and taught before clinical application. The aim of this work is to show that it is possible to use the simulation to design, train, and develop new robotic procedures.

In this work, we have focused on middle ear microsurgery. Microsurgery is an excellent scope for robotic systems [2–4] and several robots have been designed for middle ear microsurgery [5, 6]. This work is based on a teleoperated system called RobOtol [7] (Figure 1(a)). The RobOtol system is developed in order to avoid reduction of the surgical field exposure by the surgeon's hands, to stop physiological tremor [8], and to raise gesture accuracy.

The middle ear ensures the mechanical transmission of the sound wave from the tympanic membrane to the stapes footplate through the ossicular chain which conducts the sound wave to the inner ear. It is located between the outer and the inner ear and is composed of the tympanic membrane, the ossicles (malleus, incus, and stapes), the middle ear cleft, and mastoid cells (Figure 2).

When a patient suffers from otosclerosis, the stapes footplate is progressively fixed to the inner ear, which leads to conductive hearing loss. The treatment such as ossiculoplasty consists in the replacement of one or several ossicles by

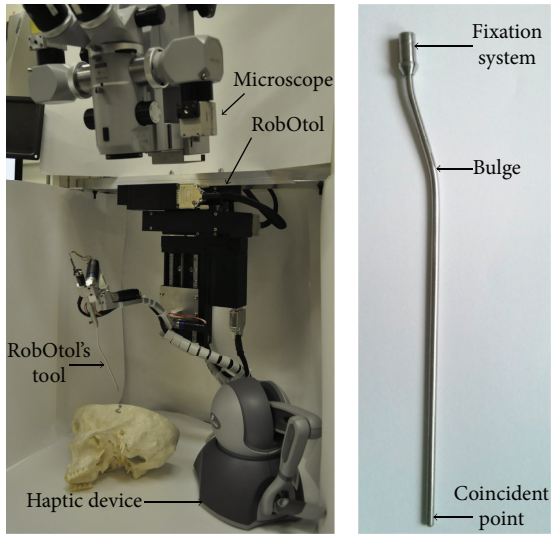

(a) RobOtol system and its environment (b) Robot's tool

FIGURE 1: RobOtol, a teleoperated system for middle ear microsurgery. (a) The surgeon uses a microscope and commands the robot with the haptic device, a Phantom Omni (Sensable, Wilmington, MA). (b) To avoid visual obstruction by the robot, a bulge is designed on the tool.

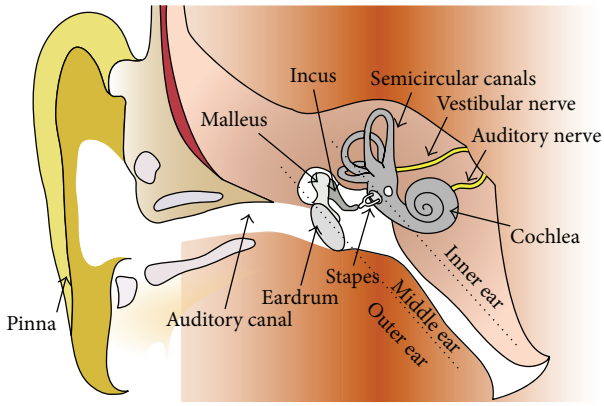

FIGURE 2: Human ear in surgical condition. Surgeons use a speculum to enlarge cartilaginous part of the external ear canal and may use up to 2 tools.

prosthesis during a microsurgery. When performing the conventional surgery through the auditory canal, surgeons have to manipulate bones of less than 4 mm high localized inside a maximized 16×16 mm cavity size at 34 mm depth. Yet, several structures including the ossicles and the facial nerve are very sensitive to injury. To perform a nontraumatic intervention, submillimetric motion inside a narrow workspace is required. Consequently, conventional gesture remains complicated and stressful for surgeons.

The use of the RobOtol system should reduce the risks of the surgery and increase physicians' confidence. The benefits of the robot were evaluated by 4 surgeons (seniors and juniors) in [9, 10]. The robot is currently being evaluated to get the approval to carry out the first clinical trials. In this context, we propose developing a new tool, based on simulation, which has two objectives: the first is to provide a simulator to adapt the robot-based procedure before a real clinical use. Consequently, the procedure can be rehearsed to fully benefit from the use of the robot and the final design of the tools of the robot can be adjusted. The second is to develop a training tool for physicians to get familiar with RobOtol handling. Since new surgical procedures and gestures are involved, it is important for surgeons to master the robot arm. Thereby virtual simulations of those complex systems are developed for practice essentially. Nevertheless, real-time simulation is mandatory to interact realistically with a system and to obtain direct outcomes from the simulation.

The use of surgical simulators is often targeted towards training of beginners. Using virtual reality technologies, the environment of the procedure is numerically reproduced. The trainee can interact with the virtual anatomy and even get force-feedback using haptic technologies. For instance, the Visible Ear [11] and the Voxel-Man TempoSurg (Voxel-Man Group, Hamburg, Germany) are currently available to simulate only the mastoidectomy surgery. This procedure consists in drilling of temporal bone and does not involve interaction with the ossicular chain. Several finite element models of the human middle ear are reported in the literature. Their goals are to analyze and reproduce the behavior of the ossicular chain with different configuration, such as intact or pathological cases [12, 13]. Those studies are not real-time simulation and thus are not suitable for training.

The main contribution of this paper is to use the surgical interactive simulation to improve the robot-based procedures: we propose using this simulator to adapt the surgical procedure and to improve the design of the robot and its tools. Moreover, the simulation is used as a training tool before clinical translation. Thus, training is not only for beginners but also for the expert surgeons that will perform the first clinical trials. The key idea is that they need to get accustomed to the robot commands, before the first use in clinic. To do

so, the simulation needs a precise modeling of the middle ear structure behavior. It is based on a finite element model (FEM). The mechanical interactions with instruments of the robots (and especially the contact response) are treated using constraint-based approaches. Moreover, the simulation has been optimized in order to reach real-time computations during the simulation. The drilling of the stapes footplate and the placing of a snap-in ossicular prosthesis on the ossicles constitute two challenging surgical procedures of the middle ear to perform in reality or to simulate.

We describe in this paper the implementation of the surgical simulation to model these two procedures with the robot. We show that the simulation is able to reproduce faithfully both of them and can improve and evaluate the robot-based procedures.

2. Material and Methods

2.1. RobOtol Description. RobOtol is a teleoperated system with 6 degrees of freedom, which is controlled by a Phantom Omni device (Sensable, Wilmington, MA) as a master arm (Figure 1(a)). Robot actuation is performed by a XYZ cross table and 3 rotary actuators with a coincident intersection point localized at the tip of the robot's tool (Figure 1(b)). An operative microscope with a focal distance of 300 mm is placed above the robot with its axis of view collinear to the Z linear stage and to the external ear meatus.

The design and the kinematics of the robot were optimized in order to reach all of the area of the middle ear, to maximize the operating field of view and the distance between the robot's body and the patient (for safety reasons) [7, 9]. The haptic device is only used as position input system since no force sensor is present on the robot.

A dead man footswitch is used to enable the actuators and to confirm the command. The command of the robot is described in [10] and is based on the equivalence relation of the master arm stylus and the robot's tool. The position-position command was used for all the experiments in this study. Thus, the robot moves to follow the master arm stylus position and stops when it reaches the target or when the surgeon releases the dead man footswitch. A homothetic parameter set at 7 for the translation and 1 for the rotation was implemented between the master and the slave arm for ergonomic reason and to gain in accuracy. The robot is able to perform delicate tasks with high dexterity in a narrow workspace.

2.2. Interactive Simulation Description. For the simulation, a FEM of the middle ear was developed and was computed at interactive rates (Figure 3). The mechanical behavior under physiological condition or under surgical stress assumptions was successfully confronted to human temporal bones observations [14]. To evaluate the level of realism of the model, we compared the results with two different measures. The first one was the evaluation of the transfer function of the ossicular chain, in the presence of an acoustic pressure wave, like in [12, 13, 15]. This test is similar to a clinical audiometry, which is used to evaluate the hearing thresholds or postoperative

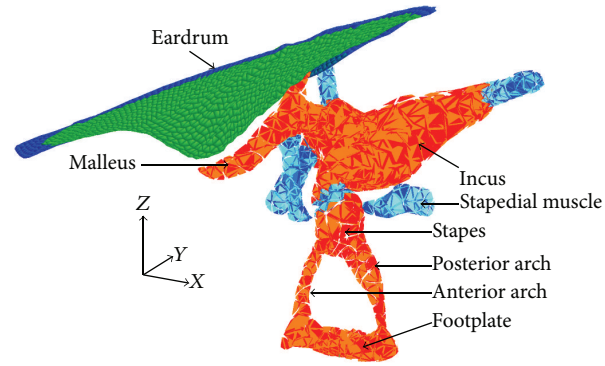

Figure 3: Finite element model of the middle ear structures. The tympanic membrane is composed of the pars flaccida, the pars tensa (green), and the tympanic annulus (blue). It is represented by triangles. Bones (red), ligaments, and tendons (blue) of the ossicular chain are modeled as tetrahedrons elements. Annular ligament is represented as springs and is attached to the footplate.

surgical outcomes. As the results of the transfer function of our FEM were in good accordance with the data measured on human temporal bones, it validated the dynamic behavior of the model at high frequencies. The second test consisted in the application of a high static pressure on the tympanic membrane in nominal and pathological cases, like in [16, 17]. This comparison with experimental data validated the deformation model in presence of large displacements as in a surgical situation. The analysis of the transfer function and the high static pressure applied to the tympanic membrane in nominal and in pathological cases was conducted to evaluate the mechanical realism of our approach. Additionally, we showed that the cochlea has a negligible effect on the mechanical behavior for frequencies below 250 Hz even when a large ossicular displacement is applied, such as situations encountered in surgical manipulation. Thereby, for surgical simulation, the cochlea could be removed, in order to reduce computation time without compromising the realistic behavior of the ossicular chain. A semiautomated algorithm allows the deformation of our model according to the anatomical dimension of the patient based on clinical imaging (cone beam computed tomography scan) [18].

The FEM was based on a geometric model obtained from a micromagnetic resonance imaging and developed for anatomical teaching [19]. The FEM was implemented in the simulation open framework architecture (SOFA, http://www.sofa-framework.org), an interactive simulation software dedicated to medical simulation [20]. A Phantom Omni device (Sensable, Wilmington, MA) with 6 degrees of freedom for positioning was used to interact with the simulation.

The ossicular chain was modeled by tetrahedral elements and the tympanic membrane by triangular (CST) elements. These constituted our mechanical atlas. Young's modulus and density parameters of all the components were set according to published data on human ear or by cross-calibration process and were reported in our previous publication [14]. The Rayleigh damping parameters were assumed to be $\alpha = 0\,s^{-1}$ and $\beta = 1.0 \times 10^{-4}$ s and the Poisson's ratio was set at 0.3

for all middle ear components. The contact response between the instruments of the robot, the ossicular chain, and the prosthesis were computed using unilateral constraints and solved using a dedicated solver that could handle snap-in tasks [21]. In order to simplify the simulation, when grasping, the prosthesis was mechanically attached to the grasper of the robot with a generalized spring.

Computation efficiency is the key of a surgical simulator, as it needs to be interactive. Nevertheless, collision detection, constraints resolution, and mechanical deformation increase time computation. However, we did not choose to decrease the realism of the simulation. The goal of this project was to build a surgical simulator for teaching and rehearsal and to enhance our robotic device. As a consequence, our approach needed to be as realistic as possible. To achieve this goal, the validated FEM was used in combination with an implicit integration scheme and an asynchronous preconditioning technique, as presented in [22]. The preconditioner did not only improve the convergence of the conjugate gradient used to solve the FEM system, but also provided a way to speed up the computation of the contact constraints. All our simulations were performed on a conventional workstation, with a backward Euler scheme and a time step of 0.04 s. A 3D viewer HMZ-T2 (Sony, San Diego, CA) was used for 3D rendering of the virtual scene.

2.3. Surgical Procedures. One of the most challenging surgical procedures in the middle ear surgery is the deposit of the ossicular prosthesis as the surgeons are in direct contact with the ossicles. Indeed, an involuntary motion may results in severe damages to the structures and could yield irreversible total deafness. The simulated surgical step consisted in performing a stapedotomy followed by the placement of a prosthesis piston through the stapes footplate, called stapedioplasty. As the goal was to provide a rehearsal surgical simulation and a platform for the development and the evaluation of new tools and procedures, it was necessary to simulate realistically these critical steps.

2.3.1. Stapedotomy. In conventional surgery, a stapedotomy consists in the perforation of the stapes footplate using either a laser or a surgical burr. The laser is a safe technic which does not need to be in contact with the ossicular chain. However this technic can raise the temperature of the footplate, which may damage the inner ear and postoperative hearing results. The drill does not have this drawback but the applied gesture needs higher accuracy. Indeed, if too much pressure is applied on the footplate, there is a risk to fracture the footplate or to push it into the inner ear (floating footplate), thus yielding complete deafness. For prosthesis with a 0.4 mm diameter, a 0.6 mm diameter hole is required. A too large opening in the footplate may induce a leak of the inner ear fluids postoperatively into the middle ear cavity, compromising the hearing.

The drilling operation was simulated using an algorithm derived from constructive solid geometry subtraction [23]. Therefore the operation required objects in which underlying geometries were based on signed distance fields. Given two of them, one called *Surface* and the other *Tool*, the computation below was done in order to update the distance field of the *Surface*:

$$Surface = \max\left(Surface, -Tool\right). \quad (1)$$

The whole process was organized around one component whose purpose was to retrieve access to the distance fields and the corresponding collision models. The drilling process was activated by a peripheral input. So the collision between the *Tool* collision model and all the *Surfaces* was checked and the rightful surfaces according to the contacts are updated. More precisely, the update was made locally around the detected contacts to avoid unnecessary computation and to save time. Figure 4 represents the updated values in green during the interaction of a *Surface* in red with a *Tool* in blue. The final rendering was currently carried out by the Marching Cubes algorithm, recreating meshes from the distance fields.

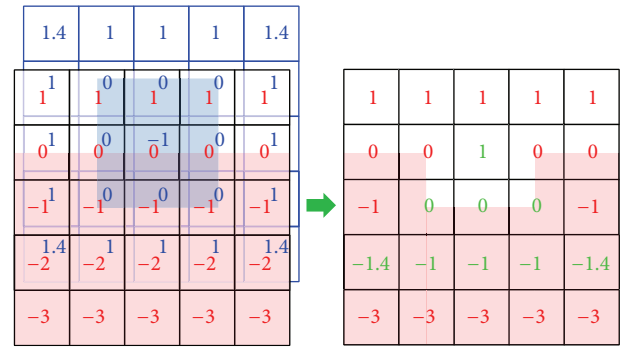

Figure 4: Application of the carving process with a cube as *Tool* (blue) and a plane as *Surface* (red) based on signed distance map. The outcome is displayed on the right side, and the local update is pictured in green.

This method was based on an unsettled model, which allowed the user to drill any part of the bones (Figures 5(a) and 5(b)). Thus an imprecise gesture or a misplacement of the stapedotomy by the resident may be simulated. Moreover to study and analyze new procedures or tools it was important to use a nondeterministic model for our simulation.

The collision detection required models that could compute the intersection between a distance field and different mesh primitives. The intersection with a point was based on the following idea: the position of the point inside the distance field can easily be computed and thus the presence of contact or not can be determined, including the distance to the surface of the object. The line and triangle intersections rested on the same basic concept, dividing the primitive in a set of points to compute the position of every one of them in the distance field. Other pairs of intersection have yet to be implemented.

To simulate the drilling surgical step, we used a sphere to represent a 0.6 mm diameter burr linked to a visual surgical hand piece. The temporal bone, the facial nerve, and a 6 mm diameter speculum were visually represented to reproduce surgical environment and visual obstacles (Figure 5(c)). Collisions were only computed between the burr and the ossicular chain. To complete the task, the surgeons had to drill

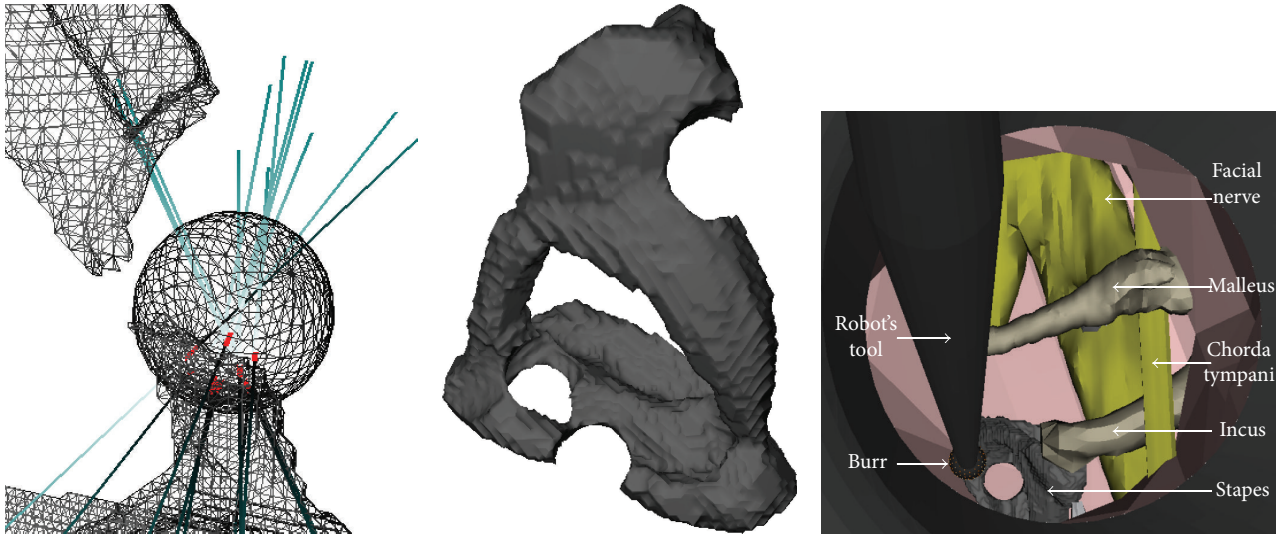

(a) Wire view (b) Nondeterministic model (c) Stapedotomy, surgical view

FIGURE 5: Simulation of a drilling procedure using a burr. (a) Contact interactions are represented in red and blue during a drill. (b) Represents the results of the marching cube algorithm. Any part of the bone can be drilled. (c) Surgical view of a stapedotomy simulation using the RobOtol.

the stapes footplate in order to obtain a 0.6 mm diameter hole. The goal of this task was also to evaluate the feasibility to drill the footplate of the stapes with a surgical hand piece mounted on the RobOtol.

The ideal position of the stapedotomy was determined initially by an expert surgeon and was not displayed to the user during the test. This optimal position was shown only at the beginning of the test during few seconds to avoid the divergence of the user position estimation. The goal was to determine user ability to reach a memorized target with the teleoperated system. The path of the robot, the distance of the burr to the optimal position, and the execution the time of the task were recorded.

2.3.2. Placement of the Prosthesis. The crimping procedure of the prosthesis piston on the incus long process is an even more critical step. Involuntary movement on the ossicular chain may induce a rupture of the incus-malleus joint or incus luxation. Severe damage occurs when forces around 0.9 N in the anterior-posterior direction (X-axis in Figure 3) or 0.7 N in the lateral-medial direction (Z-axis in Figure 3) are applied [24]. A Soft-clip (Heinz Kurz GmbH, Dusslingen, Germany) prosthesis piston with diameter of 0.4 mm and length of 4.5 mm was modeled in the simulation as hexahedral deformable elements (Figure 6(a)). The density parameter and the Young modulus of pure titanium medical grade 2 prosthesis were set at 4.5×10^3 kg/m^3 and 344 MPa. A virtual prototype of a surgical microforceps designed for the RobOtol was implemented in Sofa.

The simulation of the stapedotomy was previously performed to drill a 0.6 mm diameter hole centered on the stapes footplate. The ablation of the stapes branches was performed by a total drilling of the superstructure of the stapes. This is not the conventional procedure since the separation of the stapes superstructure to the footplate is performed by bone fracture, but this step was not yet implemented in our simulator. Nevertheless, the resulting model was used with the same mechanical parameters for the simulation of the stapedioplasty surgery. The bottom of the ossicular prosthesis was first placed through the stapes footplate, and then the upper part was set upon the incus long process. Finally, the prosthesis was pushed until it was crimped on the incus (Figure 6(b)). This is the most critical surgical step because the required forces to fix the prosthesis are close to forces that can lead to incudomalleolar articulation rupture. The execution time and the incus displacement were recorded throughout the simulation of the procedure.

2.3.3. Innovative Surgical Procedures. RobOtol enhances gestures accuracy and reduces physiological tremor. By taking advantage of these functionalities, new procedures could be performed using the robot. During the crimping of the prosthesis, the incus is moving due to the applied pressure required to push the prosthesis. To avoid this effect, an option consists in maintaining the incus using an instrument. This intervention, using two tools in contact with the ossicular chain at the same time, is almost impossible to perform in conventional surgery. The robot has the possibility to hold the same position of the tool with no tremor or tiredness effect compared to a manual surgery.

The idea was to use a second robotic arm equipped with a basic instrument, such as a microedge or a suction tool, and to place it close to the incus on the opposite side of the prosthesis approach. Thus during the crimping process the second robotic tool would restrain the incus motion inwards the middle ear cleft (Figure 7(b)). The hypothesis was to reduce the incus displacement to avoid damage of the incudomalleolar joint.

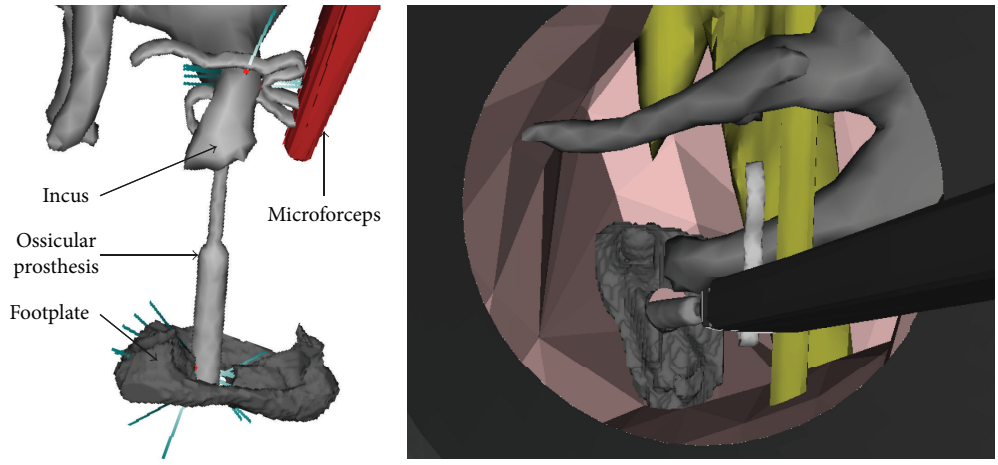

(a) Experimental view (b) Stapedioplasty, surgical view

FIGURE 6: Simulation of the placement of an ossicular prosthesis. The ossicular prosthesis is placed through the perforated stapes footplate and fixed to the incus. (a) Experimental view with the visualization of the detected collisions in blue and red lines. The prosthesis is clipped to the incus. (b) According to a surgical view, the round gray area is the view of a 6 mm diameter speculum. The prosthesis is going to be clipped.

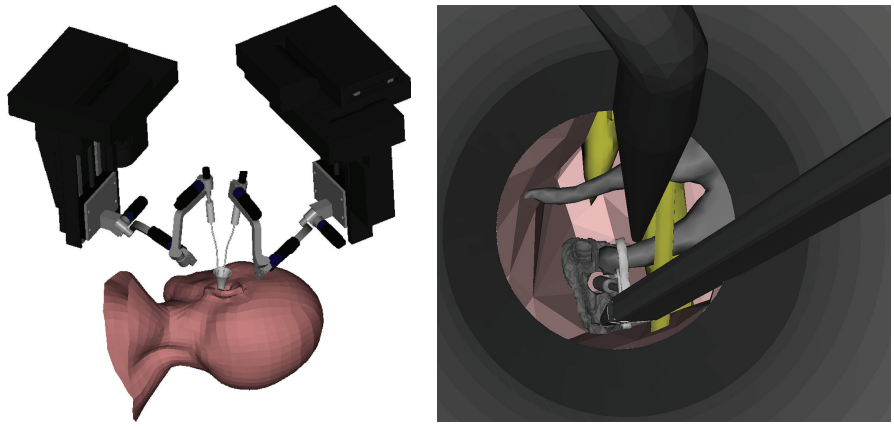

(a) External view (b) Internal view

FIGURE 7: Middle ear surgical simulation using two robot arms simultaneously. (a) External view of the surgical scene. (b) Surgical view of a stapedioplasty procedure using two arms.

However, this procedure requires two robotic arms in contact with the ossicles through the 6 mm diameter speculum. To avoid collision between the arms and to preserve as much as possible the surgical visual field, the configuration of the two robot arms in the operating room was investigated. Again, the execution time and the incus motion were recorded during the experiment.

Results were expressed as mean ± standard deviation, an unpaired t-test was used to compare our results and were analyzed with R statistical software (http://www.r-project.org).

3. Results

Robot-based stapedotomy and ossiculoplasty were successfully conducted using a haptic device interface. More than 40 frames per second were observed with no interaction between tools and organs and have dropped to 20 frames per seconds when more than 30 collisions occurred. This was the limit of acceptance for real-time interactions, but we considered that it was sufficient enough for our application. The lowest number of frames rate observed throughout all our simulations is 10 Hz and is measured during strong interaction such as drilling with 80 simultaneous collisions. Motion and deformation of the ossicular chain during a palpation with the tools were subjectively reported to be realistic by the surgeons.

The drilling algorithm based on the signed distance fields coupled to a Marching Cube algorithm allowed performing a stapedotomy. Incomplete or abnormal drilling like elliptic shaped hole was possible. The mean execution time was 80 ± 17 s ($n = 5$) with a mean duration time of 39 ± 10 s related to the descent of the robot's tool in contact with the stapes footplate. A minimal distance of 0.07 ± 0.03 mm ($n = 5$) was observed between the target position of the stapedotomy and

the different trials. The volume of the virtual stapedotomy was $0.11 \pm 0.005\,\text{mm}^3$ ($n = 5$), which corresponded to $7.3 \pm 0.33\%$ of the total volume of the stapes footplate that had been drilled.

Users were able to place the bottom of the ossicular prosthesis through the footplate with a microforceps and to place the upper part onto the incus inferior branch. The crimping process was assured by pushing the prosthesis like in manual surgery. The prototyped virtual tool preserved the surgical view (Figure 6(b)). Using a second robot's arm or a surgical hand piece mounted on the robot, surgeons were still able to move freely with the robot in the middle ear cavity. No obstruction was reported and the visual field of view was sufficient to practice surgery. No collisions between the arms, located at ±120 degrees compared to the surgeon's position, were detected (Figure 7(a)).

The mean duration time of the total stapedioplasty was 140 ± 54 s ($n = 5$) for the experiment with a single tool and 175 ± 40 s for the task with the second robot arm. The movement of the incus was 0.24 ± 0.09 mm ($n = 5$) when using a single microforceps and 0.10 ± 0.05 mm ($n = 5$) when using two tools simultaneously. A decrease displacement of the long branch of the incus was observed, while a second tool was placed against the incus ($P = 0.025$, student). A sharp decrease of the motion along the X-axis (Figure 3) was observed (0.15 ± 0.05 to 0.05 ± 0.02 mm, $P = 0.008$, student) as well as along the Y-axis (from 0.12 ± 0.04 mm to 0.06 ± 0.03, $P = 0.029$, student). However, the use of a second tool did not reduce the incus displacement along the Z-axis (0.16 ± 0.12 mm for the method with a single tool against 0.07 ± 0.06, $P = 0.198$, student).

4. Discussion

The interactive simulation presented in this paper was developed for training, rehearsal, and improving the new robotic procedures. The simulation was performed using a physics-based validated model, which ensured the realism of the mechanical behavior of the middle ear [14]. In addition to the physiological and surgical condition evaluation, the behavior of our FEM was described as realistic by expert surgeon during a palpation of the middle ear structures with the simulated robotic tools. The optimization process, implemented in SOFA, allowed simulating simultaneous interactions between the ossicular chain, a deformable prosthesis and two robot's arms controlled by an operator, at an average frame rate of 20 frames per second. However, interactions involving a relatively large number of contact points reduced the computational efficiency, suggesting that further optimizations will be needed in the future.

Two challenging procedures of the middle ear surgery were successfully performed using the RobOtol with our simulation approach: stapedotomy and stapedioplasty surgery. An unsuccessful procedure, such as misplacement of the burr during a stapedotomy, could be simulated and evaluated by the analysis of the shape of the hole or the applied forces on the footplate. For instance, as the drilled volume of the stapes footplate was relatively reproducible, an abnormal volume can indicate a bad performance. On the contrary, good achievement of those tasks validated the cinematic efficiency and abilities of the robot to perform middle ear surgery. Moreover, our simulation could constitute an alternative to temporal bone dissection for surgical training. Indeed, abundant training session is a real issue because of the diminishing availability of human temporal bones [25, 26].

The execution time of those two robot-based procedures was longer than in conventional surgery but within expected values when performing such difficult procedures. It should be noted that the duration time of the stapedotomy was rather repeatable, although it was not the case for the stapedioplasty. The high level of difficulty to perform those procedures can explain this observation. These approaches require a good positioning adjustment to place the prosthesis, which can take a variable amount of time. When using two arms at the same time, the execution time was longer. This delay of 35 s was due to the placement of the second robot's arm, although it is possible to move the two robot's arm simultaneously with two master arms. Nevertheless, the additional duration of the task was not excessive compared to the mean duration of a complete otosclerosis surgery, which is reported as 54 ± 21 minutes [27].

Between the different stapes drilling simulations, the target position was reached with 0.07 ± 0.03 mm accuracy on a footplate of 2.8×1.52 mm (elliptic shape) with a 0.6 mm diameter burr. This error relies on the memory capability of the surgeon as well as the accuracy of the teleoperated system. It means that the surgeons were able to command the robot's tool to a desired position with a mean accuracy of 0.07 mm. The drilled volume observed was around 7.3% of the total volume of the stapes footplate with a standard deviation of 0.33. That means that our experiment was very repeatable and that the robot is accurate enough to conduct a stapedotomy.

The size of the surgical burr was very important compared to a micropeak. When mounted on the robot's arm, its visual obstruction was added to the robot itself. It was important to investigate the tool arrangement in order to preserve the visual field. The different simulations suggest that the visual obstruction of the surgical burr was not a major issue, since no discomfort was reported by surgeons using the simulator.

The placement of the prosthesis using the robot was successfully simulated, with either a single or two instruments. The results suggested that we were able to reduce the global displacement of the incus during the surgical procedure by 57% with a second arm to maintain the long process of the incus. Figure 7(b) represents the surgical view using two simultaneous arms. In conventional surgery, this procedure is almost impossible to accomplish, as the manipulation of two tools simultaneously in contact with the ossicular chain requires perfect hands coordination and dexterity. The incus motions on the anterior-posterior and on the upward-backward direction were reduced by 65%. The motion on the Z-axis (Figure 3) was not significantly changed with the new approach. This could be explained by the fact that the second tool did not constrain the incus in that direction. Therefore, a new tool, similar to a microhook, could be used to decrease the displacement of the incus in that specific direction. This example of a procedure comparison, evaluated using

the simulation, shows that potential risk of incus luxation or fracture during piston crimping could be reduced using a second tool simultaneously. Obviously, this could be easily performed with two robotic arms.

The simulation and the results suggested that it was possible to improve the procedures using a robot-based system. Indeed a robot-based procedure could improve accuracy, ergonomics, fatigue, and tremor leading to increased safety of the patient and surgical outcome. Thus, our results demonstrated that two robotic arms at the same time could be used in order to decrease the risk of incus luxation or fracture. To do so, we have used the interactive simulation to test and evaluate a new surgical procedure using RobOtol.

One major middle ear surgery constraint is the bleeding phenomena. The blood fills the middle ear cleft from the bottom leading to an obstruction of the surgical workspace. The surgeons have to suck the blood using a suction cannula with their hands. However, it is very complicated to operate simultaneously with two tools through the external ear meatus. Several gestures, such as manipulation of the ossicular chain, may require both hands to stabilize the effective tool to control tremor. A second robotic arm could be placed at the bottom of the middle ear cavity for suction purpose. We showed that protection of the incus could reduce the ossicular chain motion. Thereby, to maintain the position of the incus while crimping the prosthesis, we can use a nonspecific shaped tool. The dimensions of this tool are compatible with usual suction cannula used in middle ear surgery. Thus, as a future work, we will study the possibility to use one tool mounted on a second arm to reduce bleeding embarrassment and to maintain the incus during real manipulation of the ossicles.

The simulation could also be used to train the physicians to the use of the robot and to evaluate the quality of the simulated procedure based on four evaluation criteria. The first criterion is based on the anatomical point of view, with the study of the shape, or placement of the hole in the footplate or the prosthesis on the incus compared to expert intervention. The analysis of the applied forces on the anatomical structures could be the second criterion, which allows the assessment of the surgical gesture ability. The visual obstruction duration could be taken into account to evaluate the procedure, as a third criterion. And finally the quality of the functional results of the surgical procedures could be estimated by the differential analysis of the ossicular transfer function results before and after the intervention as a fourth criterion. Equation (2) illustrates our assessment process that could provide an objective evaluation of a performed procedure. Thereby, the robot's tool prototype and different surgical approaches can be compared:

$$E = \alpha \frac{1}{S} + \beta \frac{1}{F} + \gamma \frac{1}{\mathrm{VF}} + \delta \frac{\mathrm{TF}_{\mathrm{after}}}{\mathrm{TF}_{\mathrm{before}}}, \quad (2)$$

where α, β, γ, and δ are constants; S expresses the distance to an optimal position initially determined by an expert surgeon; F takes into account the force applied on the anatomical structures such as in (3); VF corresponds to the visual obstruction time; and TF represents the transfer function results with the detailed computation reported in [14] and corresponding to the surgical outcome estimation. The execution time is not represented because we believe that it has no negative effect on the surgery result:

$$F = \mu \frac{df}{dt} + \lambda \int f \, dt. \quad (3)$$

Other contribution of this work is to offer the possibility to evaluate new tools design for our robotic system. Interactive simulation allows the surgeons to determine whenever the tool is obstructing the field of vision during the surgical intervention and to evaluate their efficiency. Based on this work, questions about the instruments are raised, such as the better side to open the microforceps jaws. Our simulation offers the possibility to see and feel what could be the surgery using these tools, thus assessing the difficulty to perform it. Thus, the development cost and time could be reduced and direct feedback from the surgeons could be taken into account during the design process.

To perform a stapedioplasty with the RobOtol, a new actuator, providing 7th degree of freedom, should be implemented in order to grasp the prosthesis. The number of mobile jaws is now set to one in order to avoid damage on anatomical structures while opening the forceps. This new degree of freedom is compatible with the current RobOtol design and can be ensured by a step motor AM 1020-A0.258 (Faulhaber GmbH, Germany). Buttons on the master arm device or on the pedal-board can control opening or closing action of the forceps. A real version of the forceps for the robot will be built and based upon the tool evaluated with our interactive simulator. Furthermore, we know that the robot's actuators are powerful enough to handle a surgical hand piece without any change of the motion performance of the robot. However, before mounting a surgical hand piece on the robot's end effector, we have to verify that the burr vibrations will not disturb the robot and its accuracy. This will now constitute our next work. The interactive simulations presented in this work allowed performing a preliminary test on the feasibility and on the design of robot-based procedures using the robot.

At any time, the robot was able to complete the procedures and did not require a manual intervention. As the robot has no force sensor, no haptic rendering was transmitted to the user. The surgeon estimated the proximity and the contacts between the virtual components with the 3D rendering using the 3D viewer and visualization of the anatomical structures displacement or deformation like in actual surgery. Results showed that the robot was compatible with these surgical procedures, even without force feedback as in the current configuration of the robot, and that the physicians can be trained to the use of the robot by the simulation.

5. Conclusion

The clinical tests of our teleoperated system, called RobOtol, will start in few months. To accustom the surgeons to the robot and to investigate new tools design and new surgical

procedures, we developed a surgical simulator of the middle ear microsurgery. Unlike most training system, the purpose here was to use the simulation for rehearsal procedures that will later be performed using a robotic system, called RobOtol. Thereby, we showed that our simulator allowed the design improvement of this teleoperated system such as the addition of new degrees of freedom and also prepared the physician to the first clinical interventions that will be performed with the robot. To reach this goal, the simulation was based on a validated finite element model of the middle ear, compatible with real-time computation. Moreover, interactive drilling was implemented and based on a nondeterministic model. Two challenging middle ear surgeries, a stapedotomy and a stapedioplasty, were simulated using the RobOtol. To our knowledge, virtual simulations of those microsurgical procedures had never been reported yet.

Moreover, the concept of using a real-time simulator to test and evaluate the new possibilities given by the robot and to design the robot tools was also original. Currently, we have already investigated the ability to use easily two robotic arms simultaneously during the robot-based procedure.

Further surgical simulations using the RobOtol will allow the development of a set of tools and to test innovative surgical procedures in order to improve surgical outcomes and patient safety.

Conflict of Interests

The authors declare that there is no conflict of interests regarding the publication of this paper.

Acknowledgment

The authors would like to thank Collin SA (Bagneux, France) for financial support for this study.

References

[1] J. Finkelstein, E. Eckersberger, H. Sadri, S. S. Taneja, H. Lepor, and B. Djavan, "Open versus laparoscopic versus robot-assisted laparoscopic prostatectomy: the European and US experience," *Review in Urology*, vol. 12, no. 1, pp. 35–43, 2010.

[2] Z. Jianxun, T. Huan, L. Wenqin, Y. Tian, and W. Shumei, "Robot assistant microsurgery system," in *Proceedings of the 6th World Congress on Intelligent Control and Automation (WCICA '06)*, pp. 9032–9036, June 2006.

[3] B. Mitchell, J. Koo, M. Iordachita et al., "Development and application of a new steady-hand manipulator for retinal surgery," in *Proceedings of the IEEE International Conference on Robotics and Automation (ICRA '07)*, pp. 623–629, Rome, Italy, April 2007.

[4] P. Dubach, B. Bell, S. Weber, and M. Caversaccio, "Image-guided otorhinolaryngology," in *Intraoperative Imaging and Image-Guided Therapy*, F. A. Jolesz, Ed., pp. 845–856, Springer, New York, NY, USA, 2014.

[5] G. M. Grande, A. J. Knisely, B. C. Becker, S. Yang, B. E. Hirsch, and C. N. Riviere, "Handheld micromanipulator for robot-assisted stapes footplate surgery," in *Proceedings of the 34th Annual International Conference of the IEEE Engineering in Medicine and Biology Society (EMBS '12)*, pp. 1422–1425, September 2012.

[6] K. Entsfellner, G. Strauss, T. Berger, A. Dietz, and T. C. Lueth, "Micro-macro telemanipulator for middle-ear microsurgery," in *Proceedings of the 7th German Conference on Robotics (ROBOTIK '12)*, pp. 1–4, 2012.

[7] M. Miroir, Y. Nguyen, J. Szewczyk, O. Sterkers, and A. Bozorg Grayeli, "Design, kinematic optimization, and evaluation of a teleoperated system for middle ear microsurgery," *The Scientific World Journal*, vol. 2012, Article ID 907372, 19 pages, 2012.

[8] C. Duval and J. Jones, "Assessment of the amplitude of oscillations associated with high-frequency components of physiological tremor: Impact of loading and signal differentiation," *Experimental Brain Research*, vol. 163, no. 2, pp. 261–266, 2005.

[9] M. Miroir, Y. Nguyen, J. Szewczyk et al., "RobOtol: from design to evaluation of a robot for middle ear surgery," in *Proceedings of the 23rd IEEE/RSJ International Conference on Intelligent Robots and Systems (IROS '10)*, pp. 850–856, October 2010.

[10] G. Kazmitcheff, M. Miroir, Y. Nguyen et al., "Evaluation of command modes of an assistance robot for middle ear surgery," in *Proceedings of the IEEE/RSJ International Conference on Intelligent Robots and Systems (IROS '11)*, pp. 2532–2538, San Francisco, Calif, USA, September 2011.

[11] P. Trier, K. Ø. Noe, M. S. Sørensen, and J. Mosegaard, "The visible ear surgery simulator," *Studies in Health Technology and Informatics*, vol. 132, pp. 523–525, 2008.

[12] R. Z. Gan, B. Feng, and Q. Sun, "Three-dimensional finite element modeling of human ear for sound transmission," *Annals of Biomedical Engineering*, vol. 32, no. 6, pp. 847–859, 2004.

[13] D. J. Kelly, P. J. Prendergast, and A. W. Blayney, "The effect of prosthesis design on vibration of the reconstructed ossicular chain: a comparative finite element analysis of four prostheses," *Otology and Neurotology*, vol. 24, no. 1, pp. 11–19, 2003.

[14] G. Kazmitcheff, M. Miroir, Y. Nguyen et al., "Validation method of a middle ear mechanical model to develop a surgical simulator," *Audiology & Neuro-Otology*, vol. 19, no. 2, pp. 73–84, 2013.

[15] J. J. Rosowski, W. Chien, M. E. Ravicz, and S. N. Merchant, "Testing a method for quantifying the output of implantable middle ear hearing devices," *Audiology and Neurotology*, vol. 12, no. 4, pp. 265–276, 2007.

[16] K. B. Huttenbrink, "The mechanics of the middle-ear at static air pressures: the role of the ossicular joints, the function of the middle-ear muscles and the behaviour of stapedial prostheses," *Acta Oto-Laryngologica, Supplement*, vol. 106, no. 451, pp. 1–35, 1988.

[17] X. Wang, T. Cheng, and R. Z. Gan, "Finite-element analysis of middle-ear pressure effects on static and dynamic behavior of human ear," *Journal of the Acoustical Society of America*, vol. 122, no. 2, pp. 906–917, 2007.

[18] G. Kazmitcheff, C. Duriez, M. Miroir et al., "Registration of a validated mechanical atlas of middle ear for surgical simulation," in *Proceedings of the Medical Image Computing and Computer Assisted Intervention (MICCAI '13)*, pp. 331–338, 2013.

[19] D. T. Nicholson, C. Chalk, W. R. J. Funnell, and S. J. Daniel, "Can virtual reality improve anatomy education? A randomised controlled study of a computer-generated three-dimensional anatomical ear model," *Medical Education*, vol. 40, no. 11, pp. 1081–1087, 2006.

[20] F. Faure, C. Duriez, H. Delingette et al., "SOFA: a multi-model framework for interactive physical simulation," in *Soft Tissue Biomechanical Modeling for Computer Assisted Surgery*, vol. 11 of

Studies in Mechanobiology, Tissue Engineering and Biomaterials, pp. 283–321, 2012.

[21] C. Duriez, C. Andriot, and A. Kheddar, "Interactive haptics for virtual prototyping of deformable objects: snap-in tasks case," *Eurohaptics*, p. 28, 2003.

[22] H. Courtecuisse, J. Allard, C. Duriez, and S. Cotin, "Asynchronous preconditioners for efficient solving of non-linear deformations," in *Proceedings of the Virtual Reality Interaction and Physical Simulation (VRIPHYS '10)*, 2010.

[23] C. Syllebranque and C. Duriez, "Six degree-of freedom haptic rendering for dental implantology simulation," in *Biomedical Simulation*, vol. 5958 of *Lecture Notes in Computer Science*, pp. 139–149, 2010.

[24] M. Lauxmann, C. Heckeler, D. Beutner et al., "Experimental study on admissible forces at the incudomalleolar joint," *Otology and Neurotology*, vol. 33, no. 6, pp. 1077–1084, 2012.

[25] S. B. Mathews, B. M. Rasgon, and F. M. Byl, "Stapes surgery in a residency training program," *Laryngoscope*, vol. 109, no. 1, pp. 52–53, 1999.

[26] J. B. Farrior, "Stapedectomy for the home temporal bone dissection laboratory," *Otolaryngology—Head and Neck Surgery*, vol. 94, no. 4, pp. 521–525, 1986.

[27] J. A. Hornung, C. Brase, A. Bozzato, J. Zenk, and H. Iro, "First experience with a new titanium clip stapes prosthesis and a comparison with the earlier model used in stapes surgery," *Laryngoscope*, vol. 119, no. 12, pp. 2421–2427, 2009.

Hindawi Publishing Corporation
BioMed Research International
Volume 2014, Article ID 416205, 9 pages
http://dx.doi.org/10.1155/2014/416205

Research Article

Speech Understanding with a New Implant Technology: A Comparative Study with a New Nonskin Penetrating Baha System

Anja Kurz,[1] Mark Flynn,[2] Marco Caversaccio,[1] and Martin Kompis[1]

[1] *Department of ENT, Head and Neck Surgery, Inselspital, University of Bern, 3010 Bern, Switzerland*
[2] *Cochlear Bone Anchored Hearing Solutions, Mölnlycke, Sweden*

Correspondence should be addressed to Martin Kompis; martin.kompis@insel.ch

Received 6 March 2014; Accepted 16 May 2014; Published 23 July 2014

Academic Editor: Nozomu Matsumoto

Objective. To compare hearing and speech understanding between a new, nonskin penetrating Baha system (Baha Attract) to the current Baha system using a skin-penetrating abutment. *Methods.* Hearing and speech understanding were measured in 16 experienced Baha users. The transmission path via the abutment was compared to a simulated Baha Attract transmission path by attaching the implantable magnet to the abutment and then by adding a sample of artificial skin and the external parts of the Baha Attract system. Four different measurements were performed: bone conduction thresholds directly through the sound processor (BC Direct), aided sound field thresholds, aided speech understanding in quiet, and aided speech understanding in noise. *Results.* The simulated Baha Attract transmission path introduced an attenuation starting from approximately 5 dB at 1000 Hz, increasing to 20–25 dB above 6000 Hz. However, aided sound field threshold shows smaller differences and aided speech understanding in quiet and in noise does not differ significantly between the two transmission paths. *Conclusion.* The Baha Attract system transmission path introduces predominately high frequency attenuation. This attenuation can be partially compensated by adequate fitting of the speech processor. No significant decrease in speech understanding in either quiet or in noise was found.

1. Introduction

With more than 100,000 implantations so far, bone anchored hearing implants [1] belong to the widest used implantable hearing aids to date, second only to cochlear implants. The principle of operation is shown in Figure 1(a): a skin penetrating abutment is attached to an osseointegrated titanium implant. A sound processor is then attached to the abutment using a snap coupling which can be adjusted or removed by the user. Although each part of the system has been improved considerably in the last years [2–4], the basic design principle has now been in use for over 3 decades [5]. Its attractiveness is based on the relatively simple surgery and on the excellent results in adults and children with conductive or mixed hearing loss or, more recently, also in single sided deafness [6–8].

Despite this success, some drawbacks are well known. One of them is a tendency to low-grade infections around the abutment [9, 10], another personal preference, and cosmetic factors. Some patients who could benefit significantly from a system such as the Baha depicted in Figure 1(a) decline because of the skin penetrating implant behind the ear.

Several solutions, in which the skin remains intact, have been proposed. The Xomed Audiant system [11] in the 1980s had an implanted magnet, but the coil of the transducer was built into the sound processor. The maximal output of the system proved to be too low for numerous patients [11], and the system was discontinued. The Sophono system [12] is available today and is based on two implanted magnets within a single implant [13]. The sound processor with the bone conduction transducer (vibrator) is attached externally over the intact skin. The contact area between the skull and the implant is relatively large (more than 2.5 cm^2) and new research suggests that its output is 10–15 dB lower than that of the Baha [14].

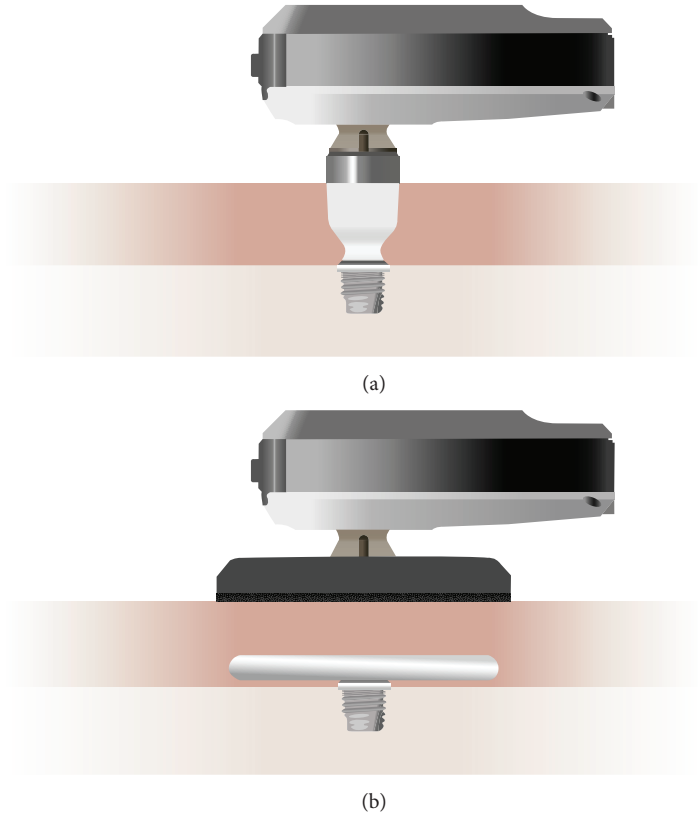

(a)

(b)

Figure 1: (a) Current Baha system with skin penetrating abutment. (b) Nonskin penetrating Baha Attract system with magnetic retention.

Recently, a new bone conduction implant, the Vibrant Bonebridge [15], has been introduced. In contrast to the other systems described so far, the transducer is fully implanted and connected to the speech processor via a radiofrequency link. The implant is significantly larger and more expensive than any of the others.

Very recently, a new system called Baha Attract has been proposed. It is shown schematically in Figure 1(b). It uses the same types of sound processors and the same osseointegrated titanium implant as the current Baha system. This results in a small contact area between the skull and the implant. Two magnetic discs are used: one with a diameter of 27.0 mm below the intact skin and another with a diameter of 29.5 mm, to which the external sound processor is attached. The choice of such a relatively large contact area results in lower skin pressures to achieve the necessary retention force.

So far, little is known about the practically important audiologic aspects of this new system and we are not aware of any peer reviewed reports or investigations. The change of the transmission path from direct bone conduction through the abutment to transmission via soft tissue might introduce differences in the acoustic transmission, most probably an additional attenuation. However, its extent and consequences for speech understanding are not known. A part of this attenuation may be compensated by different setting of the sound processor, but possibly not all of it.

The aim of this investigation is threefold. The primary aim is to compare the proposed Baha Attract transmission path to the conventional path shown in Figure 1(a) in actual Baha users. Hearing thresholds and speech understanding measured through the system are the pertinent endpoints.

The second aim is to estimate the hearing thresholds, at which candidates may be expected to experience significantly decreased speech understanding when deciding whether to choose a Baha Attract system instead of the skin penetrating solution.

The third aim is to ascertain that the differences in hearing between the two transmission paths are comparable for the two most important groups of Baha users: those with a conductive/mixed hearing loss [3] and those with single-sided sensorineural deafness (SSD) [8]. As all changes in the transmission path take place prior to sound entering the skull, we hypothesize that the attenuation and therefore the impact on speech understanding should be similar in both user groups. However, to date there is no experimental evidence to support this hypothesis.

2. Materials and Methods

2.1. Subjects. 16 adult Baha users aged 30–75, mean 58.4 years, 6 females and 10 males, participated in the study. All had an implant with a skin penetrating abutment, as shown in Figure 1(a), for a period between 6 months and 22 years (average 8.9 years, 7 right, 9 left) and used a Baha sound processor on a daily basis at the

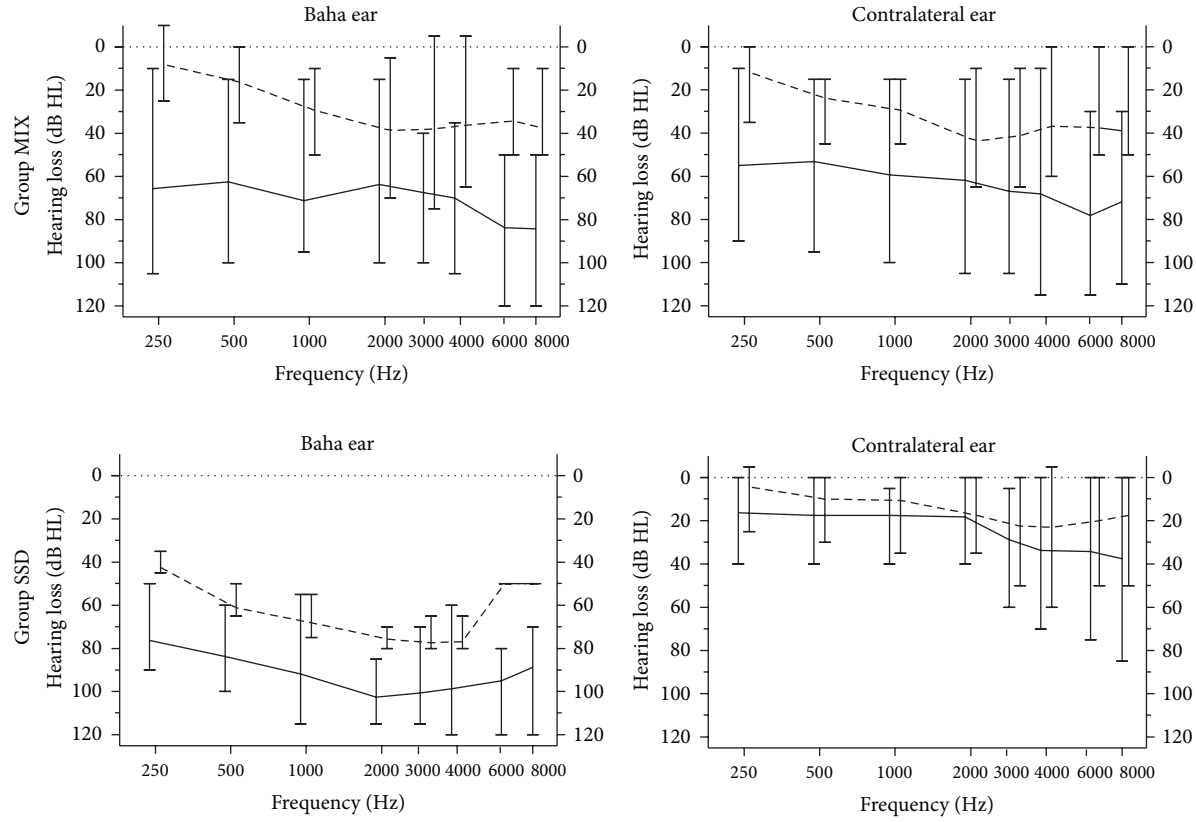

Figure 2: Pure tone audiograms of the two study subgroups MIX and SSD. Solid lines denote mean AC thresholds, broken lines mean BC thresholds, and error bars show the range.

time of testing (6 Baha BP110, 5 Baha BP100, 3 Baha Intenso, 1 Baha Divino, and 1 Baha Compact [3, 4, 16]). Eight subjects had a mixed or conductive hearing loss and this group is labelled MIX throughout the text. The other 8 subjects had a single-sided sensorineural deafness. This group is labelled SSD throughout the text. Figure 2 shows a synopsis of the unaided air conduction (AC) and bone conduction (BC) hearing thresholds for both groups.

2.2. Transmission Paths. Four different transmission paths were compared in this study. They are labelled "Abutment," "Magnet 3," "Magnet 5," and "Testband." Figure 3 shows a schematic representation of these paths. A Baha BP110 sound processor [4] (Cochlear Inc., Sweden) was used for all tests and all participants.

In the "Abutment" setting, the BP110 sound processor was attached directly to the patient's own abutments, as shown in Figure 3(a).

In the "Magnet 3" and "Magnet 5" settings, shown in Figure 3(b), a magnetic plate (diameter 27.0 mm, thickness 2.4 mm) was attached to the snap coupling. An artificial skin sample (SawBones 1485-150, Sweden, diameter 28 mm, thickness 5.6 mm) was placed directly above it. The thickness of this sample is very close to the average skin thickness of 5.5 mm on the mastoid found by Faber et al. [10]. Then the Baha Attract sound processor magnet (diameter 29.5 mm, thickness 5.1 mm) was placed above the artificial skin sample and the BP110 sound processor was attached to its snap coupling.

Five different processor magnets are available, labelled 1 through 5 by the manufacturer according to their magnetic strength. In this investigation, Magnet 3 was used as it was the weakest one that was held in place sufficiently for the experiments without falling off. Its measured retention force in the experimental setup was 0.87 N.

In the "Magnet 5" setting, the strongest magnet available was used. Its retention force in the experimental setting was measured to be 1.24 N.

In the "Testband" setting, depicted schematically in Figure 3(c), the BP110 sound processor was mounted on a standard Baha testband [17]. The plastic disc of the testband, which holds the sound processor, is shown schematically in Figure 3(c). It was placed immediately behind the patient's implant, but without touching the abutment. The "Testband" condition was included because it is simple, is frequently used preoperatively at many centers, and is expected to show similar results as the Baha Attract transmission path.

2.3. Study Protocol. The study protocol was approved by the local Ethical Committee of Bern. All tests were performed at the University Hospital of Bern in accordance with the declaration of Helsinki and all participants had given their informed consent prior to inclusion in the study.

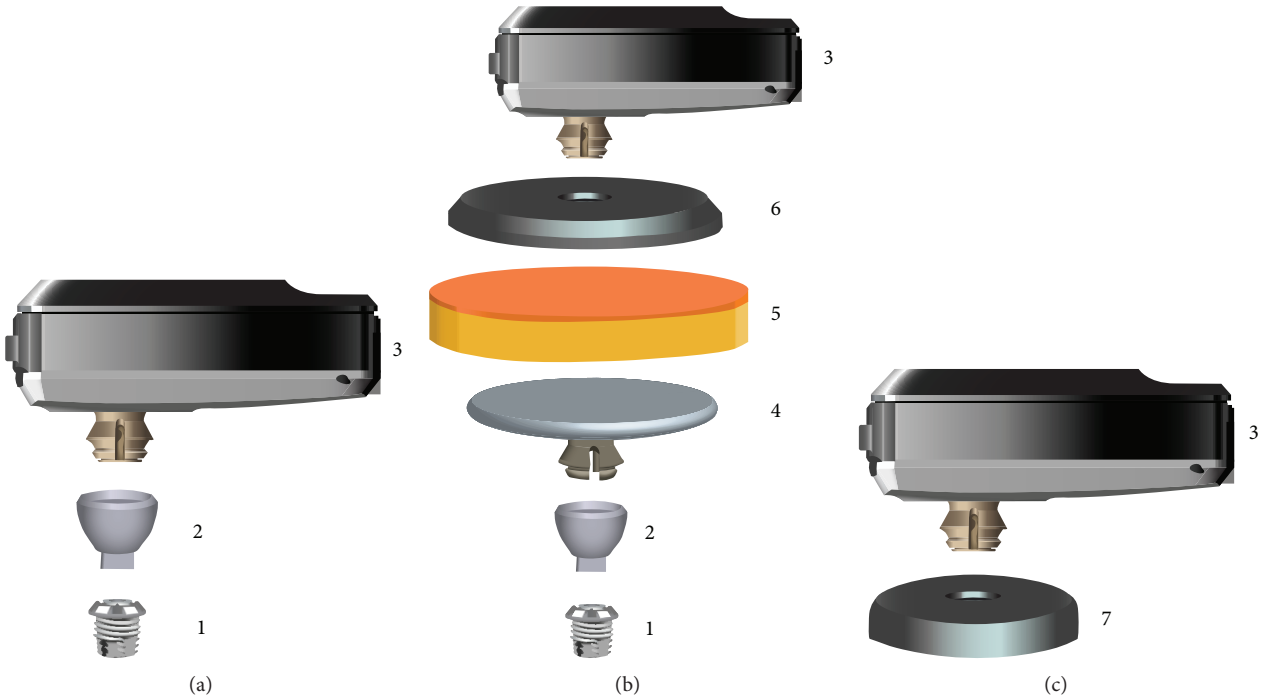

Figure 3: Transmission paths compared in the study. (a) "Abutment," (b) "Magnet 3" and "Magnet 5," and (c) "Testband" individual parts: (1) implant, (2) abutment, (3) sound processor BP110, (4) internal magnet, (5) artificial skin, (6) external magnet plate, and (7) testband (only the disc is shown, and the headband, which is attached to the disc, is not shown).

The measurements took approximately 5 hours per subject and were completed within one day for all but one participant. For each subject, AC and BC threshold were measured first in both ears. BC thresholds were measured between 250 Hz and 8000 Hz. Scale-out values were marked. They were rare, except for the poorer ear of the SSD group, as shown in the bottom left panel of Figure 2, where scale-out values were replaced by the audiometer limits for graphical purposes. Then unaided sound field thresholds were measured. For all sound field measurements, that is, aided and unaided, the ear contralateral to the Baha implant was plugged with an ear plug (E-A-Rsoft, 3M, Sweden) and covered with a Peltor Optime II hearing protector (Aero Ltd., Poynton, UK).

Then, hearing and speech understanding with each of the 4 transmission paths described in Section 2.2 were tested. The order of the transmission paths was varied systematically between subjects to minimize effects of training or fatigue.

For each new transmission path, first BC thresholds were measured directly via the BP110 sound processor (so-called BC Direct [18]). Then the processor was fitted according to the manufacturer's instructions, with the individually measured BC Direct values serving as the starting point. Version 2.0 SR 2 of the Cochlear Fitting software was used for all fittings. All automatic algorithms such as noise reduction or automatic directionality were switched off. For all tests, the everyday program was used with the following settings: microphone set to omnidirectional mode, feedback manager set to default, and position compensation set to "on." No additional fine tuning was administered.

After an acclimatization period of 30 minutes, the following three measurements were performed in the sound field: (1) aided thresholds using narrow band noise, (2) aided speech understanding in quiet using German monosyllabic words (Freiburger word test) at a presentation level of 65 dB SPL, and (3) aided speech understanding in noise using the German Oldenburger sentence test (OLSA) [19]. The OLSA uses an adaptive test procedure to estimate the signal-to-noise ratio (SNR) required for 50% speech understanding. It consists of 40 lists of 30 test sentences each and an accompanying noise signal (speech babble) generated by superimposing all test items. The noise level was held constant at 65 dB SPL and the presentation level of the test sentences was varied adaptively according to the number of correctly repeated words, as prescribed by the predefined OLSA test paradigm [19]. Two training lists were administered before the actual testing. The results of the training lists were not used.

2.4. Test Rooms and Test Equipment. All measurements took place in a double-walled sound attenuating chamber (6.0 × 4.1 × 2.2 m) with an almost frequency independent average reverberation time of 0.14 s. Speech in quiet and sound field thresholds measurements were measured with a clinical audiometer (GSI61; Grason-Stadler, Mildford, NH, USA) using an active loudspeaker (Type 1030A, Genelec, Iisalmi, Finland) placed 1 m in front of the listener. For speech understanding in noise, an Audiobox amplifier (Merz Medizintechnik, Reutlingen, Germany) and a Control 1 Pro loudspeaker (JBL Ins., CA, USA) positioned at a distance of 1 m from the listener was used.

2.5. Statistical Analysis. Results were analyzed using Prism 5 and Instat 3.10 (both from GraphPad Inc., La Jolla, CA, USA). The Friedman test (repeated measures nonparametric ANOVA) and Dunn's comparisons as posttests were used for comparisons between the different transmission paths. Mann-Whitney tests were used for comparisons between the MIX and the SSD group in Section 3.4. All statistical analyses were either performed or supervised by a certified statistician (last author Martin Kompis).

3. Results

3.1. Hearing Thresholds through the Different Transmission Paths. Hearing thresholds were measured twice through each of the 4 transmission paths: once using BC Direct, that is, measuring the BC thresholds with the sound processor as the signal generator, and once as aided sound field thresholds, where the sound processor acts as a hearing amplifier in its clinically intended way. The most important difference between the two measures was that any additional damping in the transmission path may be compensated by suitably fitting the sound processor in the sound field measurement, but not in BC Direct measurement.

Figure 4 shows the BC Direct thresholds of all 16 participants. Below 1000 Hz, all thresholds are similar and no statistically significant differences are found ($P > 0.05$). Above 1000 Hz, the Friedman test shows significant differences ($P \leq 0.0072$). The posttests reveal that the difference lies between the better threshold with the abutment and the other 3 transmission paths, but not between Magnet 3, Magnet 5, and the Testband. The difference between the abutment and the other 3 paths lies between 11.9 dB and 23.3 dB for the frequency range of 4 to 8 kHz.

Figure 5 shows the sound field thresholds in the unaided and in the aided condition using all 4 transmission paths. For all aided conditions and at all frequencies, the aided thresholds are significantly better than the unaided thresholds. Stars denote statistically significant differences ($P < 0.05$) between the aided conditions.

Aided thresholds are similar in the middle frequency range (500 to 2000 Hz) but differ at 250 Hz ($P = 0.0016$) and above 3000 Hz ($P < 0.011$). Again, the statistical posttests show that it is the difference between the abutment and the other conditions, and not between the 3 other transmission paths, which is statistically significant. In the frequency range 4000 to 8000 Hz, the difference between the abutment and the other 3 transmission paths is smaller by approximately 3 dB than that for the BC Direct measurement in Figure 4.

3.2. Aided Speech Understanding. Figure 6 shows the results for aided speech understanding in quiet at a presentation level of 65 dB. Average scores decrease from the abutment setting to the testband (difference of 17% points) with the scores for "Magnet 3" and "Magnet 5" lying in between. Despite substantial variations between the participants, the differences are statistically significant (Friedman test $P = 0.01$). Dunn's posttests reveal that the difference between "Abutment" and "Magnet 5" as well as between "Abutment" and "Testband" is significant ($P < 0.05$). No significant difference was found between Magnet 3 and Magnet 5.

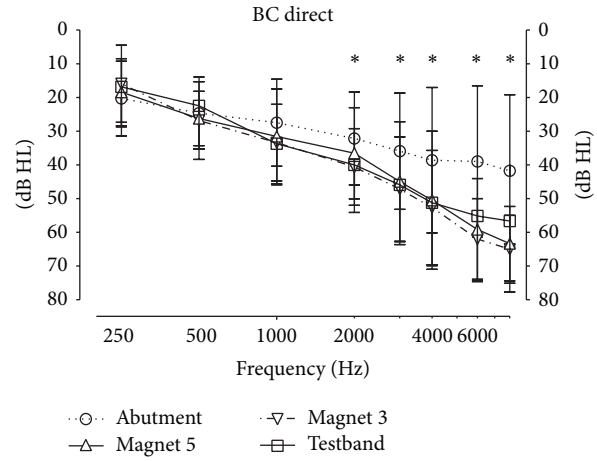

Figure 4: Hearing thresholds measured directly through the sound processor. Stars denote statistically significant difference ($P < 0.05$) between the 4 transmission paths at this frequency.

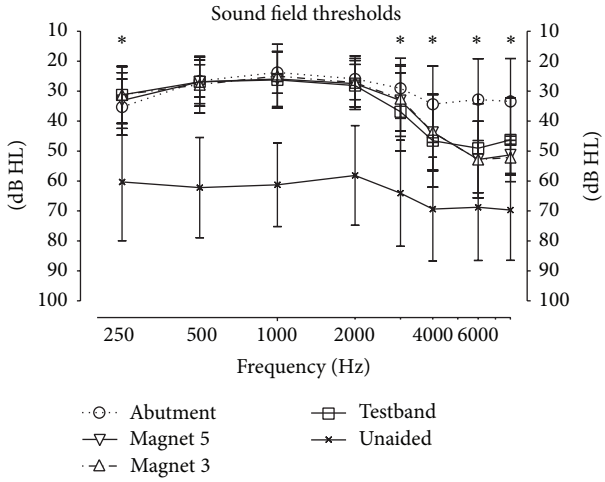

Figure 5: Unaided and aided sound field thresholds. Stars denote statistically significant difference ($P < 0.05$) between the 4 aided thresholds (4 transmission paths) at the given frequency.

Figure 7 shows the results for speech understanding in noise. Here, lower SNRs denote better speech understanding in noise. The differences between the means are small (max difference 2.0 dB) but still statistically significant ($P = 0.02$). The posttests show that the significant ($P < 0.05$) differences are between "Abutment" and "Testband" and between "Testband" and "Magnet 5." Again, no significant difference was found between "Magnet 3" and "Magnet 5."

3.3. Relationship between Unaided BC Thresholds and Speech Understanding. The attenuation introduced by the Baha Attract system can be partially compensated by proper adjustment of the sound processor. This can be seen by comparing Figures 4 and 5. Users with relatively good BC hearing thresholds can therefore be expected to experience only small

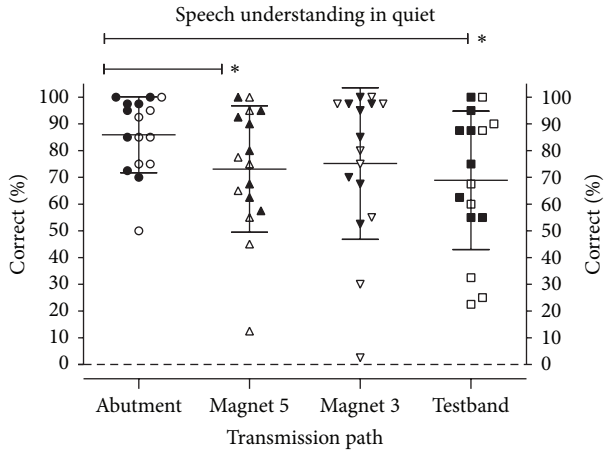

Figure 6: Monosyllabic word understanding in quiet at 65 dB SPL. Data points denote individual results (filled symbols: group SSD; empty symbols: group MIX), and horizontal lines denote mean values and standard deviations. Stars denote statistically significant differences ($P < 0.05$).

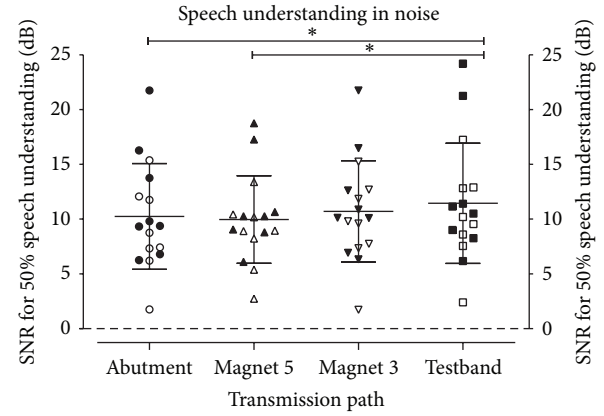

Figure 7: Speech understanding in noise. Lower SNRs denote better speech understanding. Data points denote individual results (filled symbols: group SSD; empty symbols: group MIX), and horizontal lines denote mean values and standard deviations. Stars denote statistically significant differences ($P < 0.05$).

or even no detrimental effect from using the Baha Attract system. In the higher frequency range, compensation is only partial (Figure 5). It is conceivable that mainly users with a more pronounced hearing loss might suffer a noticeable decrease in speech understanding when choosing a Baha Attract system instead of the current solution with the skin penetrating abutment.

Aided thresholds and aided speech understanding are known to correlate well with the BC threshold of the better ear [20]. This correlation is better than the correlation with, for example, AC thresholds or with the BC threshold of the poorer ear [20]. The largest difference between the "Abutment" and the "Magnet" transmission paths shows in the high frequency region above 3000 Hz. Figure 8 shows the loss of speech understanding when changing from the "Abutment" to the "Magnet 3" transmission as a function of the average BC thresholds at 4, 6, and 8 kHz. Scale-out was observed in 4 subjects at 6 or 8 kHz, never at 4 kHz. In cases of scale-out, audiometer limits were used. This may lead to a small compression at the right side of the graph in Figure 8 when compared to the real, but not readily measurable BC thresholds of these few subjects.

Both parts of the figure show the data points for each participant and an exponential (nonlinear) fit. There is a substantial spread of individual data points. Nevertheless, a tendency towards higher SNRs required for speech understanding in noise can be seen starting from around 40 dB average BC hearing loss. For speech in quiet (lower panel of Figure 8), there is a drop that similarly starts to be clinically significant around an average BC hearing loss of approximately 30 to 45 dB.

3.4. Single Sided Deafness versus Mixed Hearing Loss. So far, all data of the SSD and of the MIX group were pooled and analyzed together. This is based on the hypothesis, that the change in the transmission path should affect patients in both groups similarly, previously discussed.

To test whether this hypothesis can be substantiated by our data, the difference between the 2 groups of patients (MIX and SSD) was analyzed. For each of the 4 measurements (BC Direct, aided sound field thresholds, speech in quiet, and speech in noise), the difference between the "Abutment" and the "Magnet 3" setting was analyzed. Data for "Magnet 3" rather than for "Magnet 5" are shown here, as these differences might be expected to be larger due to the weaker coupling to the skin, although no significant differences between the two magnets were found in our data.

For the BC Direct thresholds over the 8 frequencies 250, 500, 1000, 2000, 3000, 4000, 6000, and 8000 Hz, the average difference between "Abutment" and "Magnet 3" ranges from −6.9 dB to +25.5 for the SSD group and between −1.9 dB and +26.3 dB for the MIX group. Even before correction for multiple testing, the difference between the two groups is not statistically significant at any of the 8 frequencies (Mann-Whitney test, $P = 0.37$ to 0.99).

Similarly, for aided sound field thresholds over the same 8 frequencies between 250 and 8000 Hz, the average difference between "Abutment" and "Magnet 3" ranges from −6.3 dB to +18.1 for the SSD group and between −1.9 dB and +23.1 dB for the MIX group. Again, even before correction for multiple testing, the difference between the two groups is not statistically significant at any of the 8 frequencies (Mann-Whitney test, $P = 0.22$ to 0.62).

Table 1 summarizes the comparison between the SSD group and the MIX group for speech in quiet and for speech in noise. Again, the differences between the MIX and the SSD groups are not statistically significant for either speech test.

4. Discussion

Our data suggest that the nonskin penetrating Baha Attract system should be helpful and beneficial for patients. Although on average speech understanding in quiet does decrease, if compared to the direct bone conduction through the

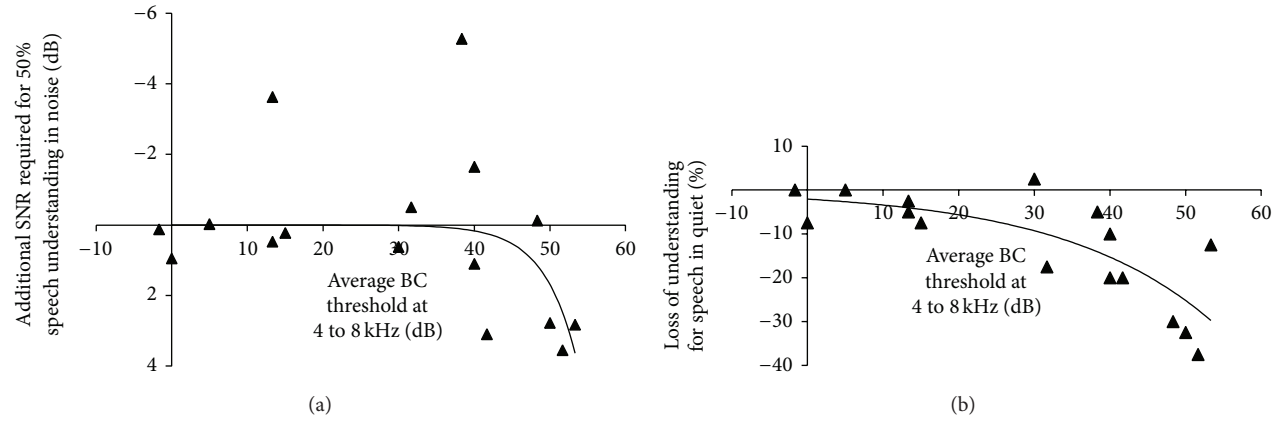

Figure 8: Difference between speech understanding in the "Abutment" and the "Magnet 3" condition as a function of the average BC hearing loss of the better ear at 4, 6, and 8 kHz. Data points for individual subjects and nonlinear regression lines are shown. (a) Speech understanding in noise. (b) Speech understanding in quiet. In both panels, data points closer to the bottom of the graph denote lower speech understanding with Magnet 3.

Table 1: The difference (decrease) in speech understanding between the "Abutment" and the "Magnet 3" transmission paths is not statistically significantly different between the two subgroups SSD and MIX either in quiet or in noise.

Measurement	Group SSD (mean ± SD)	Group MIX (mean ± SD)	Difference between groups
Speech in quiet	15.0 ± 20.8%	6.6 ± 8.3%	8.4% ($P = 0.75$)
Speech in noise	−0.8 ± 1.8 dB	0.2 ± 2.9 dB	−1.0 dB ($P = 0.80$)

abutment, the difference is small (10.8% points for Magnet 3 and 12.8% points for Magnet 5) and not statistically significant. The drop is even smaller than that for the "Testband" transmission path, which is used frequently by audiologists for preoperative testing. As a consequence, preoperative tests with a testband should be useful and valid predictors for the postoperative outcome with the Baha Attract system.

The additional attenuation of the Baha Attract system increases from around 5 dB at 1 kHz to 20–25 dB at 6 to 8 kHz, when compared to the abutment (Figure 4). In contrast, speech reception scores show only a relatively small drop. The probable reason for this difference is suggested by the aided sound field thresholds in Figure 5. As the sound processor was fitted for each transmission path separately, there is a good compensation of the additional attenuation for frequencies up to approximately 3000 Hz. For 4000 Hz to 8000 Hz, there is still a partial compensation. Thus a large portion of the frequency spectrum which is important for speech understanding remains almost unaffected. Consequently, speech understanding scores can be reasonably expected to remain high in Baha Attract users.

All tests were performed with two different magnets. No significant difference between the two magnets (3 and 5) was found in any of the tests (BC Direct, aided sound field thresholds, speech understanding in quiet, and speech understanding in noise; Figures 4 to 7). A probable reason for this finding is that the thickness of the artificial skin is not affected significantly by the pressure of the magnets. Young's modulus of the skin sample was estimated to be around 83000 N/m^2 (±11%) from a series of simple measurements. The relatively low pressures of less than 2200 N/m^2 even by Magnet 5 will therefore cause a compression of 0.15 mm or less. This small deformation does not change the density or elastic properties of the skin sample significantly.

This raises the following question: how realistic the experimental setup with the artificial skin depicted in Figure 2(b) is. Figure 4 shows the frequency dependent attenuation through the system, measured psychoacoustically using the BC Direct method. It can be seen that thresholds are not significantly different from the attenuation of the patients' own, real skin with the testband in the same figure. Similar frequency dependences and magnitudes of the sound attenuation of real skin in patients have also been published earlier by other groups (e.g., [17, 21]). This suggests that the artificial skin does indeed mimic real skin reasonably well.

It is known that skin thickness behind the ear does vary between patients [10], but different skin thicknesses were not compared in this investigation. The thickness of the artificial skin (5.6 mm) used in this study is close to the maximum thickness (6 mm) of soft tissue recommended by the manufacturer. For higher values, the manufacturer recommends soft tissue thinning. Preliminary trials with a double layer of the artificial skin, which would then correspond roughly to the upper limit of the skin thickness found on the mastoid [10], showed that even the strongest magnet currently available could not hold the sound processor in place sufficiently.

Our comparisons of the two patient groups (SSD and MIX) suggest that there are no significant differences in how hearing and speech understanding are affected by switching

from a skin penetrating abutment to a nonskin penetrating Baha Attract transmission path. These findings confirm that it is admissible to group the data of the two populations for analysis. More importantly, however, they suggest that there is currently no reason to limit the Attract system to only one of these patient groups.

5. Conclusion

The nonskin penetrating Baha Attract system offers a new approach of partially implantable bone conduction hearing aids. In the preimplantation tests reported here, it was found that there is an additional attenuation, ranging from approximately 5 dB at 1000 Hz to 20–25 dB above 6000 kHz, when compared to the conventional transmission path using an abutment. However, aided sound field hearing thresholds show that a substantial part of this attenuation, mainly in the frequency range up to 3000 Hz, can be compensated by the individual fitting of the sound processor. This is a probable explanation for the relatively minor and statistically nonsignificant differences in speech understanding in quiet and in noise between the two different transmission paths. The loss in speech understanding is even smaller than that for the transmission through a testband, a method that is commonly used preoperatively to test the system. On the basis of this preimplantation trial, it can be reasonably expected that the nonskin penetrating Baha Attract system will be useful and beneficial for patients.

Conflict of Interests

Coauthor Mark Flynn is employed by Cochlear Bone Anchored Hearing Solutions, Mölnlycke, Sweden.

Acknowledgments

The work of Anja Kurz has been supported by a research grant from Cochlear Bone Anchored Hearing Solutions, Sweden, and by Cochlear Europe.

References

[1] B. Hakansson, A. Tjellstrom, U. Rosenhall, and P. Carlsson, "The bone-anchored hearing aid. Principal design and a psychoacoustical evaluation," *Acta Oto-Laryngologica*, vol. 100, no. 3-4, pp. 229–239, 1985.

[2] H. T. Faber, C. A. J. Dun, R. C. Nelissen, E. A. M. Mylanus, C. W. R. J. Cremers, and M. K. S. Hol, "Bone-anchored hearing implant loading at 3 weeks: stability and tolerability after 6 months," *Otology and Neurotology*, vol. 34, no. 1, pp. 104–110, 2013.

[3] F. Pfiffner, M. D. Caversaccio, and M. Kompis, "Comparisons of sound processors based on osseointegrated implants in patients with conductive or mixed hearing loss," *Otology & Neurotology*, vol. 32, no. 5, pp. 728–735, 2011.

[4] A. Kurz, M. Caversaccio, and M. Kompis, "Hearing performance with 2 different high-power sound processors for osseointegrated auditory implants," *Otology and Neurotology*, vol. 34, no. 4, pp. 604–610, 2013.

[5] A. Mudry and A. Tjellström, "Historical background of bone conduction hearing devices and bone conduction hearing aids," *Advances in Oto-Rhino-Laryngology*, vol. 71, pp. 1–9, 2011.

[6] B. Håkansson, G. Lidén, A. Tjellström et al., "Ten years of experience with the Swedish bone-anchored hearing system," *The Annals of Otology, Rhinology & Laryngology, Supplement*, vol. 151, pp. 1–16, 1990.

[7] A. McDermott and P. Sheehan, "Paediatric baha," *Advances in Oto-Rhino-Laryngology*, vol. 71, pp. 56–62, 2011.

[8] J. J. Wazen, J. B. Spitzer, S. N. Ghossaini et al., "Transcranial contralateral cochlear stimulation in unilateral deafness," *Otolaryngology—Head and Neck Surgery*, vol. 129, no. 3, pp. 248–254, 2003.

[9] J. J. Wazen, B. Wycherly, and J. Daugherty, "Complications of bone-anchored hearing devices," *Advances in Oto-Rhino-Laryngology*, vol. 71, pp. 63–72, 2011.

[10] H. T. Faber, M. J. F. De Wolf, J. W. J. de Rooy, M. K. S. Hol, C. W. R. J. Cremers, and E. A. M. Mylanus, "Bone-anchored hearing aid implant location in relation to skin reactions," *Archives of Otolaryngology—Head and Neck Surgery*, vol. 135, no. 8, pp. 742–747, 2009.

[11] S. Negri, O. Bernath, and R. Häusler, "Bone conduction implants: xomed audiant bone conductor(TM) vs. BAHA," *Ear, Nose and Throat Journal*, vol. 76, no. 6, pp. 394–396, 1997.

[12] R. Siegert and J. Kanderske, "A new semi-implantable transcutaneous bone conduction device: Clinical, surgical, and audiologic outcomes in patients with congenital ear canal atresia," *Otology and Neurotology*, vol. 34, no. 5, pp. 927–934, 2013.

[13] R. Siegert, "Partially implantable bone conduction hearing aids without a percutaneous abutment (otomag): technique and preliminary clinical results," *Advances in Oto-Rhino-Laryngology*, vol. 71, pp. 41–46, 2011.

[14] M. K. S. Hol, R. C. Nelissen, M. J. H. Agterberg, C. W. R. J. Cremers, and A. F. M. Snik, "Comparison between a new implantable transcutaneous bone conductor and percutaneous bone-conduction hearing implant," *Otology and Neurotology*, vol. 34, no. 6, pp. 1071–1075, 2013.

[15] M. Barbara, M. Perotti, B. Gioia, L. Volpini, and S. Monini, "Transcutaneous bone-conduction hearing device: audiological and surgical aspects in a first series of patients with mixed hearing loss," *Acta Oto-Laryngologica*, vol. 133, no. 10, pp. 1058–1064, 2013.

[16] M. Kompis, M. Krebs, and R. Häusler, "Speech understanding in quiet and in noise with the bone-anchored hearing aids Baha Compact and Baha Divino," *Acta Oto-Laryngologica*, vol. 127, no. 8, pp. 829–835, 2007.

[17] A. J. Zarowski, N. Verstraeten, T. Somers, D. Riff, and E. F. Offeciers, "Headbands, testbands and softbands in preoperative testing and application of bone-anchored devices in adults and children," *Advances in Oto-Rhino-Laryngology*, vol. 71, pp. 124–131, 2011.

[18] M. C. Flynn and M. Hillbratt, "Improving the accuracy of Baha fittings through measures of direct bone conduction," *Clinical and Experimental Otorhinolaryngology*, vol. 5, supplement 1, pp. S43–S47, 2012.

[19] K. Wagener, T. Brand, and B. Kollmeier, "Entwicklung und evaluation eines satztestes für die deutsche sprache teil III: evaluation des oldenburger satztestes," *Audiologic Acoustic*, vol. 38, pp. 86–95, 1999.

[20] F. Pfiffner, M. Kompis, and C. Stieger, "Bone-anchored hearing aids: correlation between pure-tone thresholds and outcome in

three user groups," *Otology and Neurotology*, vol. 30, no. 7, pp. 884–890, 2009.

[21] N. Verstraeten, A. J. Zarowski, T. Somers, D. Riff, and E. F. Offeciers, "Comparison of the audiologic results obtained with the bone-anchored hearing aid attached to the headband, the testband, and to the "snap" abutment," *Otology and Neurotology*, vol. 30, no. 1, pp. 70–75, 2009.

Hindawi Publishing Corporation
BioMed Research International
Volume 2014, Article ID 532570, 9 pages
http://dx.doi.org/10.1155/2014/532570

Research Article

Definition of Metrics to Evaluate Cochlear Array Insertion Forces Performed with Forceps, Insertion Tool, or Motorized Tool in Temporal Bone Specimens

Yann Nguyen,[1,2,3] Guillaume Kazmitcheff,[2,3] Daniele De Seta,[2,3,4] Mathieu Miroir,[2,3] Evelyne Ferrary,[1,2,3] and Olivier Sterkers[1,2,3]

[1] *Otolaryngology Department, Unit of Otology, Auditory Implants and Skull Base Surgery, Hospital Pitié Salpêtrière, 47-83 Boulevard de l'Hôpital, Cedex 13, 75651 Paris, France*
[2] *Sorbonne University, "Minimally Invasive Robot-Based Hearing Rehabilitation", UPMC Univ Paris 06, UMR S 1159, 75005 Paris, France*
[3] *INSERM, "Minimally Invasive Robot-Based Hearing Rehabilitation", UMR S 1159, 75018 Paris, France*
[4] *Sensory Organs Department, Sapienza University of Rome, 00100 Rome, Italy*

Correspondence should be addressed to Yann Nguyen; yann.nguyen@inserm.fr

Received 14 February 2014; Accepted 17 June 2014; Published 15 July 2014

Academic Editor: Peter Brett

Introduction. In order to achieve a minimal trauma to the inner ear structures during array insertion, it would be suitable to control insertion forces. The aim of this work was to compare the insertion forces of an array insertion into anatomical specimens with three different insertion techniques: with forceps, with a commercial tool, and with a motorized tool. *Materials and Methods*. Temporal bones have been mounted on a 6-axis force sensor to record insertion forces. Each temporal bone has been inserted, with a lateral wall electrode array, in random order, with each of the 3 techniques. *Results*. Forceps manual and commercial tool insertions generated multiple jerks during whole length insertion related to fits and starts. On the contrary, insertion force with the motorized tool only rose at the end of the insertion. Overall force momentum was 1.16 ± 0.505 N (mean ± SD, $n = 10$), 1.337 ± 0.408 N ($n = 8$), and 1.573 ± 0.764 N ($n = 8$) for manual insertion with forceps and commercial and motorized tools, respectively. *Conclusion*. Considering force momentum, no difference between the three techniques was observed. Nevertheless, a more predictable force profile could be observed with the motorized tool with a smoother rise of insertion forces.

1. Introduction

Cochlear implant is a neural prosthesis that is inserted within the cochlea into the scala tympani in order to electrically stimulate spiral ganglion fibers from the auditory nerve. It has become the most efficient device to rehabilitate patients suffering from severe to profound deafness [1]. Three critical steps can be identified in the cochlear implantation procedure: approach to cochlea, cochlea opening, and array insertion. Minimizing trauma during the cochlear implantation procedure is critical to preserve residual hearing in case of acoustic electric stimulation or remaining inner ear structures in case of electric stimulation only [2]. Even though multiple approaches can be performed to access cochlea such as suprameatal, transcanal, or minimally invasive key-hole access, the routine exposure of the cochlea in a vast majority of cochlear implant centers is mastoidectomy followed by posterior tympanotomy [3]. The cochlea opening through the round window membrane, a cochleostomy, or an extended round window approach remains a current debate frequently discussed [4]. These two first steps determine the axis and the entry point of the array into the cochlea. Considering solutions to reduce trauma during the array insertion, most studies compared array designs [5] and evaluated histological trauma [6] or insertion forces [7]. Even though the insertion technique remains critical for inner ear structure

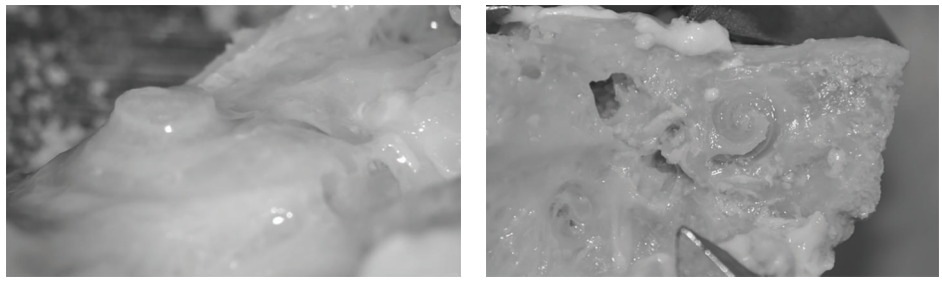

(a) (b)

Figure 1: Microdissected cochlea model. (a) A wide canal wall down mastoidectomy is performed to expose the cochlea. The otic capsule is then thinned with a diamond burr (left cochlea). (b) The scalae vestibuli and media are then carefully opened to expose the basilar membrane leaving the scala tympani intact (right cochlea).

preservation to achieve insertion with minimal trauma, it is seldom studied. The insertion technique will be influenced by tremor, insertion speed, and duration and possibilities of insertion axis modification including torque around the array body. It is usually performed manually using forceps, microforceps, or a dedicated tool depending on the array design. Arrays including a stylet can offer various insertion techniques depending on stylet removal timing [8]. Speed of insertion or use of lubricant have also been studied and have been shown to influence frictions forces [9, 10]. Manual insertion with forceps has been compared to robotic insertion [11] but has never been compared to the insertion with other technique with specific tool. Motorization of the tool could also be employed to reduce fits and start inherent to manual insertion as it is hard to insert the array in a single move with forceps grasping. The goal of the present work was to compare cochlear array insertion forces performed by forceps, an insertion tool, or a motorized tool in temporal bone specimens with the same array design.

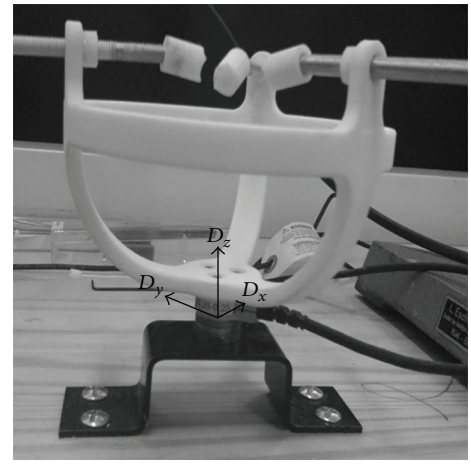

Figure 2: Insertion force measurement setup. A plastic temporal bone holder was screwed on a 6-axis force sensor (ATI Nano 17, Apex, NC) to record array insertion forces into a temporal bone.

2. Material and Methods

2.1. Human Temporal Bone Preparation. Twenty human temporal bones have been prepared. The cochlea has been exposed through a canal wall down mastoidectomy. A large approach has been chosen to ease bony otic capsule drilling and avoid direct contact of the forceps, insertion tool, or motorized tool with the temporal bone. The bony otic capsule has been thinned using diamond burrs under microscope (Figure 1(a)). The scala vestibuli and the scala media have then been carefully opened taking care to respect the basilar membrane integrity from the round window to the apex (Figure 1(b)). This allowed visualization of the array progression during its insertion by transparency through the basilar membrane. This also allowed checking basilar membrane integrity and the lack of scalae translocation during insertion. An extended round window cochleostomy has then been drilled in the inferior rim of the round window. Temporal bones were then mounted on an in-house made temporal bone holder that could be fixed to a force sensor (Figure 2). The temporal bones specimens, fixed on the force sensor, have been oriented to align the array insertion axis, the scala tympani midline, and the D_z axis of the 6-axis force sensor. Cochleostomy was irrigated with saline serum before each insertion.

2.2. Electrode Array. Hifocus 1J arrays (Advanced Bionics, Valencia, CA) have been used in this study. 1J array is a lateral wall positioning array bearing 16 electrodes. A silicon jog is placed at its base in order to push the array with an insertion tool. This jog slides into the insertion tube and serves as the contact point for array propulsion inside the insertion tube by a rod. The array has a total length of 25 mm from the jog to the tip, an active length of 17 mm, a proximal diameter of 0.8 mm, and a distal diameter of 0.4 mm. Each array was used for two insertions and then discarded.

2.3. Insertion Protocol and Insertion Force Measurements. Frictions forces between the array and the cochlea have been recorded with a 6-axis force sensor (ATI Nano 17, calibration type SI-12-0.12, resolution: 3 mN, Apex, NC). Sensor data have been recorded in real-time via the same analog to digital interface card controlling the actuator input power at

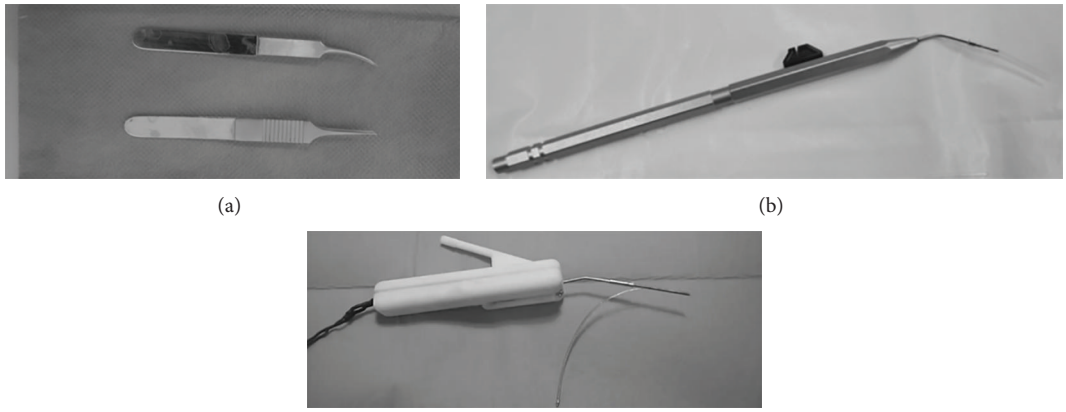

(a) (b) (c)

Figure 3: Tools and devices used in this study to insert array on temporal bones. (a) Microforceps claws, (b) Hifocus 1J tool (Advanced Bionincs, Valencia, USA), and (c) insertion with an in-house motorized tool.

a sample rate of 100 Hz. From the 6-axis sensor, insertion forces were computed only based on linear force norms (D_x, D_y, D_z).

Three insertion tools and techniques were randomly tested:

(i) manual insertion using two microforceps claws (Figure 3(a));

(ii) insertion with the Hifocus 1J electrode insertion tool (Figure 3(b)), a commercially available tool distributed with Hifocus 1J and helix array; it is composed of a handle comprising a flexible shaft connected to a slide that can eject out of an insertion tube the array by pushing its silicon jog. We have been using the metal insertion tube (AB-6135, Advanced bionics, Valencia, CA) in this study. This tool was held manually during insertion;

(iii) insertion with an in-house made motorized insertion tool (Figure 3(c)). This tool comprised a rotary actuator (RE10CLL, MDP, Miribel, France) connected to a threaded screw that pushed a blunt pin into an insertion tube loading the array. The tool was held steady by a flexible arm. No force feedback loop between this tool and the force sensor was applied. The actuator speed was controlled via laboratory power supply and set at 0.8 mm·s^{-1}.

During each insertion, a particular attention was made to avoid touching directly the temporal bone with forceps or insertions tools in order to avoid artefact recording of the force sensor. For the manual and commercial tool techniques, the operator's hands were supported on a flexible arm with a metal bar similarly to a Yasargil bar as it has been shown that supporting the wrists significantly decreases the amplitude of the tremor [12]. Force measurement was coupled to video recording through the microscope to collect force data from the beginning to the end of the insertion only.

Each temporal bone was inserted three times with the three different insertions techniques in an order that was randomized. If a basilar membrane perforation occurred during insertion, the temporal bone was excluded for analysis.

2.4. Metrics Analysis. We investigated the shape of the curve corresponding to the force versus the time. In order to do so, we have built different metrics.

(i) The peak of force applied during the insertion: this metric quantifies a potential damage of the cochlea if an excessive force is applied. Thus, the study of the peak of force allows us to identify if an insertion method may guaranty a lower maximal force.

(ii) The total change in momentum (I, in Ns) was produced during the insertion, measured by $I = \int F(t)dt$.

(iii) The number of occurrence (Th) where the applied forces were over an arbitrary threshold, fixed at 0.1 N that may yield to severe damage of anatomical structure within the cochlea: this threshold value corresponds to the peak force at the end of a complete insertion of array in temporal bones from previously published data [7].

(iv) The number of times (G) where forces (F) were increased by 50% (sudden rise) within a small time step $h = t - (t - 1) = 0.1$ s: it corresponded to the number of local discontinuities of the applied forces and possibly to the number of potential local damages into the cochlea. Consider

$$G_t = \begin{cases} G_t - 1 + 1, & \text{if } \dfrac{F_t}{F_t - 1} \geq 2, \\ G_t - 1, & \text{otherwise.} \end{cases} \quad (1)$$

(v) The smoothness of the curve, studied as "jerk" variation (J) (expressed as N·s^{-1}): it is obtained from the derivative of the force over the time. A root mean

square (RMS) function was used to analyze the jerk variation. Consider

$$\text{RMS} = \sqrt{\frac{1}{n}\sum_{i=0}^{n-1} J_i^2}, \quad \text{with } J = \frac{dF}{dt}. \tag{2}$$

2.5. Statistical Analysis. Results are expressed as mean ± standard deviation. Data were analyzed and graphics were generated by "R" statistical software (http://www.r-project.org/). Comparisons between different insertions conditions were tested by ANOVA and results are presented with the associated P value for significant data.

3. Results

3.1. Data Collection. A basilar membrane perforation occurred in 7 temporal bones (35%) out of 20. This occurred once with a forceps insertion, 3 times with the Hifocus 1J electrode insertion tool, and 3 times with the motorized insertion. The translocation rate has to be analyzed with precaution due to model preparation. While giving immediate information during insertion on array translocation, this kind of microdissected model has the drawback of potentially creating histological damages or weakening of the basilar membrane before array insertion [7].

Thus, the implants were inserted three times in the same cochlea in 13 temporal bones (39 insertions). We investigate the possible lesions of the cochlea undergone during the first insertions, in order to determine the presence of a systematic diminution of forces for the second or the third insertions. We found that force peaks of the motorized insertion on third position were significantly different compared to measurement of first and second insertion ($P = 0.0362$). Thus, third insertion could not be used for analysis and all data collected during the third insertion were discarded in all temporal bones. Consequently, insertions forces data were used for analysis in 10 manual insertions, 8 Hifocus 1J electrode insertion tool insertions, and 8 motorized insertions.

3.2. Insertion Force Profiles. Insertion force profiles had a similar shape from one temporal bone to another depending on the insertion technique. With manual forceps insertion technique (Figure 4(a1)), insertion forces remained low in the first half of the insertions with some peaks corresponding to fits and starts when the array was grasped and released multiple times from distal to proximal parts. The amplitude of these peaks rose towards the end of the insertion.

With motorized tool technique, insertion forces remained also low in the first half of the insertion (Figure 4(c1)). It rises slowly afterwards continuously without peak and reached a maximum at the end of the insertion. A plot using force versus angle representing insertions with the motorized tool is represented on Figure 5.

With the Hifocus 1J electrode insertion tool technique (Figure 4(b1)), a mix between the two previously described force profiles was observed with small amplitude peaks distributed along a force profile curve that slowly rises from the second part of the insertion toward the end.

3.3. Metric Analysis. The results from metric analysis are reported in Figure 6 and Table 1. Considering the peak force at the end of the insertion, the Hifocus 1J electrode insertion tool had higher values than techniques with forceps and motorized tool. The momentum was the same for the three techniques. There was less threshold crossing over 0.1 N with the motorized tool compared to Hifocus 1J electrode insertion tool and the forceps manual technique. Sudden rises and jerks happened also less frequently with the motorized tool compared to manual insertion and Hifocus 1J electrode insertion tool (Figures 4(a2), 4(b2), and 4(c2)).

4. Discussion

In this study, we compared cochlear array insertion forces performed manually with forceps, an insertion tool, or a motorized tool in temporal bone specimens with the same array design. We have shown that there was no difference between the three techniques for peak force and total force value. A more predictable insertion force curve with less peak and rises was seen with the motorized tool compared to the two other insertion tools.

4.1. Advantages and Drawbacks of the Three Insertion Techniques. Each of the three techniques has advantages and drawbacks. Manual insertion with forceps is commonly used because it is compatible with most of the clinically available array device, especially straight arrays. One claw forceps is used to push the array while the other is used to guide the insertion axis. Depending on array length and stiffness, full insertion of the array cannot always be performed in single step and may require multiples grasps to insert the whole array, segment after segment. These fits and starts during the insertion procedure might generate multiple short peak forces during insertion as we observed in the present study. Resistance feedback can be perceived once a physiological threshold is reached. The force feedback sensitiveness depends on wearing gloves and is clearly subject to variability between surgeons. Furthermore this technique is subject to human limitation in terms of accuracy and tremor [13].

Insertion with the Hifocus 1J electrode insertion tool is only possible with 1J and Helix arrays because it requires a silicon jog on the array. It offers an increased stability as the insertion tube can be leant on the posterior part of the posterior tympanotomy during array insertion. The tool only requires one hand to function, thus the second hand can be used as a stabilizer to further reduce tremor. Drawbacks are represented by a lack of resistance feedback feeling because friction forces within the tool and insertion tube might interfere with surgeon sensitiveness on friction forces within the cochlea [14]. Furthermore, due to insertion tube diameter, vision of the cochleostomy or round window can be reduced a little compared to a manual forceps technique. At last the stroke of the slide of the tool can require a two-step push

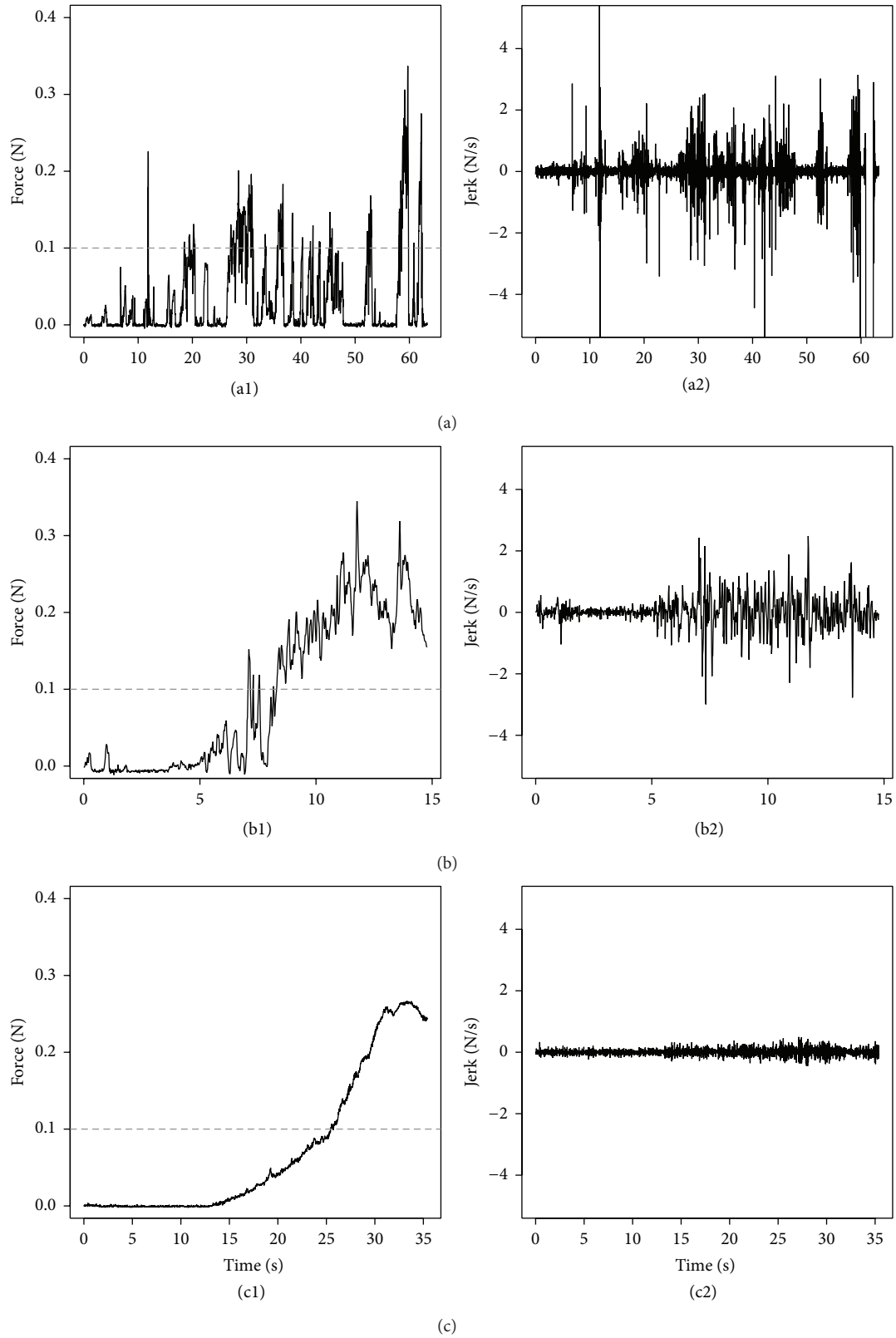

FIGURE 4: Insertion force profile and jerk of a 1J array with 3 different insertion techniques in the same temporal bone. (a) Manual insertion with microforceps claws tool, (b) insertion with Hifocus 1J electrode insertion tool, and (c) insertion with an in-house motorized tool. Left pictures ((a1), (b1), and (c1)): insertion forces profiles. Dashed line represents 0.1 N threshold. Peak forces were around 0.3 N for the three insertion techniques. Right pictures ((a2), (b2), and (c2)): jerk. Hifocus 1J electrode insertion tool provided smoother insertion with little jerk compared to manual insertion with forceps. This benefit is even more increased with a motorized tool.

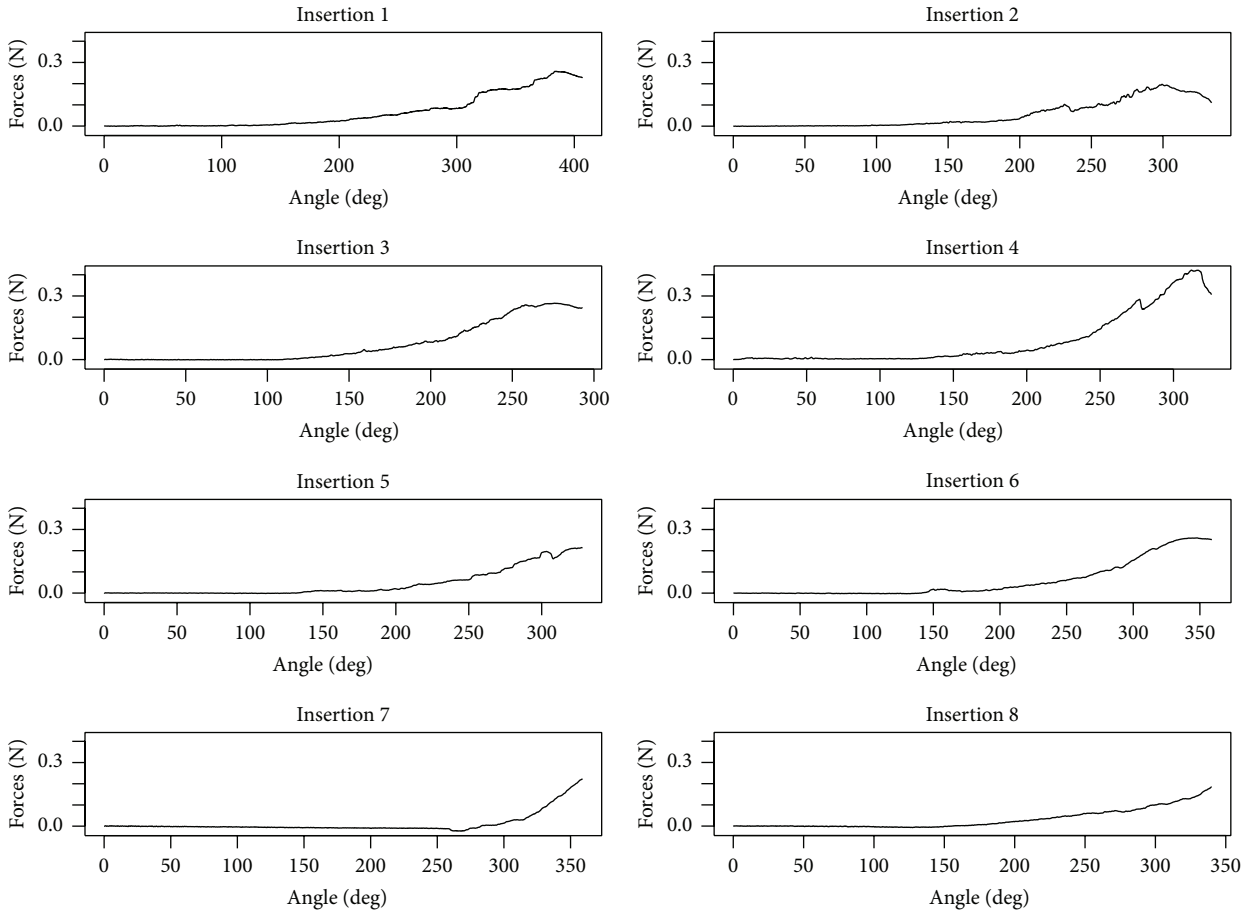

Figure 5: Plot using force versus angle representing insertions with the motorized tool. Insertion forces remain low in the first half on the insertion and then slowly rise with no peak and reach a maximum at the end of the insertion.

Table 1: Metric values recorded during of the cochlear implantation with three different insertion techniques.

Metric	Insertion technique	Mean ± SD	n	P
Peak (N)	Forceps	0.256 ± 0.061	10	NA
	Hifocus tool	0.327 ± 0.055	8	0.028
	Motorized	0.255 ± 0.075	8	NS
Momentum (Ns)	Forceps	1.16 ± 0.505	10	NA
	Hifocus tool	1.337 ± 0.408	8	NS
	Motorized	1.573 ± 0.764	8	NS
Over threshold >0.1 N	Forceps	21.00 ± 12.552	10	NA
	Hifocus tool	7.00 ± 4.036	8	0.002
	Motorized	3.38 ± 3.113	8	0.0002
Sudden rise	Forceps	90.60 ± 46.569	10	NA
	Hifocus tool	28.25 ± 15.872	8	0.0003
	Motorized	14.00 ± 6.949	8	0.00003
Jerk ($N \cdot s^{-1}$)	Forceps	0.467 ± 0.116	10	NA
	Hifocus tool	0.515 ± 0.206	8	NS
	Motorized	0.1553 ± 0.05	8	0.00008

Values are expressed as mean ± SD of n insertion. NA: not applicable; NS: not significant. "Forceps" stands for manual insertion with forceps technique, "Hifocus tool" stands for Hifocus 1J electrode insertion tool technique, and "motorized" stands for our in-house motorized insertion tool technique. Statistical analysis was performed by analysis of variance. Each technique was compared against the manual insertion with forceps technique.

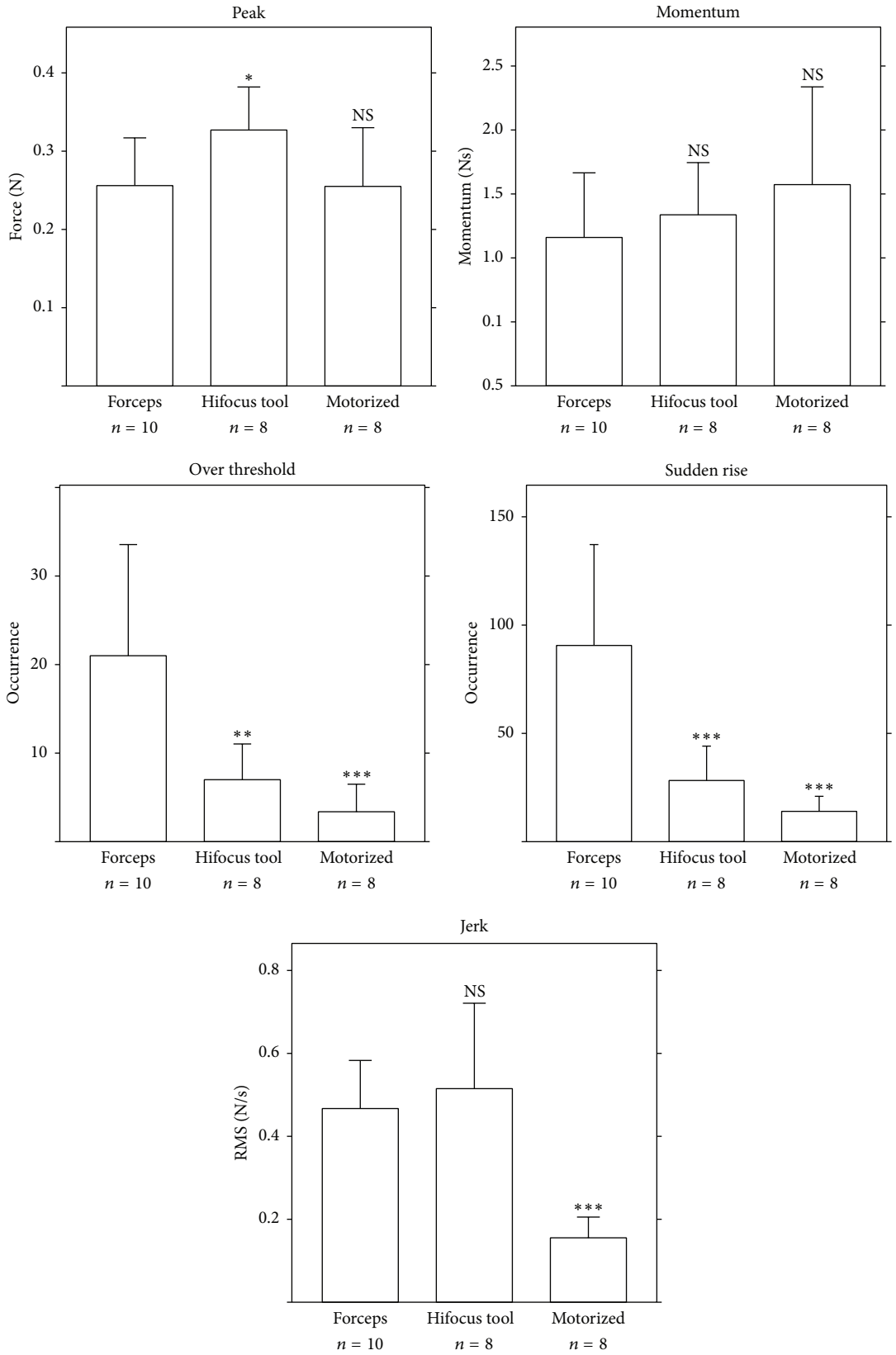

Figure 6: Comparison of insertion forces of cochlear implantation with 5 metrics. Bars represent mean ± SD of n insertions. NS: not significant. "Forceps" stands for manual insertion with forceps technique, "Hifocus tool" stands for Hifocus 1J electrode insertion tool technique, and "motorized" stands for our in-house motorized insertion tool technique. Statistical analysis was performed by analysis of variance. Each technique was compared against the manual insertion with forceps technique.

depending on the finger (thumb or forefinger) that is used to push the slide thus generating a fit and start during insertion.

Insertion with our current version of in-house motorized tool is only possible with 1J and helix because it requires a jog on the device to push the array. It provides a smooth and low speed insertion. Complete insertion can be achieved in a single step. Human hand tremor is removed as the tool is held by a flexible arm. However, force feedback is completely impaired and surgeon can only rely on visual control at the cochleostomy to detect a blockage within the cochlea that will lead to array bending at its proximal part outside the cochlea. Vision is also impaired just as with the tool from the second technique.

4.2. Previous Work on Insertion Technique Comparison and Definition of New Metrics to Study Insertion Forces. Majdani et al. had compared robotic to manual insertion with array using an advance off stylet technique in an artificial model of scala tympani [11]. It has been shown that a greater variability of frictions forces could be observed with a manual array insertion technique with more peaks compared to a robot-based insertion technique. The average force was also compared showing increased force for the robotic insertion compared to manual insertions.

We decided to define new metrics to study and compare insertion forces profiles because average force seems hard to interpret. For example manual insertion with a long duration will necessarily have a lower average force since during pauses for the duration of insertion, there is no effort on the cochlea. We could have compared the technique using forces in Newton versus angle or length of insertion. These data are easy to collect with a constant speed insertion such as the motorized tool but hard to collect with manual and Hifocus 1J electrode insertion tool because the array progression cannot be visualized through the basilar membrane as well as a transparent artificial model of scale tympani and the insertion speed during array progression with manual technique is difficult to collect. One of the limitations of this study is that we were not able to control or measure the insertion speed when using the manual or commercial tool technique.

No force sensor was mounted on the motorized insertion tool. Thus insertions with this tool were not force feedback controlled. Frictions of the array within the insertion tube of the commercial tool could impair surgeon's force feedback feeling. Thus, force feedback could only be perceived with the manual technique. This might account for the different basilar membrane perforation rates among the three techniques.

The new metrics that we have defined can help forces profiles analyses by giving absolute values such as the peak force or the forces momentum but also information on sudden forces changes or rises.

5. Conclusion and Perspectives

We have validated the use of metrics such as peak force, momentum of the force, threshold crossing over 0.1 N, sudden rises, and jerks that could be indicators of the quality of surgical gesture during cochlear implantation. The analysis of these metrics in insertion allows demonstrating that the Hifocus 1J electrode insertion with a commercial guided tool has less threshold crossing over 0.1 N and sudden rises compared to a manual insertion performed with forceps. These drawbacks are even more reduced with a motorized tool leading to a smoother insertion. Next step will be to introduce a force feedback control loop between the motorized tool and the force sensor in order to reduce the insertion peaks (in amplitude and in duration) and to stop the insertion in case of abnormal force sudden rise. If those parameters can be controlled, it should be possible to enhance the safety of cochlear implantation.

Conflict of Interests

The authors declare that there is no conflict of interests regarding the publication of this paper.

Acknowledgment

Authors would like to thank Advanced Bionics (Valencia, USA) for providing 1J Arrays, Hifocus 1J electrode insertion tools, and financial support to UMR-S 1159 for this study.

References

[1] B. S. Wilson and M. F. Dorman, "Cochlear implants: a remarkable past and a brilliant future," *Hearing Research*, vol. 242, no. 1-2, pp. 3–21, 2008.

[2] M. L. Carlson, C. L. Driscoll, R. H. Gifford et al., "Implications of minimizing trauma during conventional cochlear implantation," *Otology & Neurotology*, vol. 32, no. 6, pp. 962–968, 2011.

[3] M. E. Zernotti, A. Suárez, V. Slavutsky, L. Nicenboim, M. F. Di Gregorio, and J. A. Soto, "Comparison of complications by technique used in cochlear implants," *Acta Otorrinolaringologica Espanola*, vol. 63, no. 5, pp. 327–331, 2012.

[4] S. Havenith, M. J. W. Lammers, R. A. Tange et al., "Hearing preservation surgery: cochleostomy or round window approach? A systematic review," *Otology and Neurotology*, vol. 34, no. 4, pp. 667–674, 2013.

[5] Y. Nguyen, I. Mosnier, S. Borel et al., "Evolution of electrode array diameter for hearing preservation in cochlear implantation," *Acta Oto-Laryngologica*, vol. 133, no. 2, pp. 116–122, 2013.

[6] A. A. Eshraghi, N. W. Yang, and T. J. Balkany, "Comparative study of cochlear damage with three perimodiolar electrode designs," *Laryngoscope*, vol. 113, no. 3, pp. 415–419, 2003.

[7] Y. Nguyen, M. Miroir, G. Kazmitcheff et al., "Cochlear implant insertion forces in microdissected human cochlea to evaluate a prototype array," *Audiology and Neurotology*, vol. 17, no. 5, pp. 290–298, 2012.

[8] D. Schurzig, R. J. Webster, M. S. Dietrich, and R. F. Labadie, "Force of cochlear implant electrode insertion performed by a robotic insertion tool: comparison of traditional versus advance off-stylet techniques," *Otology & Neurotology*, vol. 31, no. 8, pp. 1207–1210, 2010.

[9] G. Kontorinis, T. Lenarz, T. Stöver, and G. Paasche, "Impact of the insertion speed of cochlear implant electrodes on the insertion forces," *Otology and Neurotology*, vol. 32, no. 4, pp. 565–570, 2011.

[10] G. Kontorinis, G. Paasche, T. Lenarz, and T. Stöver, "The effect of different lubricants on cochlear implant electrode insertion forces," *Otology and Neurotology*, vol. 32, no. 7, pp. 1050–1056, 2011.

[11] O. Majdani, D. Schurzig, A. Hussong et al., "Force measurement of insertion of cochlear implant electrode arrays in vitro: comparison of surgeon to automated insertion tool," *Acta Oto-Laryngologica*, vol. 130, no. 1, pp. 31–36, 2010.

[12] C. J. Coulson, P. S. Slack, and X. Ma, "The effect of supporting a surgeon's wrist on their hand tremor," *Microsurgery*, vol. 30, no. 7, pp. 565–568, 2010.

[13] D. Mürbe, K.-B. Hüttenbrink, T. Zahnert et al., "Tremor in otosurgery: influence of physical strain on hand steadiness," *Otology and Neurotology*, vol. 22, no. 5, pp. 672–677, 2001.

[14] M. Miroir, Y. Nguyen, G. Kazmitcheff, E. Ferrary, O. Sterkers, and A. B. Grayeli, "Friction force measurement during cochlear implant insertion: application to a force-controlled insertion tool design," *Otology and Neurotology*, vol. 33, no. 6, pp. 1092–1100, 2012.

Hindawi Publishing Corporation
BioMed Research International
Volume 2014, Article ID 656325, 7 pages
http://dx.doi.org/10.1155/2014/656325

Research Article

Feasibility Study of a Hand Guided Robotic Drill for Cochleostomy

Peter Brett,[1] Xinli Du,[1] Masoud Zoka-Assadi,[1] Chris Coulson,[2] Andrew Reid,[2] and David Proops[2]

[1] *Brunel Institute for Bioengineering, Brunel University, London UB8 3PH, UK*
[2] *ENT Department, Queen Elizabeth Hospital, Birmingham B15 2TH, UK*

Correspondence should be addressed to Peter Brett; peter.brett@brunel.ac.uk

Received 14 March 2014; Accepted 28 May 2014; Published 7 July 2014

Academic Editor: Stefan Weber

The concept of a hand guided robotic drill has been inspired by an automated, arm supported robotic drill recently applied in clinical practice to produce cochleostomies without penetrating the endosteum ready for inserting cochlear electrodes. The smart tactile sensing scheme within the drill enables precise control of the state of interaction between tissues and tools in real-time. This paper reports development studies of the hand guided robotic drill where the same consistent outcomes, augmentation of surgeon control and skill, and similar reduction of induced disturbances on the hearing organ are achieved. The device operates with differing presentation of tissues resulting from variation in anatomy and demonstrates the ability to control or avoid penetration of tissue layers as required and to respond to intended rather than involuntary motion of the surgeon operator. The advantage of hand guided over an arm supported system is that it offers flexibility in adjusting the drilling trajectory. This can be important to initiate cutting on a hard convex tissue surface without slipping and then to proceed on the desired trajectory after cutting has commenced. The results for trials on phantoms show that drill unit compliance is an important factor in the design.

1. Introduction

Drilling through bone is a common operative task in surgical disciplines (ENT, neurosurgery, maxillofacial surgery, and orthopaedics are some examples). Surgeons within these fields are faced with the same challenges of cutting without slipping on hard bone surfaces, particularly with convex surfaces [1], and in discriminating tissues and structures ahead on the tool trajectory [2, 3].

Robotic surgery has demonstrated consistent results [4–6] for certain procedures in which these systems have found a niche. For many other procedures the initial cost, setup time, surgeon training overhead, and maintenance of a large system cannot be justified. If robotic surgery is to provide a benefit to a wider range of procedures then the robotic systems need to be smaller, of lower cost, and intuitive to use and require few additional resources to be applied into clinical practice. A number of hand guided robotic systems for surgery are emerging, for example, to assist in gripping tissues (laparoscopy), in guiding hand-held instruments, and in cutting applications (knee joint replacement surgery) [7–10]. Where feasible, the simplicity of hand guided robotic type instruments for surgery compared with the complexity of extensive manipulation robot systems is attractive in terms of the application of principles to a wide range of procedures at a reasonable cost. To accomplish this there is the need to engage more extensively with the less structured state of the working environment, as the point of registration is likely to be quite different to systems registered to scan data alone, for example. In some cases the reference may be the deforming tissue. For these devices, sensing systems, protocol, and configuration take on a new set of challenges.

In this paper the extension of an automated, arm supported robotic drill, used successfully in the operating room to produce precise cochleostomies, is explored as a hand guided unit. It relies on an innovative method for tactile sensing to determine the state of the tissue being drilled and tissue about to be drilled, enabling the surgeon to achieve consistent results.

Cochleostomy formation is a key step in cochlear electrode implantation. During this step the surgeon drills through the outer bone tissue of the cochlea and ideally onto, but not through, the underlying endosteal membrane. Following this step, debris is removed from the cochleostomy and electrode is inserted into the cochlea through a pool of antiseptic gel. If a surgeon penetrates the endosteum during the drilling process then residual hearing of the patient could be compromised. Preserving the endosteum in cochleostomy is regarded as ideal and difficult to achieve reliably. The arm supported drill has been designed to produce a consistent high quality hole without penetrating the underlying membrane. The innovative sensing scheme automatically discriminates the state of tissues during the cutting process and determines the presence of tissue interfaces and underlying structures ahead on the drilling trajectory. Using these unique properties it is able to avoid penetration of delicate interfaces and underlying tissues. As a hand guided tactile sensing device it is able to offer precise and consistent cutting of tissues, with some versatility of the trajectory during the surgical process.

2. Arm Supported Robotic Drill

The arm supported robotic drill was the first autonomous surgical robot deployed able to sense its own working environment as information rather than data values in order to discriminate states attributable to conditions of the cutting process in real-time and to use this information to control progress in flexible tissues. The drilling of a cochleostomy occurs on a single axis, and the recognition of prominent states enables the automatic selection of actuation strategy to expose the correct diameter of window onto the endosteum without penetrating the membrane. This is achieved in real-time.

The system consists of linear and rotational drives to feed and rotate standard surgical burrs. Currently the drill unit is attached to a flex-lock arm, permitting free movement to align the drill on the desired trajectory and then stabilization of the drill when drilling (Figure 1). Sensing through a discriminatory process of coupled features, feed force and torque transients enable perception of the critical phenomena of the tool working environment. Anticipation of conditions ahead of the tool before they are encountered enables discrimination of the approach to the critical endosteal membrane interface before it is reached. The drilling robot is able to autonomously adjust motion strategy with respect to the deforming tissues and achieve a consistent state in the result [11, 12].

3. Drilling Process

The mathematical model, reported in [12], predicts results shown in Figure 2 that help to describe typical features used by the tactile sensing scheme to identify the approach to a tissue interface such that penetration can be avoided. The drill bit feed force and torque are plotted as functions of displacement. The characteristics indicate clear changes in

Figure 1: The surgical robot drilling system used in cochleostomy supported on a fixed flexilock arm.

transients between coupled signals that correspond to stages in the process. In this simulation feed rate is assumed to be constant. The force and torque transients clearly show the point at which hole depth is equal to the burrs radius at stage 2 at approximately 0.5 mm and is indicated by an observable change in gradient of the torque transient. Onset of breakthrough occurs at stage 3 at approximately 1.3 mm resulting in the sharp increase and subsequent roll-off in the force signal. Amongst other properties and tissue behaviour, these coupled features of the sensory transients are used to anticipate the position of the tissue interface precisely. If drilling did not cease at this point then the hole would be completed at stage 4, at approximately 1.4 mm. The force and torque would then fall to zero when full penetration occurred. If penetration is allowed to take place, then in reality the tip of the drill bit will have penetrated much further beyond the tissue interface than is necessary to complete the removal of bone tissue of the cochlea as the tissues are flexible and will have deflected significantly in response to tool forces prior to penetration. Avoiding penetration is important in the process to minimise trauma of the hearing organ, as is the amplitude of disturbances induced during the drilling process [13].

When drilling in practice the force transients are affected by many disturbances and are not as clear as indicated in Figure 2. In reality tissue inconsistency, debris, involuntary disturbances of the patient, and other disturbances are present. By using the automated discriminatory approach above, the system is able to identify the approaching condition of interface penetration before it occurs.

The process of sensing and robot control is entirely through a hardwired control unit with the surgeon retaining executive control. Autonomous perception of critical phenomena and structures is completed using the coupled force and torque drilling transients, described above, in real-time. The automated selection of control strategies enables a precise and consistent result with respect to the flexible tissues to be achieved. The most important objective of the system is to prepare the window on the endosteum.

In Figure 3, the surgeon is holding the handset that enables executive control of fine alignment and on-off control of the autonomous process in operating room. Feedback is by observation of behaviour under the binocular microscope [12, 13]. Standard surgical drilling burrs are used. On completion of the drilling process, the surgical robot is removed. As

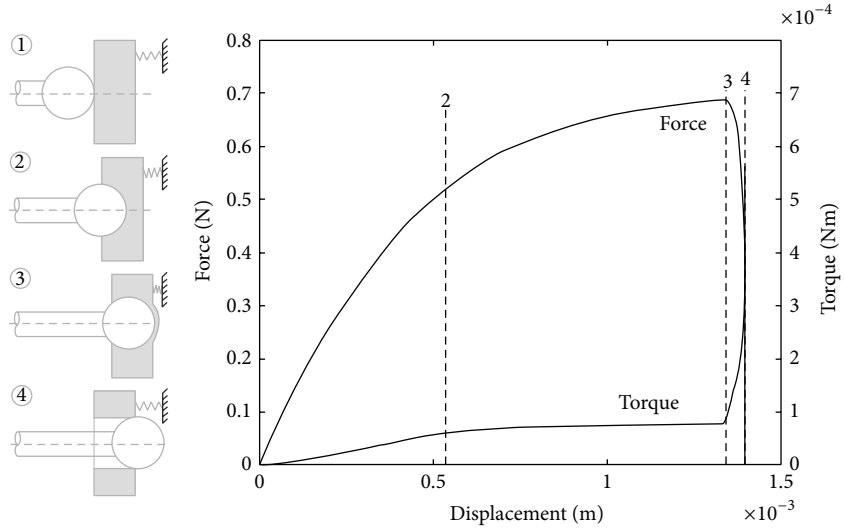

Figure 2: Simulated coupled drilling feed force and torque (assuming drilling through in cochleostomy) showing principal characteristics [12].

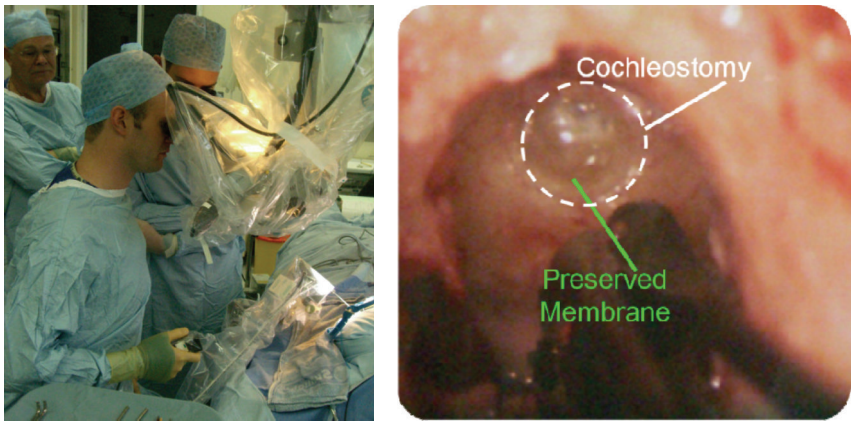

Figure 3: The arm supported drill used in operating room preparing a cochleostomy [12].

described earlier, the cochlear electrode is then fed through a droplet of antiseptic gel placed within the cochleostomy. The smooth prepared access enables smooth insertion of the electrode.

4. Disturbances

The innovative sensing method used is well proved for discriminating tissue types, tissue structures, and tissue behaviour in the drilling process. Exposure to different disturbances has shown that involuntary patient disturbances are automatically classified as different types, as are knocking and a variety of manual types of disturbance while drilling from a flex-lock arm. The automated drilling process and ability for sensing have been shown to be unaffected on drilling trajectories up to 45 degrees from the perpendicular to a tissue interface [14].

During trials for robustness with respect to forced disturbance [14] the drilling system was exposed to impact disturbance to the support arm applied to different axes when drilling eggshells and porcine cochlea. A laser Doppler vibrometer was used to obtain noncontact evaluation of disturbance velocity amplitude. Figure 4 shows the experimental setup. Disturbances by controlled knocking at the support arm from different directions and supporting table were introduced to simulate inadvertent physical disturbance with the drilling system in the operating room. The successful results showed automatic discrimination of disturbance type, whether patient/operator or tissue induced, and led to the appropriate automatic control action toward completing or aborting the process. As would be expected a certain degree of compliance is helpful to the process.

Figure 5 shows an example of a completed hole and the corresponding disturbance velocity transients applied to the arm. Peak amplitude is 20 mm/s. The corresponding hole shown in Figure 5 is through the shell of a raw egg, a phantom for the cochlea, which is typical of many trials [10]. The figure shows that the tissue of the shell has been removed to expose

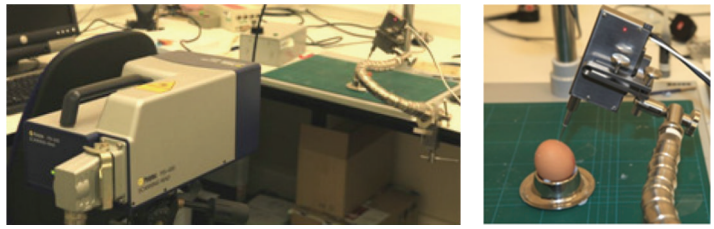

Figure 4: Setup of a laser Doppler vibrometer to evaluate disturbance velocity amplitude [14].

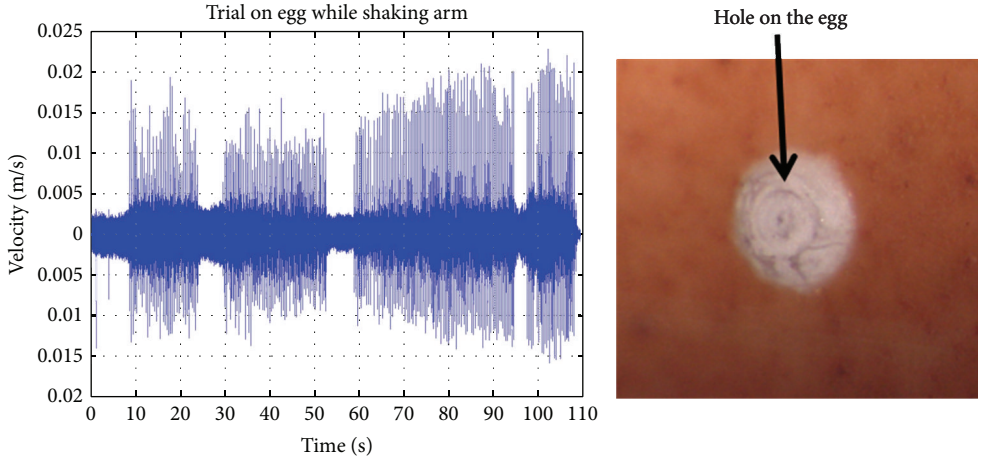

Figure 5: Completed hole and corresponding disturbance velocity transients [14].

a window onto the membrane of a diameter required for electrode insertion. The process of controlled knocking has not confused the system and the task has been accomplished without being disturbed. This shows that the sensing scheme of the drill offers robustness to environmental disturbances. The tolerance to disturbances also suggests tolerance to a variety of operator disturbances when guided by hand. The results from the current investigation on operator disturbance levels are not complete at this time and will affect the design of the drill unit.

5. Hand Guided Drill

There are many drilling tasks in surgery where flexibility in the drilling trajectory is needed during the process. A good practical example is when drilling into a convex hard surface, as is the case when drilling into the basal turn of the cochlea. Initial cutting without slip is achieved more readily when the drilling trajectory is normal to the surface. When initial cutting has been achieved, the drill can be orientated onto the desired trajectory toward the scala. A surgeon can identify this trajectory through exposed anatomical features following a posterior tympanotomy.

Similar to the arm supported system described earlier, the hand guided system consists of (1) a drilling unit, (2) a hard-wired unit for interpreting sensory signals and drill drive control, and (3) a PC screen for operator visual feedback. The system elements are shown in Figure 6.

The drill unit comprises drill bit rotation drive and sensing elements and is shown in Figure 7. Standard drill bits

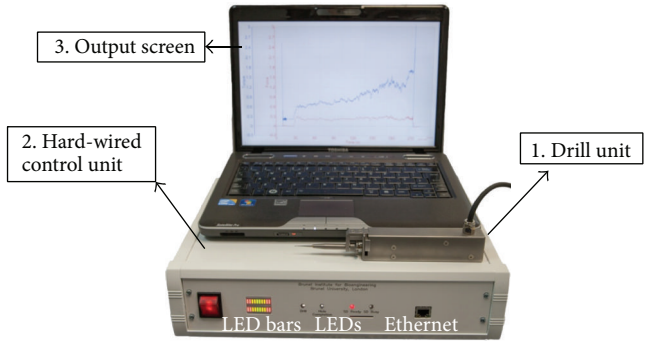

Figure 6: The experimental hand guided surgical robot drill system.

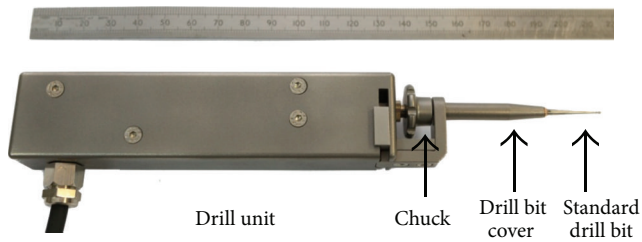

Figure 7: The hand guided robotic drill unit.

are readily changed using the chuck. Feed force is measured by a displacement sensor and torque is measured using

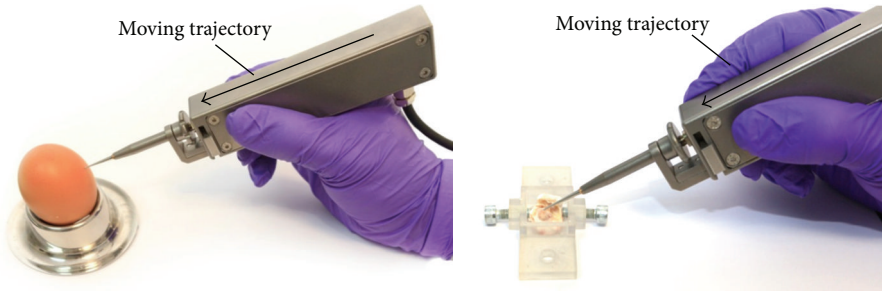

(a) (b)

Figure 8: Drilling configurations with the drill unit held by the operator on raw eggshell and porcine cochlea.

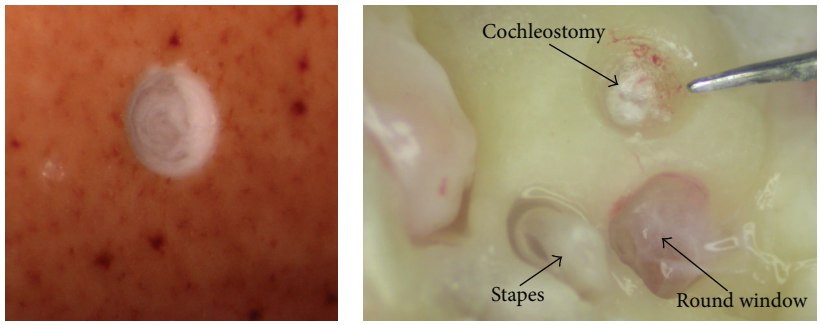

(a) (b)

Figure 9: Intact underlying membranes following drilling through bone shell tissue of a raw egg and a porcine cochlea, respectively.

drive current of the DC motor. The control unit has a two-tier hierarchy: servo level and high-level controllers. The servo controls the rotation drive of the drill at 40 Hz and communicates with the PC through ethernet connection. The high-level controller responds to key stages and states of the drilling process by selecting predefined strategies. The selection is based on the interpreted state of the drilling process where the high-level controller discriminates characteristics in the coupled sensory transients indicating the onset of breakthrough. All control system and sensory functions operate in hardware. Progress of the procedure is relayed to the clinician on the screen. The drilling process is also indicated by the LEDs on the control unit. The drill will stop rotating when the cochleostomy is complete. The LED bars on the control unit indicate contacting force level between the drill bit and tissue and provide indication to the operator on the most suitable feed force range for the task. This arrangement for the bars works well in experimental trials and demonstrates a useful principle for practice.

6. Results

Results presented here relate to laboratory trials on phantoms. The purpose was to assess the feasibility and performance of guiding such a robotic device by hand. The shell of raw eggs and porcine cochlea were used to present appropriate media and tissue interfaces. In all experimental investigations 1 mm diameter diamond burrs were used. The trials were first carried out on eggshells where there is similarity to the structure of a cochlea. Porcine cochleae have similar properties to human cochlea [15]. These were used in trials to demonstrate the production of cochleostomies with intact endosteum.

In Figure 8 the experimental configuration is shown. During these trials, the drill unit was gripped in the hand of the operator between thumb and forefinger with the hand providing support by resting on the bench. The arrow indicates the trajectory of motion imparted on the drill by the operator. Typical drilling results are presented in Figure 9 for both raw eggshell and porcine cochlea. In each case the underlying membrane remained successfully intact.

Typical coupled force and torque transients for drilling a porcine cochlea are shown in Figure 10. Usual sensory characteristics are present for contact, force building, and completion to the interface. The force level during drilling has a mean value of 1.99 N over the range from 1.4 N to 2.86 N. The operator begins by increasing feed force to ensure that the drill is cutting and is stable on the surface. The result is an initial force building transient. Following this period, the fluctuating force amplitude is primarily due to unsteady motion imparted by the operator.

Figure 11 provides contrast between reactive forces transients of hand guided and automated arm supported drill when drilling in the laboratory. As would be expected, the amplitude of disturbances is significantly greater for the hand guided system as opposed to the arm supported system since the stiffness of the drill unit in the feed direction is similar and the system is subject to involuntary operator disturbances.

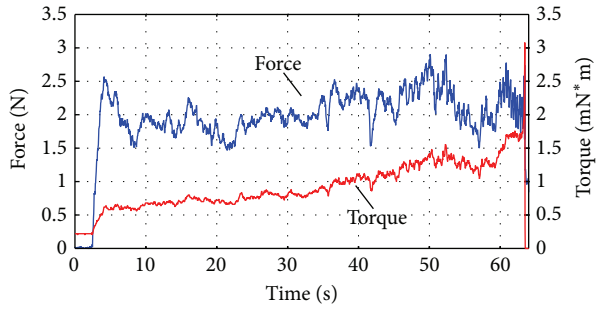

Figure 10: Typical coupled force and torque transients of the hand guided drill.

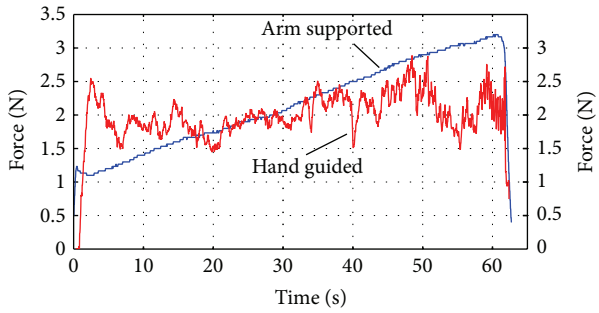

Figure 11: Contrasting force transients between the hand guided and automatically actuated drill in the laboratory.

In the real operating environment both systems will be subjected to patient disturbances of similar and even greater disturbance amplitude [12]. The figure shows that peak feed force values are similar. There is a difference in operation between the two systems; the arm supported drill begins with a lower peak whereas the initial force peak under operator guidance is greater to reinforce stability. The hand guided system guides the operator toward a constant value of feed force whereas the automatic system increases over the period shown. The feed force is limited when using the automatic arm supported drill; however in the test result shown the force limit had not been reached. These results indicate the need to adjust compliance for the hand guided system and to achieve the compromise that will attenuate operator induced disturbances while maintaining stability.

7. Conclusion

This paper describes an investigation to contrast automated drilling by a surgical robot, supported by a fixed arm, with a robotic device that is hand guided. In each case the advanced discriminatory sensing scheme was used to control the state of the drilling process for cochleostomy formation in the laboratory. These trials had the aim of demonstrating preservation of the underlying endosteum while bone tissue is removed. Raw eggshells and porcine cochlea were phantoms used. These enabled investigation of the penetration of hard bone shell tissue and the physical verification of the intact membrane on hole completion.

The hand guided tool has advantage of versatility of the drilling trajectory and the tolerance to initiate cutting on a hard convex surface. The automated system imposes less force and disturbance level; however both systems can achieve the same ideal results. In these early results, the compliance was insufficient to reduce disturbances imparted by the operator when compared to the arm supported drill. Experimentation with the means to minimise reactive force disturbance is a subject of current investigation as the sensing approach and tolerance of the system to disturbances in the delicate procedure of cochleostomy offer feasibility of advantage in practice.

Conflict of Interests

The authors declare that there is no conflict of interests regarding the publication of this paper.

References

[1] T. Cao, X. Li, Z. Gao, G. Feng, and P. Shen, "Automatic identification of otological drilling faults: an intelligent recognition algorithm," *The International Journal of Medical Robotics and Computer Assisted Surgery*, vol. 6, no. 2, pp. 231–238, 2010.

[2] C. James, K. Albegger, R. Battmer et al., "Preservation of residual hearing with cochlear implantation: how and why," *Acta Oto-Laryngologica*, vol. 125, no. 5, pp. 481–491, 2005.

[3] J. Zou, P. Bretlau, I. Pyykkö, J. Starck, and E. Toppila, "Sensorineural hearing loss after vibration: an animal model for evaluating prevention and treatment of inner ear hearing loss," *Acta Otolaryngologica*, vol. 121, no. 2, pp. 143–148, 2001.

[4] G. S. Guthart and K. J. Salisbury Jr., "Intuitive telesurgery system: overview and application," in *Proceedings of the IEEE International Conference on Robotics and Automation (ICRA '00)*, pp. 618–621, April 2000.

[5] M. Jakopec, F. Rodriguez y Baena, S. J. Harris, P. Gomes, J. Cobb, and B. L. Davies, "The hands-on orthopaedic robot "acrobot": early clinical trials of total knee replacement surgery," *IEEE Transactions on Robotics and Automation*, vol. 19, no. 5, pp. 902–911, 2003.

[6] J. H. Lonner, T. K. John, and M. A. Conditt, "Robotic arm-assisted UKA improves tibial component alignment: a pilot study," *Clinical Orthopaedics and Related Research*, vol. 468, no. 1, pp. 141–146, 2010.

[7] J. H. Lonner and G. J. Kerr, "Robotically assisted unicompartmental knee arthroplasty," *Operative Techniques in Orthopaedics*, vol. 22, no. 4, pp. 182–188, 2012.

[8] A. Jaramaz, C. Nikou, and A. Simone, "Naviopfs for unicondylar knee replacement: early cadaver validation," *The Bone & Joint Journal B*, vol. 95, no. 28, p. 73, 2013.

[9] B. Schuller, G. Rigoll, S. Can, and H. Feussner, "Emotion sensitive speech control for human-robot interaction in minimal invasive surgery," in *Proceedings of the 17th IEEE International Symposium on Robot and Human Interactive Communication (RO-MAN '08)*, pp. 453–458, August 2008.

[10] C. A. Nelson, X. Zhang, B. C. Shah, M. R. Goede, and D. Oleynikov, "Multipurpose surgical robot as a laparoscope assistant," *Surgical Endoscopy*, vol. 24, no. 7, pp. 1528–1532, 2010.

[11] P. N. Brett, R. P. Taylor, D. Proops, M. V. Griffiths, and C. Coulson, "An autonomous surgical robot applied in practice,"

in *Proceedings of the 13th Annual International Conference on Mechatronics and Machine Vision in Practice*, pp. 144–150, Toowoomba, Australia, December 2006.

[12] R. Taylor, X. Du, D. Proops, A. Reid, C. Coulson, and P. N. Brett, "A sensory-guided surgical micro-drill," *Proceedings of the Institution of Mechanical Engineers C: Journal of Mechanical Engineering Science*, vol. 224, no. 7, pp. 1531–1537, 2010.

[13] C. J. Coulson, M. Zoka Assadi, R. P. Taylor et al., "Smart micro-drill for cochleostomy formation: a comparison of cochlear disturbances with manual drilling and a human trial," *Cochlear Implants International*, vol. 14, no. 2, pp. 98–106, 2013.

[14] X. Du, M. Z. Assadi, F. Jowitt et al., "Robustness analysis of a smart surgical drill for cochleostomy," *The International Journal of Medical Robotics and Computer Assisted Surgery*, vol. 9, no. 1, pp. 119–126, 2013.

[15] J. P. Pracy, A. White, Y. Mustafa, D. Smith, and M. E. Perry, "The comparative anatomy of the pig middle ear cavity: a model for middle ear inflammation in the human?" *Journal of Anatomy*, vol. 192, no. 3, pp. 359–368, 1998.

Hindawi Publishing Corporation
BioMed Research International
Volume 2014, Article ID 904803, 7 pages
http://dx.doi.org/10.1155/2014/904803

Research Article

Quality Assurance of Multiport Image-Guided Minimally Invasive Surgery at the Lateral Skull Base

Maria Nau-Hermes,[1] Robert Schmitt,[1] Meike Becker,[2] Wissam El-Hakimi,[2] Stefan Hansen,[3] Thomas Klenzner,[3] and Jörg Schipper[3]

[1] *Chair for Metrology and Quality Management, RWTH Aachen University, Steinbachstr. 19, 52074 Aachen, Germany*
[2] *TU Darmstadt, Graphisch-Interaktive Systeme, Fraunhoferstr. 5, 64283 Darmstadt, Germany*
[3] *Hals-Nasen-Ohren-Klinik, Universitätsklinikums Düsseldorf, Moorenstr. 5, 40225 Düsseldorf, Germany*

Correspondence should be addressed to Maria Nau-Hermes; m.nau@wzl.rwth-aachen.de

Received 13 February 2014; Accepted 28 May 2014; Published 3 July 2014

Academic Editor: Stefan Weber

For multiport image-guided minimally invasive surgery at the lateral skull base a quality management is necessary to avoid the damage of closely spaced critical neurovascular structures. So far there is no standardized method applicable independently from the surgery. Therefore, we adapt a quality management method, the quality gates (QG), which is well established in, for example, the automotive industry and apply it to multiport image-guided minimally invasive surgery. QG divide a process into different sections. Passing between sections can only be achieved if previously defined requirements are fulfilled which secures the process chain. An interdisciplinary team of otosurgeons, computer scientists, and engineers has worked together to define the quality gates and the corresponding criteria that need to be fulfilled before passing each quality gate. In order to evaluate the defined QG and their criteria, the new surgery method was applied with a first prototype at a human skull cadaver model. We show that the QG method can ensure a safe multiport minimally invasive surgical process at the lateral skull base. Therewith, we present an approach towards the standardization of quality assurance of surgical processes.

1. Introduction

True obligatory standards for surgery do not exist. The operation rather depends on other skills like the experience or education of the surgeon or technical and clinical infrastructure. Routine surgical procedures at the lateral skull base depend on stepwise exposure of landmarks due to the individual anatomy of each patient within the temporal bone like the sigmoid sinus, horizontal semicircular canal, or boundary to the dura mater. In this context a large opening cavity is performed by the surgeon to reach a distinct target. The obligatory drilling is time consuming and requires an appropriate skin incision. Other areas of surgery revealed clear benefits of minimally invasive procedures like shorter length of hospital stay, less postoperative pain, earlier postoperative recovery, and a lower complication rate compared to open surgery [1, 2]. In this connection, different procedures at the lateral skull base (e.g., insertion of an electrode during a cochlear implantation or removing a tumor) could be performed without a conventional mastoidectomy or other extensive drilling procedures of the temporal bone. The feasibility of a single-port approach was shown by several groups in preclinical setups [3–8]. Multiport image-guided minimally invasive surgery at the lateral skull base is an innovative increment of existing single-port minimally invasive—or "keyhole"—surgery. The use of multiple ports will enlarge the surgical possibilities when targeting a certain anatomy within the temporal bone. Thus, two ports can be used for instruments like a suction device plus forceps or other microinstruments, while the third port is used for an endoscope to visualize the surgical steps. Due to the high anatomic complexity of the temporal bone and its neighboring structures, a strict risk management is necessary to avoid the damage of critical neurovascular structures during the drilling process.

This includes not only the drilling itself but also the entire preoperative and intraoperative management.

For medical products risk management as a part of the quality management system is mandatory as stated, for example, by the US Food and Drug Administration (FDA) [9], in the German Medical Devices Act [10] and by the International Organization for Standardization [11]. Concerning the quality assurance of a surgical process, so far there is no standardized method applicable independently from the surgery. An approach to the evaluation of surgical innovations can be found in a series in the Lancet journal [12–14]. The authors propose the so-called IDEAL paradigm which focusses on establishing new surgical procedures and on showing their efficacy by systematic studies. Still, this proposed procedure does not specifically include presurgical investigations or risk assessments. An approach to the calculation of probability of a successful surgery was proposed by Noble et al. [15]. It takes into account the drill's positioning error at the target. The probability of success is calculated before the surgery and estimates the risk regarding this specific aspect; thus it is not used to secure the whole process chain. Besides, functional and cosmetic results of a surgery are evaluated by the patient and the estimation of a surgery's success is mainly still executed by the surgeon alone. The surgical process is characterized by "standardized" medical access paths, which are defined based on the anatomy and the surgeons' experience. Therefore, in times of increased technology in medicine, an advancing urge to standardize preoperative and intraoperative processes is stated.

As stated above using the example of medical products, in the manufacturing industry in which, for example, product development processes run repeatedly, there exist a variety of methods to manage risks. Possibilities are, for example, to apply methods for fault prevention and to ensure capable processes. One approach to secure process chains is the method of quality gates (QG). QG are defined measuring points that divide the process into different phases or sections. They cannot be surmounted by process outcomes which do not meet previously defined requirements. Interim process results are evaluated regarding the fulfillment of these requirements at each quality gate [16]. This is also the main difference between quality gates and milestones. Milestones are often linked to a specific time and state, for example, that a task has to be finished by a specific date. They primarily define what needs to be done and usually do not indicate who has to provide the information and who is responsible for the process. This last aspect also applies for checklists. The quality gate method aims for measurable criteria and clear responsibilities and has therefore become an integral part of product development and production ramp-up, for example, in the automotive industry, and has also been the object of research for several years [17–19].

In this paper we adapt and apply the quality gate method to multiport image-guided minimally invasive surgery at the lateral skull base in order to secure the innovative surgical process. The defined quality gate requirements are evaluated during a first prototype surgery at a human skull cadaver model.

2. Materials and Methods

According to Pfeifer the method of quality gates can be structured into six steps [16].

(1) Division of the entire process into natural process sections.

(2) Development of measuring points (including the definition of requirements that need to be fulfilled).

(3) Development of quality management plans.

(4) Monitoring of process progress.

(5) Monitoring of measuring points.

(6) Synchronization of progress.

In this work the six steps of the QG method have been adapted and applied to a multiport image-guided minimally invasive surgery at the lateral skull base. The team that has elaborated the quality gates consists of otosurgeons, computer scientists who focus on medical imaging and image processing, and engineers from the field of metrology and quality management. In the following, we describe each step and how the QG method has been transferred and adapted accordingly.

In the first step of the QG method the process is defined and divided into several sections. If a standard operating procedure (SOP) exists that describes the relevant process, the description of the process and its division into sections can be based on the SOP. For the minimally invasive process that is analyzed here, no SOP exists. Therefore, three QG are defined in an interdisciplinary team which divide the process into four sections (Figure 1). In the second step the requirements that need to be fulfilled at each QG, the QG criteria (Table 1), are defined. This includes that the "customer" and "supplier" for each piece of information are identified. For surgical processes the "customer" of information is the responsible surgeon. The "supplier" is defined for each QG criterion. In order to ensure that everyone accepts the criteria it is important to involve the responsible people in the definition process, for example, in a workshop. For minimally invasive surgery at the lateral skull base the QG criteria was developed in a team of otosurgeons, engineers, and computer scientists. Thus, the person who will carry out the procedure later as well as experts for different technical details are included. The level of detail of the QG criteria is also defined in this group. It should be chosen in such a way that all crucial aspects for the process are covered on the one hand, but on the other hand it should not be too detailed or repeat existing process descriptions to ensure acceptance and applicability to clinical practice.

Up to the first defined QG for this surgical process, the patient has not been exposed to additional radiation compared to the standard procedure. This is the first natural break point of the process. Before anesthetization it is therefore checked if the available data suggests that a minimally invasive surgery could be possible for the given patient. Furthermore, the patient should know about potential risks. These aspects are considered in the defined QG1 criteria. In the section between QG1 and QG2 the surgery is planned

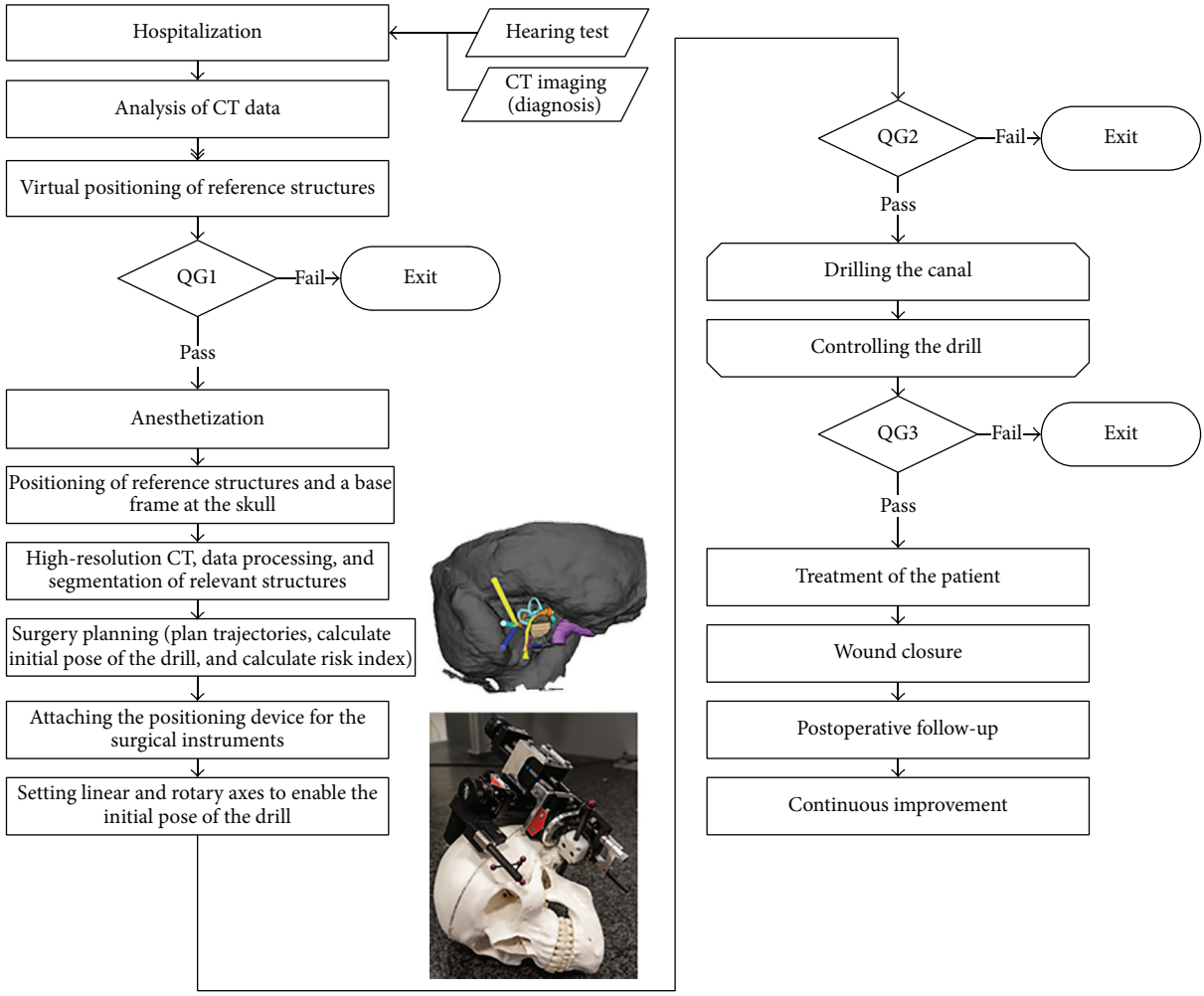

Figure 1: Process for image-guided minimally invasive surgery at the lateral skull base divided into four phases by quality gates. If a quality gate cannot be passed the surgeon should exit the minimally invasive procedure and switch to an established invasive approach.

in detail which includes a high-resolution CT scan of the temporal bone, the segmentation of relevant structures [20], the planning of trajectories [21] that meet in the target area, and the setting of a positioning system for the drill [22]. Before the actual drilling process starts, QG2 ensures that the risk of damaging sensitive structures is justifiable by calculating the so-called therapeutic risk index (TRI) [22, 23]. This index is based on standards and guidelines from production metrology that have been transferred to the medical domain: the TRI takes into account the distance from the planned trajectory to the next sensitive structure, the uncertainty of CT imaging, and segmentation of the relevant sensitive structure as well as the uncertainty of setting the initial pose of the drill. With the third QG it is checked if the drill canals have been applied according to the planning and if no sensitive structures have been damaged (QG3 criteria).

In the industrial environment people try to avoid that "customer" and "supplier" are the same person in order to ensure a control function. Looking at a surgical process it is obvious to define the responsible surgeon as the process owner and the "customer" of information. As the surgeon is also responsible for supplying information it is recommended to involve a second person in the decision regarding the requirements' fulfillment. This can, for example, be another doctor for the QG1 criteria, a nurse trained for surgical environment for the QG2 criteria, or a resident for the QG3 criteria.

The third step in the quality gate method is the development of a quality management plan. The necessary steps to fulfill QG criteria and pass the gate are described in the process description. When transferring the method to surgical processes it is necessary to define what has to be done if QG cannot be passed. In our current application it is decided that the intervention needs to be switched to a classical, nonminimally invasive approach which we indicate as "exit" (Figure 1).

The fourth step—monitoring of the progress—ensures that deviations from the requirements or parallel activities are recognized and harmonized at an early stage, also between the defined measuring points. This aspect is especially important if several processes run in parallel for a certain time and need to be linked later. Since our current application does not

Table 1: Catalogue of criteria for the quality gates of a minimal invasive image-guided surgery at lateral skull base. The customer is the responsible surgeon as he/she is responsible for the outcome of the surgery.

		Supplier
	QG1 Criteria	
(1.1)	Presence of all documents of diagnosis: (i) anamnesis, clinical examinations, (ii) indication/necessity of surgery is stated in the patient chart, (iii) hearing test, (iv) CT data set	Patient chart
(1.2)	In principle the target area is accessible by minimally invasive surgery	Surgeons
(1.3)	Available CT data suggests based on the patient's anatomy that it is possible to position drill trajectories. Sensitive structures are not unusually close	Surgeon/radiologist
(1.4)	Patient has been informed of advantages and disadvantages of a minimally invasive surgery. The information is available in the patient chart	Patient chart
	QG2 Criteria	
(2.1)	Reference structures have been fixed firmly to the patient's skull	Surgeon and residence
(2.2)	High-resolution CT images have been taken and are available	Radiology
(2.3)	High-resolution images have been processed. Risk structures (including cochlea, semicircular canals, facial nerve, chorda tympani, ossicles, internal carotid artery, and internal and external auditory canal) are segmented and drill trajectories are planned; anatomical structures and reference structures are clearly visible. The therapeutic risk index (TRI) is larger than or equal to 1. The uncertainties of the navigation process and the medical imaging have been taken into account for its calculation	Software
(2.4)	The mechanical positioning device to adjust the drill has been attached to the skull. The axes' position (linear and rotary axis) has been checked based on their scale and the calculated positions from the software	Surgeon and resident
	QG3 Criteria	
(3.1)	The continuous process control (using a C-arm) during insertion of the drill has not shown any abnormalities	Surgeon
(3.2)	The target area has been reached. The surgeon can insert an endoscope and has visual contact to the target area. The target area can furthermore be reached by a surgical instrument	Surgeon and resident
(3.3)	No vital structures have been affected (C-arm scan shows no damage of defined sensitive structures and heart rate has been normal)	Surgeon, anesthetist

include parallel running processes, this step is neglected in this example.

In step five it is monitored if the target for each process section has been achieved. To do this, the "supplier" gives an evaluation regarding the degree of fulfilment of the defined criteria to the "customer." If the "customer"—in this example the surgeon—agrees that the aim has been achieved, the process section is concluded. Step six should ensure to document and revisit acquired knowledge so that it can be used to improve future applications.

With the above definitions and descriptions we have established the quality gates to secure the complete process chain in our example.

3. Results and Discussion

In order to evaluate the previously defined QG criteria, this minimally invasive surgical process has been applied for the first time with a human skull (Figure 2). The target point was set at the porus acusticus internus since this is a common surgical target for tumors of the inner ear canal and cerebellopontine angle (neuromas). A second marker was set anteriorly as a reserve but was not used in the described setup. To validate the results experimentally (Figure 1), we performed additional measurements, obviously not possible on real humans: the position of the reference structures and the target area have been measured with a coordinate measuring machine (CMM) giving accurate space coordinates, which are important to ensure traceable measurements. The following changes to the process were made for the experimental validation.

(i) Glass markers were glued to the skull to ensure a better contrast of reference structures in the cone-beam projections acquired with a C-arm system. They have a slightly higher attenuation factor as bone and therefore can be easily localized in the 2D projections. In addition, they are not producing strong streak-like artifacts, which are typical for metal fiducials. Two additional plastic markers were positioned in the skull, one in the target area and one close to it. These two markers have a relatively low attenuation factor and are therefore ignored during the automatic marker detection process. Nevertheless, they are well

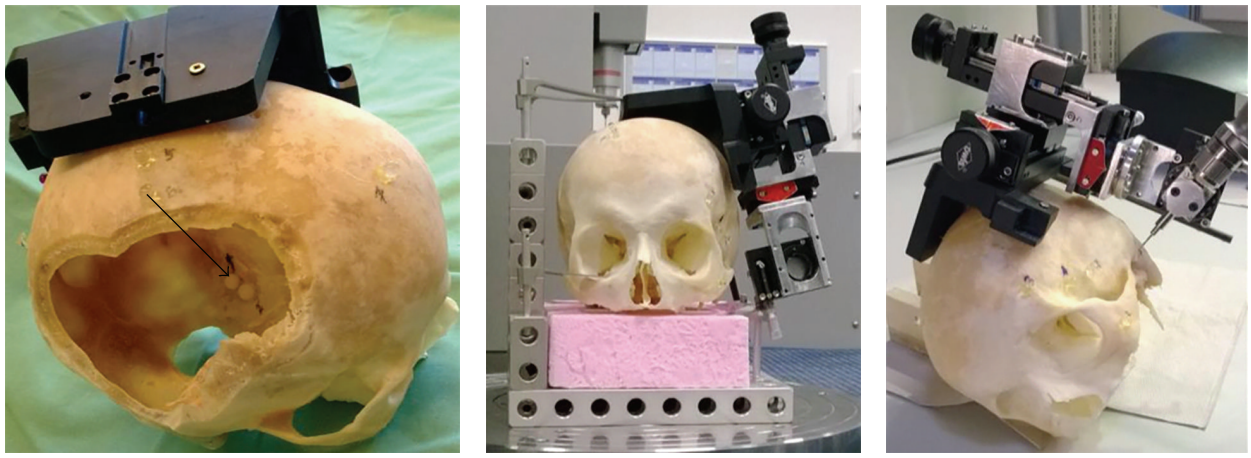

(a) (b) (c)

Figure 2: Skull used for prototype evaluation with attached base plate on the left cadaver site, reference structures on the outside of the skull (arrowhead), a target structure inside the scull (arrow), which was placed after opening the right parietal region of the head (a); on the CMM (b), and during the drilling process (c).

recognizable in the reconstructed 3D volume, so that they can be used to define the target point.

(ii) In order to calculate the drill's positioning error, the actual drill position has to be measured and matched to the planned trajectories. Therefore, at least two projections have to be acquired to compute the spatial location of the instrument. The scanner acquisition direction should thereby be perpendicular to the instrument main axis and the angle between the two projection planes should be maximized, with 90° being the ideal value. A 2D/3D registration was performed to align the 2D projections to the preoperative CT data. This was done in two steps: a point based registration followed by an intensity based one. First, the fiducial markers were automatically segmented in the 3D preoperative volume based on knowledge about marker form, size, and attenuation. The challenging task of localizing markers in 2D projections, in presence of form distortion and structure overlapping, was carried out using a recently developed method called particle path segmentation. The achieved fiducial localization error in this step was—mean (std)—0.059 mm (0.062 mm). The point correspondence and the pose estimation were solved with the SoftPosit method [24], which combined the iterative softassign algorithm and the iterative POSIT method. The first algorithm aimed to find correspondences and the second aimed to compute object pose by assuming a full-perspective camera model. A refinement of the estimated projection parameters was then performed by an intensity based registration [25], achieving a target registration error of 0.13 mm (std: 0.02 mm). After segmenting the drill in both projection images, the drill axes were back projected based on the estimated projection parameters. The intersection of the back-projected lines defined the drill position relative to the preoperative data. Lastly, the target localization error was computed as the Euclidean distance between the drill tip and the correspondent planned target.

As a skull was used for this first evaluation of the QG method it occurs that some defined QG criteria cannot be fulfilled because they are not applicable in this setting or because the information is missing. This is, for example, the case with criteria (1.1) and (1.4). For each of these criteria it has to be decided (in the team) whether it can be substituted by other requests (like (1.1), see below) or if it is not applicable and does not need to be considered. If a criterion that cannot be substituted and cannot be neglected is not fulfilled the surgeon should switch to an invasive approach as the process is not secured.

Regarding QG1, all applicable and relevant requirements are fulfilled.

(1.1) The "patient" does not have a patient chart and was not accompanied with additional information. Usually this would mean a failure to pass QG1. The missing anamneses, clinical examination, hearing test, CT scan, and decision about the necessity of a surgery are in this case substituted by the determination of the target area carried out by an otosurgeon.

(1.2) The defined target area, the porus acusticus internus, is generally accessible by minimally invasive surgery.

(1.3, 1.4) These criteria are not applicable for the process with the defined changes as no CT data from previous tests is available and the "patient" cannot be informed.

Therefore, the process can be continued. For this example, the first two QG2 criteria are fulfilled.

(2.1) The reference structures were fixed to the skull (Figure 2(a)).

(2.2) High-resolution images have been acquired and are available for further processing.

Criterion (2.3) cannot be fulfilled entirely: the risk structures are segmented, drill trajectories are planned, and anatomical structures as well as reference structures are clearly visible. A TRI of −0.44 is calculated. Based on the definition of the TRI, an index of at least 1 is recommended [23]. This means that when taking into account the previously assessed uncertainties of the initial positioning of the drill and the medical imaging the available distance from the planned trajectory to the next sensitive structure is too small. As this is an index for the capability of the process, an appropriate TRI is essential for the patient's safety. Therefore, the minimally invasive procedure would not be applied in this case if it was a real patient.

In order to be able to evaluate also the QG3 criteria and taking in mind that no real patient is used in this stage, the process was continued, although the risk of damaging the semicircular canals is high. The device for setting the drill to its initial position is fixed to the skull and the axes' parameters are set according to the plan. If these settings are checked and are correct, criterion (2.4) can be fulfilled.

The QG (3.1) criterion is not fulfilled, as the position of the drill was not checked during the drilling process. However, it could be shown that this process step can be successful when computing and matching the drill position to the planned trajectories as mentioned above. Therefore, criterion (3.1) was substituted by this experiment.

The target area, represented by the middle of a plastic ball in the inner auditory canal, was hit with the drill. This means that the inner auditory canal has been reached and QG (3.2) criterion is fulfilled.

Criterion (3.3) is not fulfilled as the semicircular canal was damaged. We expected this due to the previously calculated TRI. Therefore, the decision against a minimally invasive procedure based on the TRI would have been correct in this case and the applied QG method would have succeeded in preventing the damage of a sensitive structure.

4. Conclusion

In this paper we show that the quality gate method according to Pfeifer can be transferred to multiport image-guided minimally invasive surgery at the lateral skull base in order to ensure the quality of the surgical process. As this method is established in different fields of industry it is a reasonable possibility to also secure a surgical process chain. Although we focus on one example of multiport surgery at the lateral skull base, this method can also be applied to other single-port surgeries at the head. Necessary changes would be the definition of measuring points and their requirements. In comparison with other methods like checklists [26] or milestones that are also used to standardize processes and to prevent safety hazards, quality gates go one step further by stating responsibilities and by establishing a control function by defining "customers" and "suppliers" of information. Of course, it would be possible to extend checklists in such a way but it is usually not done. The control function is an important aspect of the QG method. Therefore, we ensure this in our example by the requirement of a four-eyes-principle if the "customer" and the "supplier" are the same person.

In an expert team we elaborated the quality gates for multiport surgery at the lateral skull base and applied this method to a cadaver skull for the first time. Furthermore, we showed that the defined measuring points and requirements are useful to ensure a safe minimally invasive surgical process at the lateral skull base. This work is a first approach towards the standardization of minimally invasive surgery which can eliminate or at least reduce potential errors. Therewith, the quality gate method can help to reduce the risk of such a surgery for the patient. For complex surgical processes especially as described in our example, when the surgeon cannot rely on his knowledge and skill alone to carry out the procedure safely but needs software and technical systems for support, the quality gates can help to secure the process when implemented in clinical practice. In order to achieve implementation in clinical practice it is important to integrate the responsible people into the process, for example, during workshops, and to ensure that the defined QG criteria do not contradict existing documents and do not extend the procedure too much.

Conflict of Interests

The authors declare that there is no conflict of interests regarding the publication of this paper.

Acknowledgment

We would like to thank the German Research Foundation DFG for the support and the funding of the depicted research within the research group MUKNO (FOR 1585).

References

[1] S. Sauerland, T. Jaschinski, and E. A. Neugebauer, "Laparoscopic versus open surgery for suspected appendicitis," *Cochrane Database of Systematic Reviews*, no. 10, Article ID CD001546, 2010.

[2] F. Keus, J. A. de Jong, H. G. Gooszen, and C. J. van Laarhoven, "Laparoscopic versus open cholecystectomy for patients with symptomatic cholecystolithiasis," *The Cochrane Database of Systematic Reviews*, no. 4, Article ID CD006231, 2006.

[3] N. Gerber, B. Bell, K. Gavaghan, C. Weisstanner, M. Caversaccio, and S. Weber, "Surgical planning tool for robotically assisted hearing aid implantation," *International Journal of Computer Assisted Radiology and Surgery*, vol. 9, no. 1, pp. 11–20, 2014.

[4] H. Hiraumi, N. Yamamoto, T. Sakamoto, and J. Ito, "A minimally invasive approach for cochlear implantation using a microendoscope," *European Archives of Oto-Rhino-Laryngology*, vol. 270, no. 2, pp. 477–481, 2013.

[5] B. Bell, C. Stieger, N. Gerber et al., "A self-developed and constructed robot for minimally invasive cochlear implantation," *Acta Oto-Laryngologica*, vol. 132, no. 4, pp. 355–360, 2012.

[6] Y. Nguyen, M. Miroir, J. L. Vellin et al., "Minimally invasive computer-assisted approach for cochlear implantation: a human temporal bone study," *Surgical Innovation*, vol. 18, no. 3, pp. 259–267, 2011.

[7] R. F. Labadie, J. H. Noble, B. M. Dawant, R. Balachandran, O. Majdani, and J. M. Fitzpatrick, "Clinical validation of percutaneous cochlear implant surgery: initial report," *The Laryngoscope*, vol. 118, no. 6, pp. 1031–1039, 2008.

[8] G. B. Wanna, R. Balachandran, O. Majdani, J. Mitchell, and R. F. Labadie, "Percutaneous access to the petrous apex in vitro using customized micro-stereotactic frames based on image-guided surgical technology," *Acta Oto—Laryngologica*, vol. 130, no. 4, pp. 458–463, 2010.

[9] U.S. Food and Drug Administration, "Quality System Regulation," Code of Federal Regulations Title 21, Chapter 1, Part 820, 2013.

[10] Bundesministerium der Justiz, *Gesetz für Medizinprodukte*, vol. 28, 2011.

[11] International Organization for Standardization, "Medical devices—application of risk managmenet to medical devices," ISO 14971, 2013.

[12] J. S. Barkun, J. K. Aronson, L. S. Feldman, G. J. Maddern, and S. M. Strasberg, "Evaluation and stages of surgical innovations," *The Lancet*, vol. 374, no. 9695, pp. 1089–1096, 2009.

[13] P. L. Ergina, J. A. Cook, J. M. Blazeby et al., "Challenges in evaluating surgical innovation," *The Lancet*, vol. 374, no. 9695, pp. 1097–1104, 2009.

[14] P. McCulloch, D. G. Altmann, W. B. Campbell et al., "No surgical innvoation without evaluation: the IDEAL recommendations," *The Lancet*, vol. 374, pp. 1105–1112, 2009.

[15] J. H. Noble, R. F. Labadie, R. H. Gifford, and B. M. Dawant, "Automatic determination of optimal linear drilling trajectories for cochlear access accounting for drill-positioning error," *International Journal of Medical Robotics and Computer Assisted Surgery*, vol. 6, no. 3, pp. 281–290, 2010.

[16] T. Pfeifer, "Quality management—strategies, methods, techniques," *Hanser*, pp. 60–66, 2002.

[17] T. Prefi, *Qualitätsorientierte Unternehmensführung [Habilitation thesis]*, P3—Ingenieurgesellschaft für Management und Organisation, 2003.

[18] T. Flore, "NetQGate—tool support for quality gate processes," in *Proceedings of the Conference on Quality Engineering in Software Technology (CONQUEST '06)*, Berlin, Germany, 2006.

[19] C. Hammers and R. Schmitt, "Governing the process chain of product development with an enhanced quality gate approach," *CIRP Journal of Manufacturing Science and Technology*, vol. 1, no. 3, pp. 206–211, 2009.

[20] M. Becker, M. Kirschner, and G. Sakas, "Segmentation of risk structures in the temporal bone using the Probabilistic Active Shape Model," in *Medical Imaging*, vol. 9036 of *Proceedings of SPIE*, 2014.

[21] M. Becker, S. Hansen, S. Wesarg, and G. Sakas, "Path planning for multi-port lateral skull base surgery based on first clinical experiences," in *Clinical Image-Based Procedures. Translational Research in Medical Imaging*, Lecture Notes in Computer Science, pp. 23–30, Springer, Berlin, Germany, 2014.

[22] M. Nau, S. Pollmanns, and R. Schmitt, "Assessing the risk of minimally-invasive surgery: a metrological approach," in *Proceedings of the 16th International Congress of Metrology*, pp. 1–5, 2013.

[23] M. Nau, S. Pollmanns, and R. Schmitt, "Uncertainty evaluation for surgical processes," in *Proceedings of the 11th International Symposium Seires on Measurement Technology and Intelligent Instruments (ISMTII '13)*, CD 07_14, 2013.

[24] P. David, D. Dementhon, R. Duraiswami, and H. Samet, "SoftPOSIT: simultaneous pose and correspondence determination," *International Journal of Computer Vision*, vol. 59, no. 3, pp. 259–284, 2004.

[25] P. Markelj, D. Tomaževič, B. Likar, and F. Pernuš, "A review of 3D/2D registration methods for image-guided interventions," *Medical Image Analysis*, vol. 16, no. 3, pp. 642–661, 2012.

[26] B. M. Gillespie, W. Chaboyer, L. Thalib, M. John, N. Fairweather, and K. Slater, "Effect of using a safety checklist on patient complications after surgery: a systematic review and meta-analysis," *Anesthesiology*, vol. 120, no. 6, pp. 1380–1389, 2014.

Hindawi Publishing Corporation
BioMed Research International
Volume 2014, Article ID 379295, 7 pages
http://dx.doi.org/10.1155/2014/379295

Research Article

Minimally Invasive Multiport Surgery of the Lateral Skull Base

Igor Stenin,[1] Stefan Hansen,[1] Meike Becker,[2] Georgios Sakas,[2] Dieter Fellner,[2] Thomas Klenzner,[1] and Jörg Schipper[1]

[1] *Department of Otorhinolaryngology, University Hospital Düsseldorf, 40225 Düsseldorf, Germany*
[2] *Interactive Graphics Systems Group, Technical University Darmstadt, 64283 Darmstadt, Germany*

Correspondence should be addressed to Stefan Hansen; stefan.hansen@med.uni-duesseldorf.de

Received 14 February 2014; Accepted 2 June 2014; Published 2 July 2014

Academic Editor: Marco Caversaccio

Objective. Minimally invasive procedures minimize iatrogenic tissue damage and lead to a lower complication rate and high patient satisfaction. To date only experimental minimally invasive single-port approaches to the lateral skull base have been attempted. The aim of this study was to verify the feasibility of a minimally invasive multiport approach for advanced manipulation capability and visual control and develop a software tool for preoperative planning. *Methods*. Anatomical 3D models were extracted from twenty regular temporal bone CT scans. Collision-free trajectories, targeting the internal auditory canal, round window, and petrous apex, were simulated with a specially designed planning software tool. A set of three collision-free trajectories was selected by skull base surgeons concerning the maximization of the distance to critical structures and the angles between the trajectories. *Results*. A set of three collision-free trajectories could be successfully simulated to the three targets in each temporal bone model without violating critical anatomical structures. *Conclusion*. A minimally invasive multiport approach to the lateral skull base is feasible. The developed software is the first step for preoperative planning. Further studies will focus on cadaveric and clinical translation.

1. Introduction

Today, minimally invasive procedures (MIPs) are well established in various surgical fields. In MIPs, small incisions and miniaturized instruments are used to minimize iatrogenic tissue damage. MIPs lead to a shorter length of hospital stay, less postoperative pain, earlier postoperative recovery, and a lower complication rate compared with open access surgery [1–3]. While MIP approaches to the frontal skull base are increasingly used, surgery of the lateral skull base still requires a wide exposure of the anatomical landmarks and the intraoperative, direct identification of the critical anatomical structures by the surgeon. As an example, the common surgical technique of cochlear implantation is mainly based on mastoidectomy and posterior tympanotomy.

Minimally invasive, single-port approaches to the lateral skull base have been attempted by several authors using neuronavigated drilling [4–9]. Bell et al. developed an image-guided robot and performed the drilling of one access tunnel for the insertion of an electrode in a temporal bone specimen [6]. Labadie et al. demonstrated percutaneous single-port access to the cochlea in vitro and in vivo using preoperative computed tomography, bone-implanted fiducial markers, and a customized microstereotactic frame [8, 10]. This concept was further extended by Wanna et al., who created percutaneous single-port access to the petrous apex in a cadaveric temporal bone specimen using the same setup [9].

In contrast, we envision a minimally invasive *multiport* setup that provides access to the lateral skull base similar to that used in laparoscopic surgery, with one port for visualization via an endoscope and two ports for instruments. The use of three ports enables advanced manipulation, direct visual feedback, and use for more indications compared with a single-port approach. Furthermore, the intersection of the three trajectories at the target forms a cavity, which creates additional space for manipulation around the site of interest (Figure 1). Possible indications are tumor removal, biopsy, drug delivery, brachytherapy, or cochlear implantation via two instruments and under direct endoscopic visual control. Liu et al. showed the possibility of da Vinci Si-assisted cochlear implant surgery with augmented reality in cadaveric feasibility study [11]. The planning and future realization of

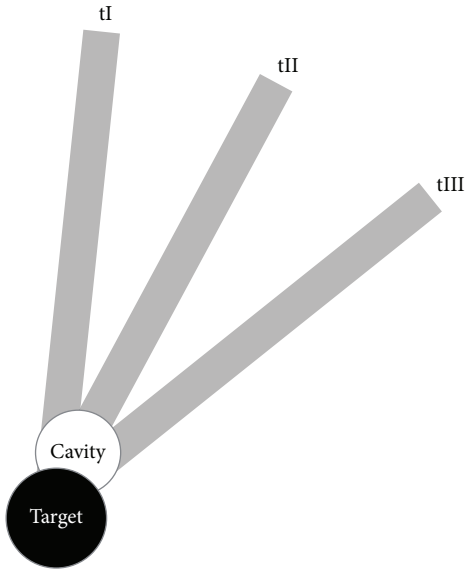

Figure 1: Multiport approach: intersection of the trajectories (tI–III) at the target and the cavity.

multiple minimally invasive ports could be used to implement a similar master slave system. Prior to drilling, the location and direction of the ports must be planned and simulated with preoperative planning software utilizing adequate radiological data. The outcome of the planning software should be (1) clarification of the general feasibility of such an approach preoperatively, (2) prediction of the possible diameters and angles of all three canals, and (3) calculation of trajectories that do not violate critical neurovascular structures.

The aim of this study was to develop and evaluate a software tool for a patient-specific determination of three collision-free trajectories (CFTs) toward various targets within the temporal bone. We developed a planning tool for multiport surgery of the lateral skull base, which facilitates the planning of trajectories inside patient-individual three-dimensional (3D) temporal bone models derived from preoperative computed tomography (CT) scans. Using the planning tool, we analyzed the feasibility of three trajectories, the position of the trajectories, and the maximum drill diameters in twenty different native CT scans of the temporal bone. The internal auditory canal (IAC), round window (RW), and petrous apex (PA) were chosen as representative target points. Possible applications are biopsy and resection of benign and malignant lesions (e.g., metastases, vestibular schwannoma, and paraganglioma), drug delivery (e.g., biologicals, stem cells), drainage of cholesterol granuloma, or cochlear implant insertion. A set of three CFTs was simulated for each target without violating critical structures.

2. Materials and Methods

2.1. Preprocessing. To plan and simulate a minimally invasive multiport procedure in the temporal bone, individual anatomical 3D models were extracted from actual CT image data. Twenty regular CT scans obtained using a standard clinical scanning protocol for temporal bone (Siemens Somatom, Siemens, Eschborn, Germany) average resolution $0.19 \times 0.19 \times 0.39\,\text{mm}^3$ were used. The following anatomical structures were defined as essential: the internal carotid artery and jugular vein bulb, facial nerve and chorda tympani, cochlea and labyrinth, internal and external auditory canal, ossicles, brain, and cranial bone. All structures except for the cranial bone and brain were manually segmented with the ITK-Snap freeware software [12] within each slice of the CT scans (Figure 2). The cranial bone was automatically extracted using simple thresholding. For segmentation of the brain, a safety margin was extracted semiautomatically using a pixel-based approach. It is specifically designed for a certain volume of interest and uses a ray casting approach. The segmentations were verified and manually corrected via visual control of all processed slices by an experienced skull-base surgeon. The chorda tympani could not be identified in one dataset. After segmentation, a triangle mesh was extracted using the Marching Cubes algorithm [13]. The triangle meshes of the anatomical structures were loaded into the planning tool.

2.2. Planning Tool and Selection of Drill Path Combinations. Our planning tool software uses the public domain physical simulation C++ library "Simulation Open Framework Architecture" (SOFA) [14] running on a standard personal computer with a Windows operating system. For CFT planning, a custom graphical user interface (GUI) was added to SOFA. The protocol was as follows: first, a region for candidate entry points of the trajectories is defined on the surface of the 3D triangle mesh skull model. By clicking on the surface of the model the center point of the area of candidate entry points is marked. Then all triangle center points of the skull's triangle mesh within a user defined distance to the chosen point are added to the set of candidate entry points. The target of the trajectories can be defined by clicking on a point in the 3D model or inside the axial CT image. Furthermore, the GUI allows for definition of a drill path radius, a minimum safety distance to the critical structures, and the inaccuracy of the drill. After determining all variables, the software computes and displays all CFTs from the entry points at the skull to the target point, fulfilling the above constraints. The CFTs are color-coded based on their distance to the closest critical structure as follows: the reddish (hot) color indicates a small distance, which is associated with higher risk drillings, whereas the bluish (cold) color indicates a larger distance to the risk organs, that is, safer paths (Figure 3). The planning software allows the definition of an individual safety margin (minimum safety distance to the critical structures and the inaccuracy of the drill). The required value of the safety margin highly depends on the actual clinical setup, for example, the quality of the CT scan, the fiducial markers, drilling process, and so forth. Therefore we decided not to set a fixed safety margin value in this general feasibility study.

A set of three CFTs can then be selected by clicking on the displayed trajectories. The GUI displays the angles between the paths, the length of the individual paths in millimeters

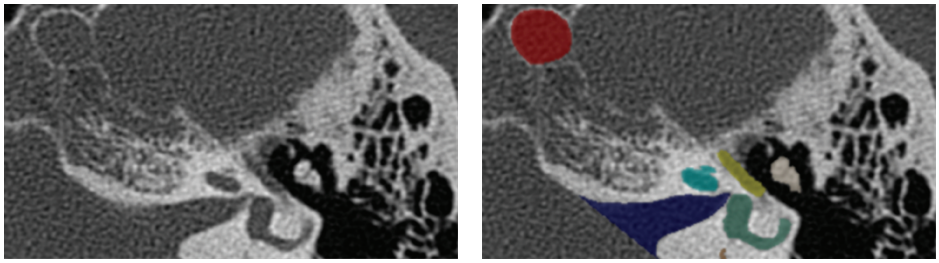

(a) (b)

Figure 2: Manual segmentation of the anatomical structures: the left (a) image shows the axial plane of a temporal bone CT scan. The internal carotid artery (red), internal auditory canal (blue), cochlea (teal), labyrinth (green), facial nerve (yellow), and ossicles (beige) were manually segmented in the right (b) image.

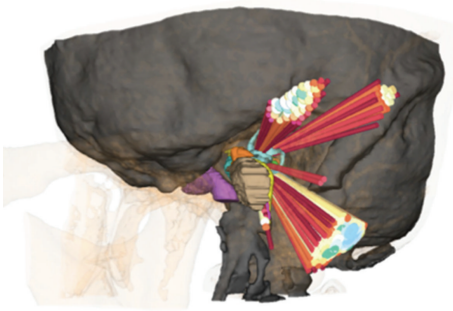

Figure 3: Color-coded CFTs to the internal auditory canal; reddish (hot) colors indicate a small and bluish (cold) colors indicate a larger distance to the risk organs.

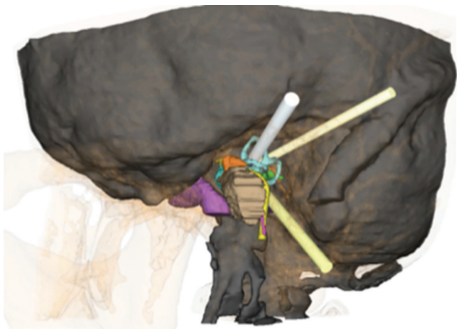

Figure 4: A set of three CFTs selected by the evaluator.

(mm), and the distance to the closest critical anatomical structure in mm (Figure 4). Two criteria were considered in the selection of the optimal CFTs: the maximization of (1) the distance from each drill path to critical structures and (2) the distance between the entry points, that is, the angles between the CFTs (see the next section).

The planning of a set of three CFTs was performed according to the above-described protocol in each of the twenty patients, targeting the RW, IAC, and PA. The drill path diameter was set to 1 mm in each case. The sum of the defined diameter and the safety distance in mm represents the largest possible diameter of a CFT. Thus, the resulting set of CFT does not necessarily have the same diameters. The diameters can be varied as needed in a future intervention, for example, one small diameter for the endoscope and two larger diameters for instruments. In each case, the target structure itself was labelled as noncritical and was therefore not considered for collision detection. We envision the implantation of a cochlear implant as the main indication for targeting the RW. Therefore, the ossicles were labeled as noncritical, as residual hearing is not relevant in this case.

2.3. Analysis of Virtual Drilling Canals and Statistics. The software SPSS (Statistical Package for the Social Sciences) 11 (IBM, USA) was used to perform the statistical analysis and generate the graphs. Boxplots were employed to account for the individual anatomical variations and the consequential differences in the location and diameter of the drill paths. In the following section, we show the median diameter of the drill paths, along with the first and third quartiles, the minimum and maximum values, and the outliers. The data are displayed separately for each target area and subdivided by anatomical region. Ultimately, the cumulative values of each anatomical region are presented. Three angles were calculated between corresponding pairs of the 3 CFTs, and the degrees of these three angles were summed. We termed the resulting value the cumulative angle (CA) and used this value as an indication benchmark. Specifically, a high CA value indicates the preferable configurations because the drill paths are further spread apart, and, therefore, the intersection of the paths occurs at a closer distance to the target.

3. Results

3.1. Software and Protocol. Our software and protocol proved to be stable. The software was optimized by clinician feedback during the study in terms of workflow and user comfort. For example, the color labeling was added and the user interface was developed in close cooperation between clinician and computer scientists. CFTs to the three target structures were calculated for all 20 patients. Of all the generated CFTs, a set of three was chosen by employing the color-coding scheme and considering the displayed angles between trajectories. To enable a more intuitive evaluation of the results, we defined the following five anatomical regions for better visualization and presentation: suprameatal (SM), superior

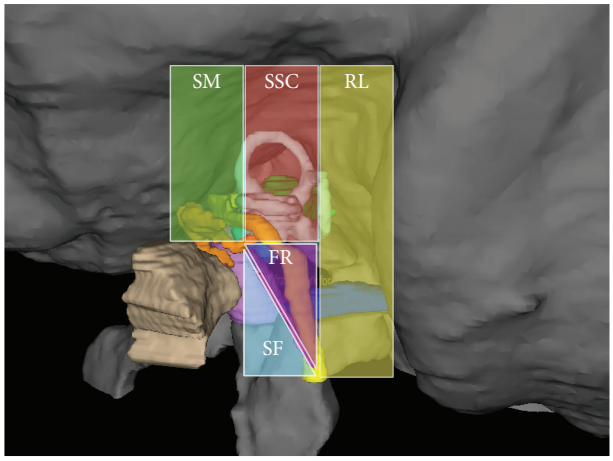

Figure 5: Five anatomic regions for passing CFTs: suprameatal (SM), superior semicircular canal (SSC), retrolabyrinthine (RL), chorda-facial recess (FR), and subfacial (SF).

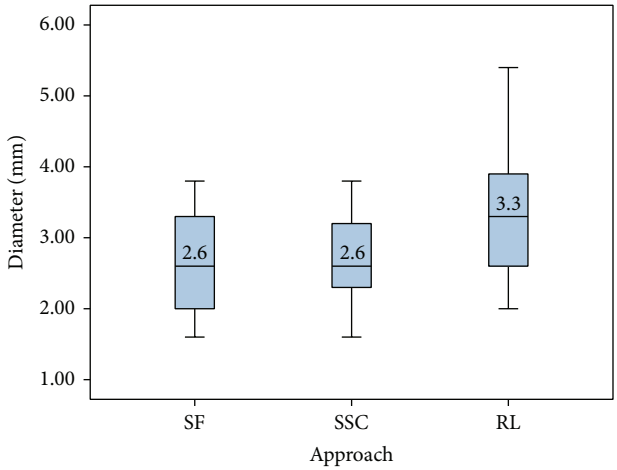

Figure 6: Diameters and anatomical regions of the CFTs for the IAC target point (subfacial (SF), superior semicircular canal (SSC), and retrolabyrinthine (RL)).

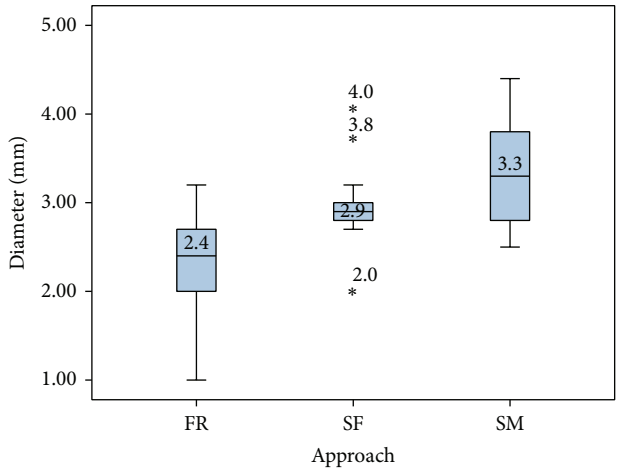

Figure 7: Diameters and anatomical regions of the CFTs for the RW target point (facial recess (FR), subfacial (SF), and suprameatal (SM)).

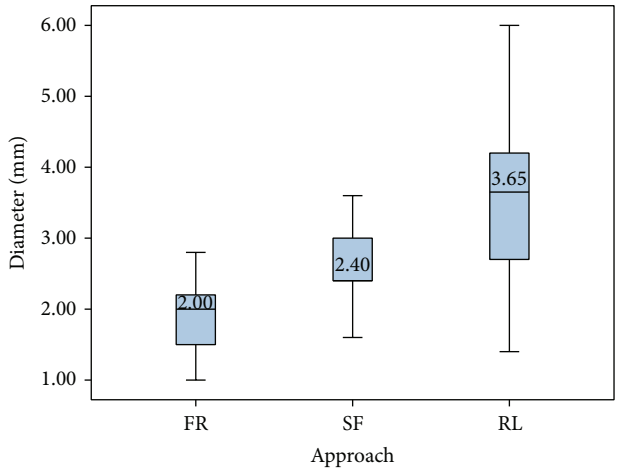

Figure 8: Diameters and anatomical regions of the CFTs in mm for the PA target point (facial recess (FR), subfacial (SF), and retrolabyrinthine (RL)).

semicircular canal (SSC), retrolabyrinthine (RL), chorda-facial recess (FR), and subfacial (SF) (Figure 5).

3.2. Collision-Free Paths and Diameters. In each of the 20 cases, the evaluators determined three CFTs to the IAC, representing three alternative and valid configurations for each patient. Of all 60 defined paths to the IAC, 53% were inside the retrolabyrinthine area, 40% passed through the SSC, and 23% passed subfacially. The region with the largest possible median drilling diameters was found to be the retrolabyrinthine (3.3 mm), followed by the SSC (2.6 mm) and the SF area (2.6 mm). Overall, the collision-free path with the largest diameter (5.4 mm) was located in the retrolabyrinthine, and the CFT with the smallest diameter (1.6 mm) was located subfacially and in the SSC (Figure 6).

Three collision-free drill paths to the RW were also found in all 20 cases. The 60 possible paths were localized in the FR, SM, and SF in 33%, 43%, and 23% of all calculated CFTs, respectively. The largest median diameters were found in the suprameatal area (3.3 mm), followed by the subfacial area (2.9 mm) and the facial recess (2.4 mm). The collision-free path with the overall largest diameter passed through the SM area (4.4 mm), while the path with the smallest diameter was found in the facial recess (Figure 7).

Last, we simulated three CFTs to the PA in all 20 cases. The most common region to intersect with the CFTs was the retrolabyrinthine (67%), followed by the subfacial area (22%) and the facial recess (12%). The median CFT diameters for the RL, SF, and FR were 3.7, 2.4, and 2.0 mm, respectively. The collision-free path with the overall largest diameter (6.0 mm) was found in the retrolabyrinthine area and the path with the smallest diameter (1 mm) passed through the facial recess (Figure 8).

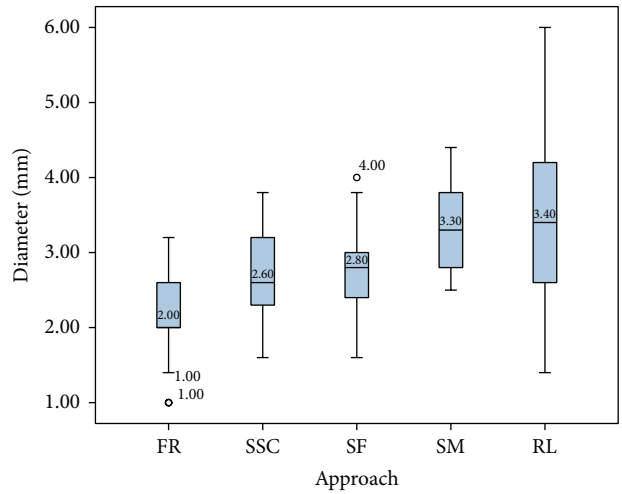

Figure 9: Diameters of the CFTs for all three target points by anatomical region/approach (facial recess (FR), superior semicircular canal (SSC), subfacial (SF), suprameatal (SM), and retrolabyrinthine (RL)).

Table 1: The cumulative angle (CA) for each target point. The values represent the CA in degrees (internal auditory canal (IAC), round window (RW), and petrous apex (PA)).

Region	IAC	RW	PA
Median	98	112	40
STD deviation	27	30	12
Minimal value	13	42	19
Maximal value	126	153	62

To evaluate the appropriateness of each of the 5 anatomical regions as an entry-point area, we evaluated each region for all targets combined to determine the average available space for CFTs in that region. The retrolabyrinthine region showed the largest possible average diameter (3.4 mm). It is notable that this region had not only the largest maximum diameter (6.0 mm) but also the largest range, with a minimum diameter of 1.4 mm. The suprameatal, subfacial, and SSC regions allowed for mean diameters of 3.3, 2.8, and 2.6 mm, respectively. The facial recess approach provided the smallest space, with a mean CFT diameter of 2.0 mm and a minimum diameter of only 1 mm (Figure 9).

The CA was dependent on the target. For example, the largest average CA of 112° was found when targeting the RW. The IAC and PA targets displayed smaller average CAs of 98° and 40°, respectively (Table 1).

4. Discussion

In this study, we developed a software program for the planning and evaluation of multiple trajectories toward a designated target within the temporal bone. Based on 20 conventional CT scans of the temporal bone, it was possible to calculate and visualize for each patient a set of three alternative CFTs to the RW, internal auditory canal, and petrous apex (i.e., 9 CFTs per patient) without violating critical structures. The CFTs were chosen with the aim of maximizing both the drilling diameter and the angles between CFTs. The CFTs originated in five anatomical regions with an average measured diameter of 3.4 mm for the RL, 3.3 mm for the SM, 2.8 mm for the SF, 2.7 mm for the SSC, and 2.1 mm for the FR region. The diameters exhibited high variability, especially in the deeper regions of the temporal bone (internal auditory canal and petrous apex), because of anatomical variations, such as a high sinus bulb, low dura, or narrow chorda-facial recess.

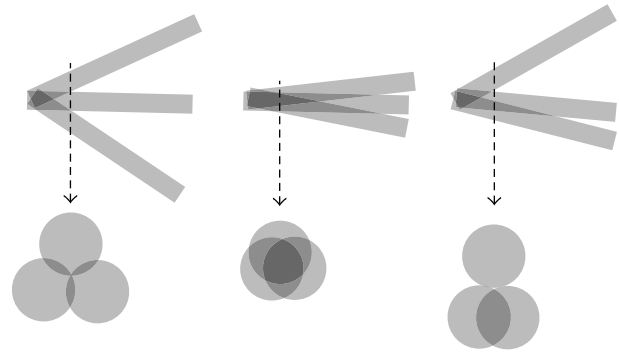

Figure 10: Different possibilities of intersection point of the canals.

The current planning process from a regular CT scan to the three CFTs requires approximately 2 hours. This includes manual segmentation, mesh extraction, transfer, and planning. The most time-consuming procedure is the manual segmentation. The first procedures required approximately twice as long. There was a learning curve since (i) segmentation times improved, especially when using a graphic tablet, and (ii) the surgeons gained experience with the workflow and the user interface of the software. The last step, planning of the trajectories with the SOFA planning tool, usually requires less than 15 minutes. We are currently working on semiautomatic segmentation of all anatomical structures and automatic transfer into SOFA in order to improve the duration of the process.

The data demonstrate the feasibility of a multiport strategy within the temporal bone. Although several authors have demonstrated single-port approaches for MIPs in the skull base, to the best of our knowledge, a MIP multiport approach with three ports in the lateral skull base has not been previously reported. As stated above, the rationale for employing three ports is that this approach provides advanced manipulation capability and visual control. Although we were able to find three alternative, valid CFTs for each patient and target region in all 20 cases, the following aspects should be considered (Figure 10). In the multiport setup, the trajectories inevitably intersect at a variable distance before they reach the actual target. The intersection point depends on the diameter and the intertrajectory angles. A distal intersection occurring immediately at the target forms a cavity and creates additional space for manipulation around the target, which is desirable. An intersection that is too proximal may lead to fusion into two or even one path and, possibly, the loss of space for one or two instruments. The optimal relationship between

the diameter and angle of the trajectories has not yet been evaluated.

The navigation, imaging, segmentation, and drilling process all have a major impact on the success of a procedure. High-resolution imaging and navigation are key factors. The mean target registration error (TRE) for commercially available otolaryngologic navigation systems with skin-affixed fiducial marker registration or bone-implanted fiducials has been reported to be at least 0.91 ± 0.28 mm [15, 16]. The use of microstereotactic frames allows for further reduction of the TRE to 0.45 ± 0.15 mm [17] or even 0.37 ± 0.18 mm [10]. Bartling et al. showed that submillimetric surgical navigation accuracy is possible by using flat panel-based volume computed tomography (TRE: 0.46 ± 0.22 mm) rather than 16-slice CT (TRE: 0.82±0.35 mm) [18]. A recent study by Bell et al. presented an image-guided robot system for drilling of one minimally invasive tunnel to the round window for cochlear electrode insertion. The group reported an error of 0.15 ± 0.08 mm at the target [19].

Manual segmentation is the gold standard but is still dependent on the quality of the imaging and even more dependent on the experience of the surgeon. To the best of our knowledge, the intra- and intersurgeon variability and/or deviation from the "ground truth" have not been reviewed for skull base datasets and must be accounted for when defining the safety margin for the drilling paths. In the final setting, this operator-dependent error requires further reduction of the drill path diameter to increase the safe distance to risk structures. Currently, this safety strategy may unreasonably exclude certain patients from a MIP scenario due to the small diameter of at least one canal. A possible future solution would involve an automatic, validated segmentation protocol that may eliminate human error and that is currently under investigation by our group. Currently, the additional safety value can be manually adjusted, as appropriate, by our planning software and may be included in an individualized patient-specific therapeutic regimen.

The multiport MIP approach to the otobasis demands specially fitted, miniaturized instruments; surgery through tiny bony channels in a narrow space pushes the boundaries of "conventional" instruments. Emerging technologies, for example, piezosurgery, optical coherence tomography, or microendoscopy, may be applied for tissue ablation [20, 21]. The use of robotics may further enhance the precision of the operation; robotic systems can reduce human tremor, provide haptic feedback, and improve motor skills and articulation capabilities. The exact requirements for the instruments depend on the individual case; even with current instruments, applications such as biopsy and local injection of drugs (e.g., "targeted therapy") may become possible due to the minimal trauma and predictable risks afforded by MIPs. Another challenge is the sufficient visualization of the region of interest in a rigid, complex region such as the otobasis. The ongoing miniaturization of the endoscope and improvement of the image quality may enable the use of the smallest drill channels for direct visualization; rigid endoscopes, commonly known as Hopkins rods, are currently available in diameters <0.9 mm and deliver better image quality than fiber optic and chip-on-tip technology [22].

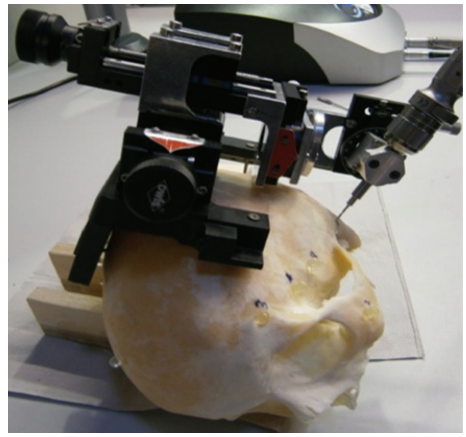

Figure 11: Positioning of a drill based on computed trajectories in a cadaveric scull.

Our results demonstrate that planning of minimally invasive multiport paths, providing access to the lateral skull base, is feasible. The presented planning and simulation of the trajectories are the first, necessary steps to successful minimally invasive multiport surgery of the otobasis. The translation from planning to actual cadaveric model testing is currently underway in our laboratory (Figure 11).

5. Conclusion

Our study shows that planning of minimally invasive multiport paths, providing access to the lateral skull base, is feasible. A future approach based on this planning may minimize iatrogenic damage and deliver a reproducible result with high outcome predictability, thereby improving patient satisfaction and safety. Cadaveric and clinical studies are required to further verify this approach to the lateral skull base.

Conflict of Interests

The authors declare that there is no conflict of interests regarding the publication of this paper.

References

[1] X. Li, J. Zhang, L. Sang, W. Zhang, Z. Chu, and Y. Liu, "Laparoscopic versus conventional appendectomy —a meta-analysis of randomized controlled trials," *BMC Gastroenterology*, vol. 10, article 129, 2010.

[2] S. Sauerland, T. Jaschinski, and E. A. Neugebauer, "Laparoscopic versus open surgery for suspected appendicitis," *Cochrane Database of Systematic Reviews*, no. 10, Article ID CD001546, 2010.

[3] F. Keus, J. A. F. de Jong, H. G. Gooszen, and C. J. van Laarhoven, "Laparoscopic versus open cholecystectomy for patients with symptomatic cholecystolithiasis.," *Cochrane Database Of Systematic Reviews*, no. 4, Article ID CD006231, 2006.

[4] N. Gerber, B. Bell, K. Gavaghan et al., "Surgical planning tool for robotically assisted hearing aid implantation," *International*

Journal for Computer Assisted Radiology and Surgery, vol. 9, pp. 11–20, 2014.

[5] H. Hiraumi, N. Yamamoto, T. Sakamoto, and J. Ito, "A minimally invasive approach for cochlear implantation using a microendoscope," *European Archives of Oto-Rhino-Laryngology*, vol. 270, no. 2, pp. 477–481, 2013.

[6] B. Bell, C. Stieger, N. Gerber et al., "A self-developed and constructed robot for minimally invasive cochlear implantation," *Acta Oto-Laryngologica*, vol. 132, no. 4, pp. 355–360, 2012.

[7] Y. Nguyen, M. Miroir, J. Vellin et al., "Minimally invasive computer-assisted approach for cochlear implantation: a human temporal bone study," *Surgical Innovation*, vol. 18, no. 3, pp. 259–267, 2011.

[8] R. F. Labadie, J. H. Noble, B. M. Dawant, R. Balachandran, O. Majdani, and J. M. Fitzpatrick, "Clinical validation of percutaneous cochlear implant surgery: Initial report," *Laryngoscope*, vol. 118, no. 6, pp. 1031–1039, 2008.

[9] G. B. Wanna, R. Balachandran, O. Majdani, J. Mitchell, and R. F. Labadie, "Percutaneous access to the petrous apex in vitro using customized micro-stereotactic frames based on image-guided surgical technology," *Acta Oto-Laryngologica*, vol. 130, no. 4, pp. 458–463, 2010.

[10] R. F. Labadie, J. Mitchell, R. Balachandran, and J. M. Fitzpatrick, "Customized, rapid-production microstereotactic table for surgical targeting: description of concept and in vitro validation," *International Journal of Computer Assisted Radiology and Surgery*, vol. 4, no. 3, pp. 273–280, 2009.

[11] W. P. Liu, M. Azizian, J. Sorger et al., "Cadaveric feasibility study of da Vinci Si-assisted cochlear implant with augmented visual navigation for otologic surgery," *JAMA Otolaryngology–Head & Neck Surgery*, vol. 140, no. 3, pp. 208–214, 2014.

[12] P. A. Yushkevich, J. Piven, H. C. Hazlett et al., "User-guided 3D active contour segmentation of anatomical structures: significantly improved efficiency and reliability," *NeuroImage*, vol. 31, no. 3, pp. 1116–1128, 2006.

[13] W. E. Lorensen and H. E. Cline, "Marching cubes: a high resolution 3D surface construction algorithm," *ACM Siggraph Computer Graphics*, vol. 21, no. 4, pp. 163–169, 1987.

[14] J. Allard, S. Cotin, F. Faure et al., "SOFA—an open source framework for medical simulation.," *Studies in Health Technology and Informatics*, vol. 125, pp. 13–18, 2007.

[15] R. F. Labadie, B. M. Davis, and J. M. Fitzpatrick, "Image-guided surgery: what is the accuracy?" *Current Opinion in Otolaryngology and Head and Neck Surgery*, vol. 13, no. 1, pp. 27–31, 2005.

[16] P. Pillai, S. Sammet, and M. Ammirati, "Application accuracy of computed tomography-based, image-guided navigation of temporal bone," *Neurosurgery*, vol. 63, no. 4, pp. 326–333, 2008.

[17] R. Balachandran, J. E. Mitchell, B. M. Dawant, and J. M. Fitzpatrick, "Accuracy evaluation of microTargeting platforms for deep-brain stimulation using virtual targets," *IEEE Transactions on Biomedical Engineering*, vol. 56, no. 1, pp. 37–44, 2009.

[18] S. H. Bartling, M. Leinung, J. Graute et al., "Increase of accuracy in intraoperative navigation through high-resolution flat-panel volume computed tomography: experimental comparison with multislice computed tomography-based navigation," *Otology and Neurotology*, vol. 28, no. 1, pp. 129–134, 2007.

[19] B. Bell, N. Gerber, T. Williamson et al., "*In vitro* accuracy evaluation of image-guided robot system for direct cochlear access," *Otology and Neurotology*, vol. 34, no. 7, pp. 1284–1290, 2013.

[20] M. Dellepiane, R. Mora, F. A. Salzano, and A. Salami, "Clinical evaluation of piezoelectric ear surgery," *Ear, Nose and Throat Journal*, vol. 87, no. 4, pp. 212–216, 2008.

[21] M. Schlee, M. Steigmann, E. Bratu, and A. K. Garg, "Piezosurgery: basics and possibilities," *Implant Dentistry*, vol. 15, no. 4, pp. 334–340, 2006.

[22] L. A. Kahrs, T. R. McRackan, and R. F. Labadie, "Intracochlear visualization: comparing established and novel endoscopy techniques," *Otology & Neurotology*, vol. 32, no. 9, pp. 1590–1595, 2011.